FLOW-MEDIATED MECHANOTRANSDUCTION IN MOUSE PROXIMAL TUBULE

by

YI DUAN

A dissertation submitted to the Graduate Faculty in Biomedical Engineering in partial fulfillment of the requirements for the degree of Doctor of Philosophy, The City University of New York

2009

This manuscript has been read and accepted for the
Graduate Faculty in Biomedical Engineering in satisfaction of the
dissertation requirement for the degree of Doctor of Philosophy.

	Dr. Sheldon Weinbaum
Date	Chair of Examining Committee
	Dr. Mumtaz Kassir
Date	Executive Officer

Dr. Tong Wang

Dr. Alan Weinstein

Dr. John M. Tarbell

Dr. Bingmei Fu
Supervision Committee

THE CITY UNIVERSITY OF NEW YORK

ABSTRACT

FLOW-MEDIATED MECHANOTRANSDUCTION IN MOUSE PROXIMAL TUBULE

By

Yi Duan

Adviser: Professor Sheldon Weinbaum

The most important unresolved mystery in kidney proximal tubule is that the fractional reabsorption of salt and water remains constant despite the large variations in glomerular filtering load, i.e. glomerular tubular balance (GTB). In the proximal tubule of rat kidneys, the Na^+ and HCO_3^- reabsorption vary proportionally with changes in axial flow rate, a behavior termed "perfusion-absorption balance". This feature is a critical component of GTB, but the basic mechanism by which the tubule epithelial cells sense axial flow rate and convert the mechanical signal to physiological responses remains unexplained. The purpose of this thesis is to investigate flow-mediated mechanotransduction in mouse proximal tubule cells. We begin by demonstrating that "perfusion-absorption balance" is also present in isolated mouse proximal tubule. A global mathematical model was utilized to calculate the force and torque distribution on microvilli. *In vitro* microperfusion studies were performed on mouse proximal tubule, in

which volume and HCO_3^- reabsorption were recorded and used as an input to the model. The model shows a perfectly linear relationship between hydrodynamic torque and Na^+ and HCO_3^- reabsorption, indicating that the torque signals transporter activities in response to flow. In addition, this flow-dependent Na^+ and HCO_3^- reabsorption was greatly reduced by cytochalasin D, an actin disrupting drug, suggesting that the actin cytoskeleton plays an important role in regulating this flow-dependent behavior. Next, we selected a mouse proximal tubule cell line to examine the structural and functional responses of these cells to fluid shear. Cytoskeleton reorganization was dramatic. We witnessed flow-induced disappearance of stress fibers from cell base, formation of tight and adherens junctions, and accumulation of focal adhesions. Upregulation and trafficking of the transporters were seen on both luminal and peritubular sides of the cell membrane. An intact cytoskeleton network is necessary to facilitate the flow-mediated transporter activities, but not all proteins are dependent on the actin cytoskeleton. These studies investigate the mechanotransduction cascade in mouse proximal tubule cells, and will enhance on understanding of the mechanism of flow-dependent proximal tubule transport.

DEDICATION

This thesis is dedicated to my parents. They are the reason that I have chosen this path.

Also, this thesis is dedicated to my husband who has been a great source of motivation and inspiration.

Finally, this thesis is dedicated to all those who believe in the richness of learning.

ACKNOWLEDGEMENTS

I would first like to thank my advisor and supervisor, Professor Sheldon Weinbaum, for his endless support, abundant encouragement, advice and patience, for always stimulating my confidence and providing me with an environment which allowed me to do research independently, for his leading me to enter biomedical engineering, an interdisciplinary and challenging field of research. His mentoring has been extremely valuable to me in guiding me through this process and helping to build the foundation of my future career. The sheer energy with which he approaches any challenge has been inspirational.

I would also like to thank the members of my thesis committee: Professor Tong Wang (Yale), Dr. Alan Weinstein (Cornell), Dr. John M. Tarbell (CCNY) and Dr. Bingmei Fu (CCNY). They have been a source of encouragement and advice that have contributed a great deal in the course of my Ph.D. work. And also, extra thanks to Dr. Wang for her guidance and help over the years in encouraging me to be an independent researcher. It has not always been an easy road, but she has been an anchor of support throughout the years. I am also indebted to Dr. Lisa M Satlin and her kind lab members in Mount Sinai for their efforts to teach me lab techniques and train me to be an experimentalist.

My fellow members of the Wang Lab have also been invaluable not only in helping with the research problems along the way, but also in making the lab a fun and exciting place to work. My thanks to Nanami Gotoh, Qingshang Yan, and Zhaopeng Du for their

leadership in the lab and their patience in always being willing to address whatever questions I may bring them. And thanks also to the other students (and former students) in City College who have been a great source of support and friendship: Qianhong Wu, Yuefeng Han, Xiaobing Zhang, Chi Bang, Yilin Wang, Yuliya Vengrenyuk, Parisa Mirbod. Also thanks to Carol Bamberger and Pat Cupid for their administrative help.

Finally, I would like to thank the people that have been the most important over the years. First and foremost, my husband Chris Arnold should be at the top of any list. He has been an amazing support and lifeline over the years. I have put him through more than he ever could have bargained for, but he has somehow remained by my side through it all. I truly could not have accomplished anything without him there encouraging me and not allowing me to ever give up. His strength of character and beautiful spirit have carried me through many difficult times. Thank you, Chris, for being so amazing. I love you!

I would also like to thank my family for their support. My parents have always given me their full support and unconditional love. They have provided me with every opportunity to succeed, and have never stopped believing in me while never putting any undue pressure on me. They have sacrificed a lot for me to be able to pursue my education, and I am eternally grateful.

Table of Contents

List of Tables

List of Figures

Chapter 1 Physiological Background

1.1 Introduction

The major functions of the kidney are regulation of body fluid osmolality and volume, regulation of electrolyte balance, regulation of acid-base balance, and the production and secretion of hormones. They also remove the metabolic end products, such as urea and urea acid, and preserve the substances essential to life, such as water, sugars, amino acids, and electrolytes (sodium, potassium, bicarbonate and chloride). Thus, the kidneys are regulatory organs to maintain homeostasis in the body by regulating components of the interstitial fluid within a narrow range of values.

The basic structural and functional unit of the kidney is the nephron. In humans, a normal kidney contains 600,000 to 1.4 million nephrons. Two general classes of nephrons are cortical and juxtamedullary nephrons (Figure 1-1), both of which are classified according to the location of their associated renal corpuscle. Cortical nephrons have their renal corpuscle in the superficial renal cortex, while the renal corpuscles of juxtamedullary nephrons are located near the renal medulla. Functionally, cortical and juxtamedullary nephrons have distinct roles. Cortical nephrons (85% of all nephrons in humans) mainly perform excretory and regulatory functions, while juxtamedullary nephrons (15% of nephrons in humans) concentrate and dilute urine. Each nephron is composed of a filtering component (the “renal corpuscle”) and a tubule specialized for reabsorption and secretion (the “renal tubule”). The renal corpuscle, composed of a glomerulus and

Bowman's capsule, filters out large solutes from the blood, delivering water and small solutes to the renal tubule. The renal tubules are responsible for altering the urine after the glomerular filtrate is filtered through the Bowman's Capsule. The first segment of the renal tubule is proximal tubule. It reabsorbs fluid in bulk from the filtrate, including two-thirds of the filtered salt and water and all filtered organic solutes. After that, the filtrate passes through the Loop of Henle, distal convoluted tubule, connecting tubule, and eventually collecting duct system.

The nephron carries out nearly all of the kidney's functions. Most of these functions concern the reabsorption and secretion of various solutes such as ions, carbohydrates, and amino acids. Properties of the cells that line the nephron change dramatically along its length; consequently, each segment of the nephron has highly specialized functions. This thesis mainly focuses on the proximal tubule.

1.2 Anatomy of the Proximal Tubule

The proximal tubule begins abruptly at the urinary pole of the glomerulus. It consists of an initial convoluted portion, the pars convolute, which is a direct continuation of the parietal epithelium of Bowman's capsule, and a straight portion, the pars recta, which is located in the medullary ray. The length of the proximal tubule is approximately 10 mm in the rabbit, 8 mm in the rat, and 4-5 mm in the mouse, compared with approximately 14 mm in the human. The outside diameter of the proximal tubule is about 40 mm. In the rat, three morphologically distinct segments-S1, S2, and S3- have been identified (56).

Interestingly, a recent ultrastructural study found no evidence of structural segmentation along the proximal tubule of the mouse (99). Since the current research mainly uses mouse as the animal model, I will not specify the different structural features in between these three segments, but rather emphasize the general features for all proximal tubule cells in the following section.

1.2.1 The ultrastructure of proximal tubule cells

In most adult mammals, the proximal tubule epithelium consists of a single layer of highly polarized cuboidal cells. The height of the cells is 5-7 μm excluding the brush border (99). The most distinctive characteristic of these cells is their brush border. On the luminal side, the cells are covered with densely packed microvilli forming a border readily visible under the light microscope (Figure 1-2). Morphometric studies performed on isolated segments of rabbit proximal tubules found that the brush border increases the apical cell surface 36-fold (94). The basolateral plasma membrane forms extensive lateral invaginations, and lateral cell processes extending from the apical to the basal surface interdigitate with similar processes from adjacent cells (Figure 1-3). This structural feature serves to increase the intercellular space and the area of the basolateral plasma membrane, where the Na^+/K^+-ATPase (Na^+ pump) is located.

Elongated mitochondria are located in the lateral cell processes in close proximity to the plasma membrane (Figure 1-4), an arrangement that is characteristic of epithelia involved in active ion transport. With standard transmission electron microscopy, these organelles

appear rod-shaped and tortuous; however, studies using high-voltage electron microscopy of 0.5- to 1.0-mm-thick sections have revealed that many mitochondria in the proximal tubule are branched and anastomose with one another (5). The proximal tubule cells contain large quantities of smooth and rough endoplasmic reticulum, and free ribosomes are also abundant in the cytoplasm. A well-developed Golgi apparatus is located above and lateral to the nucleus in the midregion of the cell.

A large number of lysosomes are present in proximal tubule. Lysosomes are membrane-bound, heterogeneous organelles that are involved in the degradation of material absorbed by endocytosis, and often contain multiple electron-dense deposits such as proteins. Lysosomes also play a role in the normal turnover of intracellular constituents by autophagocytosis, and autophagic vacuoles containing fragments of cell organelles are often seen in the proximal tubule (56).

1.2.2 The cytoskeletal network of proximal tubule cell

The proximal tubule cell cytoskeleton consists of several filamentous components that are structurally and functionally distinct. These include actin microfilaments (together with several actin-associated proteins including spectrin, ankyrin, and myosin), microtubule network, and intermediate filaments (Figure 1-5). It has been convincingly demonstrated that this complex cytoskeletal network plays important roles in the generation and maintenance of the polarized epithelial cell pheonotype.

In proximal tubule cells, the actin cytoskeleton forms unique arrangements at the apical and basal cell poles (Figure 1-6) that help to define the unique structure and properties of these membrane domains, thereby contributing to the development and maintenance of cell polarity. The apical membrane domain contains the brush border, which can be divided into microvilli and terminal web (6). Each microvillus consists of 20-30 longitudinally oriented, polarized (barbed or plus end at the microvillus tip) actin microfilaments that extend into the terminal web area. Specific actin bundling proteins such as fimbrin and villin crosslink the actin filaments. Attachment to the lateral portions of the microvillus membrane likely involves both ezrin and myosin (83). These proteins have both actin- and membrane-binding domains. The attachment to the tips of the microvillus involves a poorly characterized protein complex. Microvillar actin is stabilized in the terminal web region by its interactions with villin, tropomyosin, spectrin, and non-muscle myosin II. The terminal web contains a dense meshwork of actin and associated proteins and intermediate filaments that are oriented primarily perpendicular to the microvilli (14). The proteins in the terminal web region are heavily crosslinked, but must also be dynamic enough to permit the passage of molecules and vesicles through this active transport area. The lower aspect of the terminal web consists of a prominent band of actin/myosin filaments forming a girdle around the cell at the level of the adherens junctions, which is a major site of contact between neighboring cells.

While the actin cytoskeleton plays a large part of maintaining the overall three dimensional structure of the cells, the microtubule cytoskeleton is involved in providing a

track or road for the membrane vesicles (80). Consequently, the microtubule cytoskeleton participates in the regulation and delivery of membrane components to their correct membrane domain. Microtubules are tubular polymers composed of α- and β-tubulin dimmers, which assemble in a polarized fashion to produce microtubules that have a distinct function polarity. The more rapidly growing end of microtubules is known as the plus (+) end, and the other end is the minus (-) end. During the establishment of polarity, long cortical bundles of microtubules with the same polarity (minus ends of microtubule oriented toward the apical surface of the cell) form parallel to the lateral membrane along the apicobasal axis of the cell (33); whereas the other short sets of microtubules, often with mixed polarity, reside either in the subapical membrane cytoplasm or along the basal membrane (Figure 1-7). It has been suggested that the orientation of microtubule assembly in the apicobasal axis is determined by linkage of microtubules to cytoskeletal complexes on lateral and basal membranes, or to the actin cytoskeleton forming under the apical membrane domain. Experimental evidence has not been provided. Coincident with microtubule reorganization, compartments of the secretory apparatus that are involved in protein sorting become localized to the apical (Golgi, TGN, and apical endosome) and basal (basolateral endosome) cytoplasm (60). Microtubule organization is required to maintain these distributions, but again, the mechanism involved are not well understood.

1.2.3 Cell-cell contacts

As a result of the extensive interdigitations of lateral and basal processes between adjacent cells, a complex extracellular compartment in proximal tubule cells is formed. It is referred to as the basolateral intercellular space. This space is separated from the tubule lumen by a specialization of the plasma membrane called tight junction.

The tight junction (zonula occludens) encircles the apex of the cell forming a barrier to intradomain movement of intrinsic membrane proteins and outer leaflet phospholipids (the "fense" function), and to paracellular movement of solutes between biological compartments ("gate" function) (50). Three cytoplasmic tight junction-associated proteins have been identified, ZO-1, ZO-2, and cingulin, and two transmembrane protein, occludin and claudin, which comprise part of the tight junction strands observed by freeze-fracture analysis. Proximal tubule cell is found to possess the "leakiest" tight junctions. As observed using electron microscopic techniques, tight junction in proximal tubule cells is shallow in the apicobasal direction and consists of a typical two-strand complex as opposed to five or more strands in some other tight epithelia such as the frog urinary bladder (12). At the functional level, tight junctions function as charge- and size-selective "paracellular tight-junction" channels (79), physiological characteristics that are thought to be conferred by integral membrane proteins that cluster together at the tight junction (98); changes in the expression of these proteins can have marked effects on permeability (27).

The second junction underneath the tight junction is the zonula adherens (adherens junction). It is a seven-layered structure formed by the two adjacent, triple-layered plasma membranes separated by a narrow upper extension of the intercellular space. At the molecular level, the adherens junction is regarded as specialized forms of cadherin-based adhesive contacts. The E-cadherin, one of the classical cadherins known to be essential for the formation and maintenance of epithelia, form a subfamily defined by a highly conserved cytoplasmic domain which binds cytoplasmic proteins termed catenins. Actin cytoskeleton colocalizes with cadherin-catenin complexes at sites of cell-cell contact and is believed to be an important mechanism by which catenins contribute to cadherin-mediated adhesion (3).

Below the zonula adherens are the desmosomes (macula adherens) that are distributed randomly at variable distances beneath adherens junction. These seven-layered structures are also formed by the two adjacent plasma membranes and the intervening intercellular space. However, they are disc-shaped rather than belt-like in configuration and they are responsible for cell-cell adhesion.

The final junction that is found on the lateral membrane is the gap junction (65). They are specialized connections between adjacent cells where the plasma membranes are separated by a 2-nm gap that contains characteristic subunits. This junction is believed to provide a pathway for the movement of low molecular weight ions (approximately 1,000-dalton molecules) between cells.

Similar to points of cell-cell contact, focal adhesions are points of contact between the cell surface and a specific extracellular substrate. At these points, actin bundles terminate on integrins that bridge the plasma membrane to form a link between the extracellular matrix and the actin cytoskeleton (41). Clearly, focal adhesions are important in first determining cell polarity by defining the basal domain of the cell that is locked onto the underlying basement membrane or extracellular matrix. The connecting network of proteins at focal adhesions includes an array of actin-binding proteins including α-actinin, talin, zyxin, and vinculin. These complexes potentially provide communication and signal transduction between the cell cytoskeleton and the extracellular milieu via specific protein kinases, such as p125.

1.3 Na^+ and HCO_3^- Reabsorption in Proximal Tubule

The key function of the proximal tubule is the near-isosomotic reabsorption of two thirds to three quarters of the glomerular ultrafiltrate. This encompasses the reabsorption of approximately 65% of filtered Na^+ and 70-80% HCO_3^-.

Na^+ reabsorption contains both paracellular and transcellular pathways. The transcellular pathway (Figure 1-7), which is also the focus of this thesis, is driven by Na^+/K^+-ATPase located in the basolateral membrane. The active transport of Na^+ out of the cell across the basolateral membrane creates a lumen-to-cell concentration gradient for Na^+. Apically, Na^+/H^+ exchanger and the Na-dependent glucose, amino acid, and phosphate cotransporters provide the entry sites in the transport of Na^+. In addition, Na^+/H^+

exchanger plays an important role in the robust absorption of HCO_3^-; this absorption of HCO_3^- serves to increase the luminal concentration of Cl^-, which in turn increases the driving forces for the passive paracellular transport of both Na^+ and Cl^-.

HCO_3^- reabsorption in the proximal tubule is determined to be H^+ secretion rather than direct HCO_3^- reabsorption. The general features of HCO_3^- reabsorption are shown in Figure 1-7: apical H^+ secretion, basolateral Na^+ coupled HCO_3^- exit from the cell, and facilitation by both membrane bound and cellular carbonic anhydrase. Apical H^+ secretion occurs by both an apical NHE3 and an H^+-ATPase. The apical secreted H^+ reacts with filtered HCO_3^- to form H_2CO_3. In the presence of carbonic anhydrase (type IV), luminal H_2CO_3 rapidly dehydrates to $CO_2 + H_2O$ that are readily permeable across all membranes of proximal tubule. Inside the cell, dissociation of H_2O into OH^- and H^+ is promoted by hydroxylation of CO_2 ($OH^- + CO_2 \Rightarrow HCO_3^-$) to generate bicarbonate, catalyzed by soluble (type II) carbonic anhydrase. Bicarbonate exits the cell through the Na/HCO_3^- cotransporter, NBC1, and the Na+ independent Cl^-/ HCO_3^- exchange. The net result is that $NaHCO_3$ disappears from the lumen and appears in the blood-side of the proximal tubule cells .

1.4 Regulation of Na^+ and HCO_3^- Reabsorption

1.4.1 Glomerular tubular balance

Regulation of Na^+ and HCO_3^- reabsorption along the proximal tubule is by glomerular-tubular balance (GTB): changes in glomerular filtration rate (GFR) are balanced by

equivalent changes in tubular reabsorption, thus maintaining a constant fractional reabsorption of fluid and Na^+. This highly regulated intake of salt and water in the proximal tubule is critical to the survival of an organism.

Schnermann et al. (76) first demonstrated the GTB in rats using the micropuncture technique four decades ago. Their classical experimental result is shown in Figure 1-8. In this experiment, inulin is used as the marker molecule. Inulin is small in size for filtration and it is neutral. Thus, it can freely filter into the Bowman's capsule from the glomerular capillaries. However it is larger in size for reabsorption and secretion and its absolute amount will not change along the tubule when infused. If the concentration of inulin in some part of the tubular fluid is more than that in plasma, indicating some volume must be absorbed by the tubule. The reabsorption fraction can be obtained in term of the ratio of inulin concentrations in the tubule and in the plasma. Let r denote the ratio of C_{PT}, the inulin concentration at the end of the proximal tubule, to C_{PL}, the inulin concentration in plasma,

$$r = \frac{C_{PT}}{C_{PL}} . \tag{1.1}$$

The reabsorption ratio κ can be expressed in term of r

$$\kappa = 1 - \frac{1}{r} . \tag{1.2}$$

In their experiment, Schnermann et al. (76) found that the ratio r remained the same despite the four fold increase in glomerular filtration rate. This ratio is 2.27 and the corresponding fractional reabsorption rate is 56%.

However, data from *in vitro* microperfusion setting was not in agreement with the former *in vivo* experiment. Burg and Orloff (9) found no flow-dependent reabsorption, and concluded that GTB was "not an intrinsic property of the proximal tubule". In subsequent work, flow-dependent Na^+ reabsorption has never been found in rabbit tubules by any investigators, and it has been an open question as to whether this difference between rat and rabbit tubules truly required an intact kidney or was a species difference. In Chapter 2, we reexamine the flow-induced changes in Na^+ and HCO_3^- reabsorption by perfusion of proximal tubule in vitro from mouse kidney to test our hypothesis that GTB is an autoregulatory mechanism that is independent of neural and systemic hormonal regulations.

1.4.2 Underlying mechanism of glomerular tubular balance

The mechanisms of GTB include both peritubular capillary effects and luminal factors (22, 95). Perhaps the most important luminal factor is the effect of luminal flow on tubular reabsorption, i.e. perfusion-reabsorption balance (95). An enhancement of GFR increases salt and water reabsorption in rat and dog studies by renal clearance and free-flow micropuncture *in vivo* (31, 76). Chan et al (10) reported that a three-fold increase in luminal flow rate produced a doubling of the rate of both Na^+ and HCO_3^- reabsorption.

The underlying mechanism for flow-activated changes in Na^+ and HCO_3^- reabsorption, however, has not been established. As mentioned previously, transepithelial movement of fluid, electrolytes, and large molecules is achieved by the activity of a host of specialized transporting proteins that are located on the apical and basolateral domain of the membrane. "Perfusion-absorption balance" in turn becomes a question of how flow could activate changes in membrane transporter activities. The major challenge to researchers in this field is the identification of the mechanism(s) by which the magnitude of the fluid flow in the lumen are detected and converted in the brush border epithelial cells into a sequence of biological responses. Therefore, mechanotransducers, where force transmission becomes transduction, are the first elements that need to be clarified.

Guo et al. (35) proposed that brush border microvilli serve as a mechanosensor in proximal tubule, because (1) they form an ordered hexagonal array of uniform height hair-like membrane projections that are directly exposed to the fluid flow in the lumen of proximal tubule, (2) they are relatively stiff, which allows them to transmit the signal (hydrodynamic torque) into the cell body, without significant bending. They suggested that the critical component was the actin cytoskeleton, which is abundant within and beneath the brush border (57). Model calculations in this paper (35) describe how the actin-filament bundle that is the central core of the microvillus deforms under hydrodynamic loading. The proposed role for microvilli is that they can not only sense fluid drag forces, but have the capability of greatly amplifying the forces through their lever arm as they are transferred to the intracellular cytoskeleton at the terminal web,

where the actin-filament bundle within the microvillus attaches at its roots to the main cell body (90). In this scheme of signaling transduction, specific interaction between the proximal tubule cytoskeleton and the luminal membrane transporter is a critical feature. Ezrin (48), an actin-binding protein, has been illustrated to link NHE3 to the actin cytoskeleton.

1.5 Brief Introduction of the Following Chapters

This thesis explores the mechanism of flow-mediated mechanotransduction in mouse proximal tubule. In particular, we investigate the candidate mechanotransducers of proximal tubule cells, examine flow-induced rearrangement of proximal tubule cell cytoskeletal structure, and study the role of cytoskeletal reorganization in modulating downstream ion exchanger activities in response to axial flow.

The model in Guo et al. (35) enables us to obtain the fluid drag and torque distribution on each microvillus. However, it does not allow us to determine easily how the drag and torque on the microvilli change with flow and tubule diameter because it requires that we determine the detailed flow around each microvillus as their spacing changes in response to tubule diameter changes. To address this issue, in Chapter 2, we construct a simpler global model in which the detailed geometry of the microvilli and their spacing is not needed. In this model, a ratio of hydrodynamic torque at any perfusion rate and diameter relative to a reference state is expressed as a function of tubule inner diameter, perfusion rate, and the length of each microvillus. This critical relationship enables us to relate

water reabsorption J_v to hydrodynamic torque T so as to compare mathematical theory and experimental results. The results delineate a perfectly linear relationship between J_v and T as well as J_{HCO3} and T, indicating that the flow-dependent changes of transport activity are modulated directly by the changes in microvillus torque (17, 19), thus providing strong support for the hypothesis that brush border microvilli serve as a mechanosensor. We also find that addition of cytochalasin D, an actin depolymerizing agent, abolishes both water and HCO_3^- reabsorption without changing its baseline at the low flow rate, which provided the evidence for our hypothesis that an intact actin cytoskeleton is critical to the flow-dependent Na^+ and HCO_3^- transport.

Based on the previous observations, we are also interested in the effect of fluid shear stress (FSS) on cytoskeletal reorganization of the proximal tubule epithelial cells. In marked contrast to endothelial cells (23, 28), there are very few studies on cytoskeletal reorganization of proximal tubule cells in response to laminar FSS under carefully monitored flow conditions. One recent study (25) has shown that mouse proximal tubule cells undergo a change in phenotype in response to FSS, and there is massive redistribution of F-actin. This study was limited to only F-actin and was largely observational. In Chapter 3, I show that immortalized mouse proximal tubule cells exposed to defined laminar FSS exhibit a cytoskeletal reorganization of actin and junctional related proteins, which, surprisingly, is nearly exactly opposite that observed in rat fat pad endothelial cell exposed to FSS for the same duration (81). These paradoxical observations are explained in terms of a conceptual model which relates cytoskeletal

reorganization of actin to the redistribution of various junction and actin associated proteins.

From the structure-function standpoint, one would expect this flow-induced dramatic cytoskeletal reorganization to greatly impact membrane transporter trafficking and activities in the proximal tubule. In our isolated single tubule perfusion studies documented in Chapter 2, luminal flow has been suggested to play a major role in modulating apical NHE3 and H^+-ATPase activity and addition of cytochalasin D, largely abolished this flow-dependent behavior (17, 19), indicating a potential role for the actin cytoskeleton in regulating flow-activated apical membrane transporter activities. However, no direct evidence has been reported regarding this issue. In addition, the effect of luminal flow on peritubular transporters remains undefined. Weinstein et al. (93) suggested that as luminal flow increases "peritubular transporter density must increase in the same manner as the apical transporters" in order to keep a constant cell volume. This leads us to propose that flow-dependent regulation in proximal tubule occurs in both apical and peritubular transporters and the regulation may be associated with the alterations of actin cytoskeleton. In Chapter 4, I use immunostaining and Western blot to examine the subcellular distribution of transporters (NHE3, H^+-ATPase and Na^+/K^+-ATPase) in response to flow. The role of the actin cytoskeleton is determined by adding the cytochalasin D to the perfusate. This work leads to an understanding of the molecular steps associated with the regulatory role of the actin-based cytoskeleton on major epithelial transport functions. The basis of this interaction lies on the regulation by actin-

binding proteins and adjacent structures, of actin filament organization which in turn, modulates transporter activity.

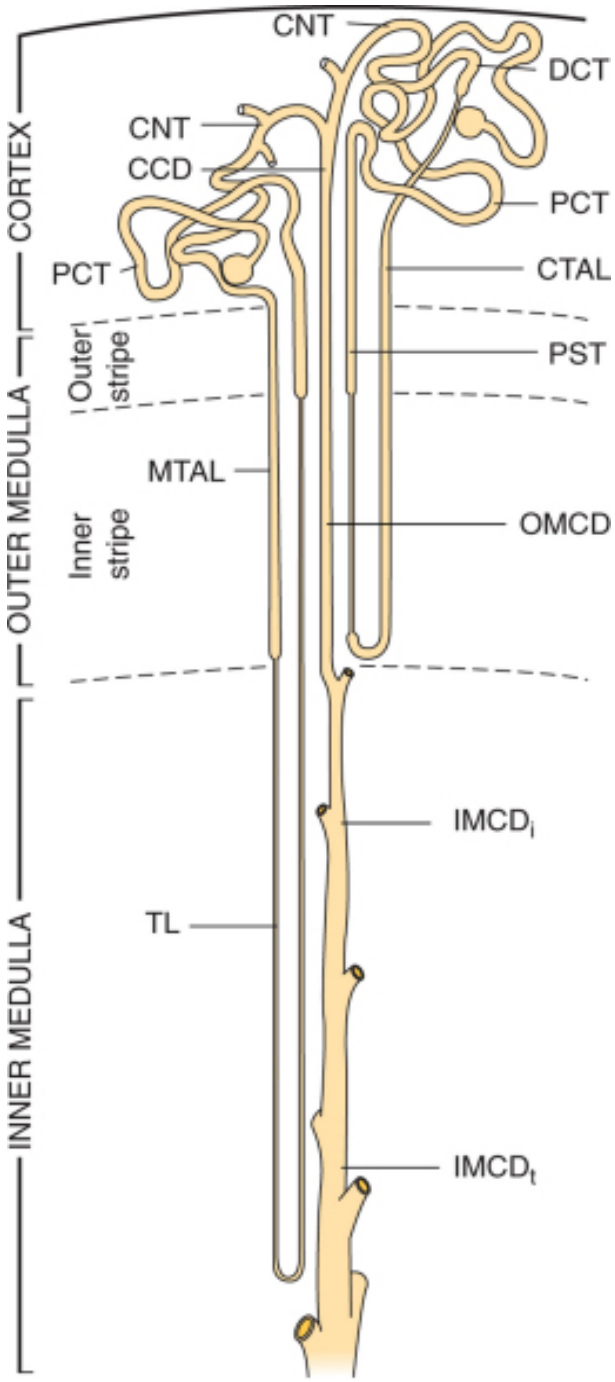

Figure 1−1 Diagram illustrating cortical and juxtamedullary nephron.

CCD, cortical collecting duct; CNT, connecting tubule; CTAL, cortical thick ascending limb; DCT, distal convoluted tubule; IMCDi, initial inner medullary collecting duct; IMCD, terminal inner medullary collecting duct; MTAL, medullary thick ascending limb; OMCD, outer medullary collecting duct; PCT, proximal convoluted tubule; PST, proximal straight tubule; TL, thin limb of loop of Henle. (Modified from (53))

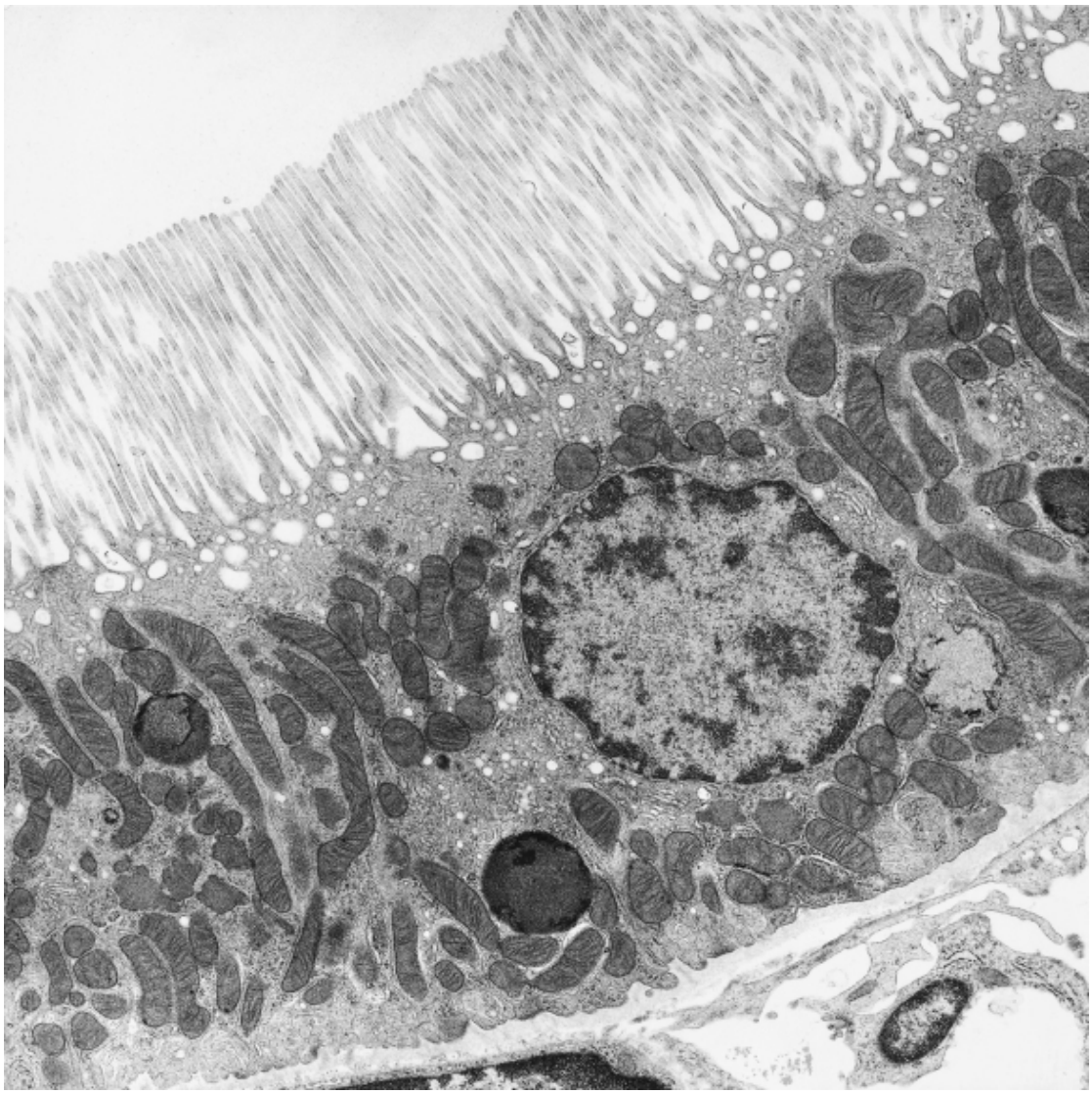

Figure 1−2 Transmission electron micrograph of S1 segment of rat proximal tubule.

The cells are characterized by a tall brush border, a prominent endocytic-lysosomal apparatus, and extensive invaginations of the basolateral plasma membrane. (Magnification, ×10,600.)
From: Brenner: Brenner and Rector's The Kidney, 8th ed.

Figure 1−3 Scanning electron micrograph of proximal convoluted tubule illustrating prominent lateral cell processes.

Arrow on adjacent proximal convoluted tubule denotes small basal processes (52). (Magnification, ×8200.)

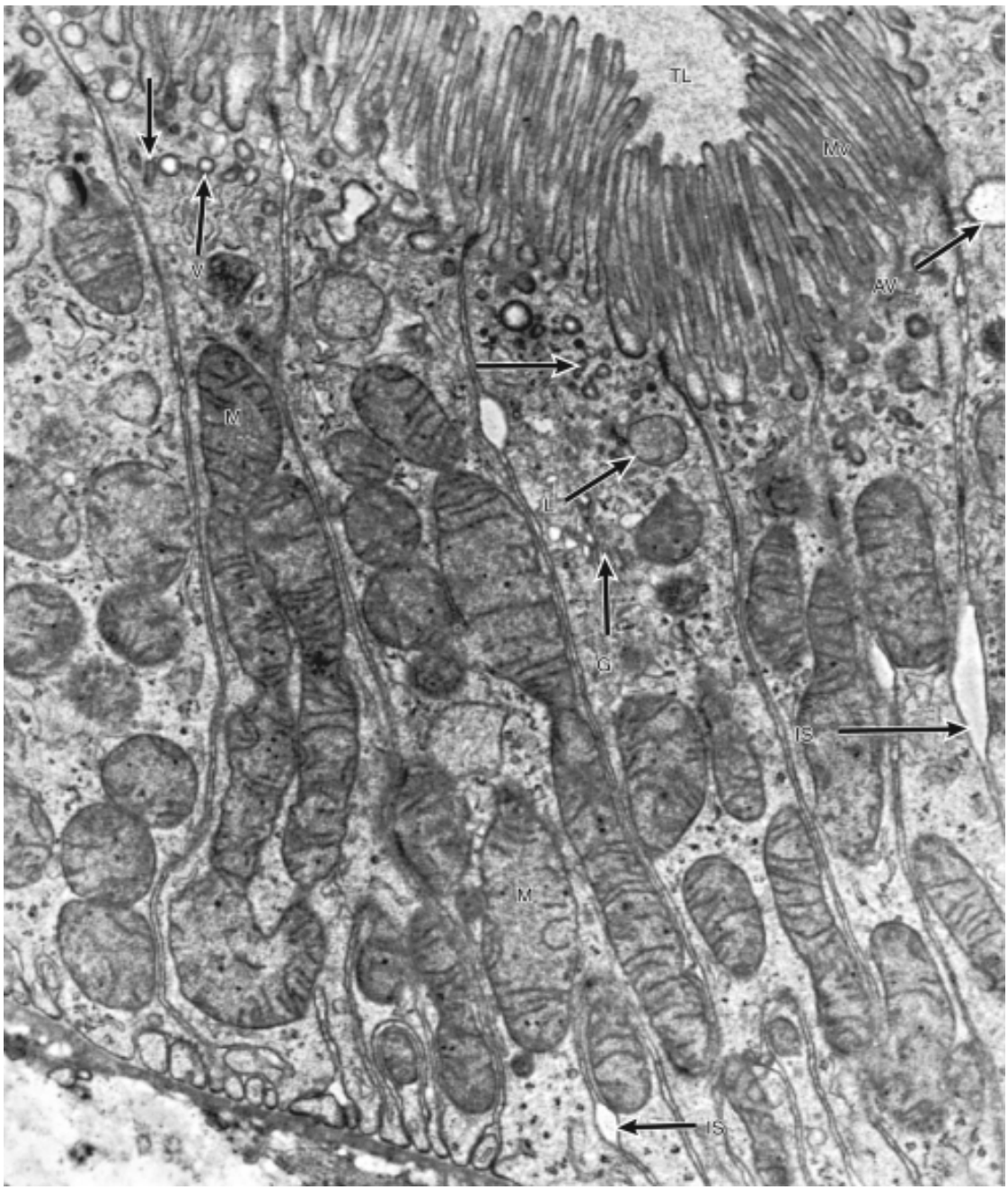

Figure 1−4 Electron micrograph of the pars convoluta of the proximal tubule from a normal human kidney.

The mitochondria (M) are elongated and tortuous, occasionally doubling back on themselves. The endocytic apparatus, composed of apical vacuoles (AV), apical vesicles (V), and apical dense tubules (arrows), is well developed. G, Golgi apparatus; IS, intercellular space; L, lysosome; Mv, microvilli forming the brush border; TL, tubule lumen. (Magnification, ×15,000.)

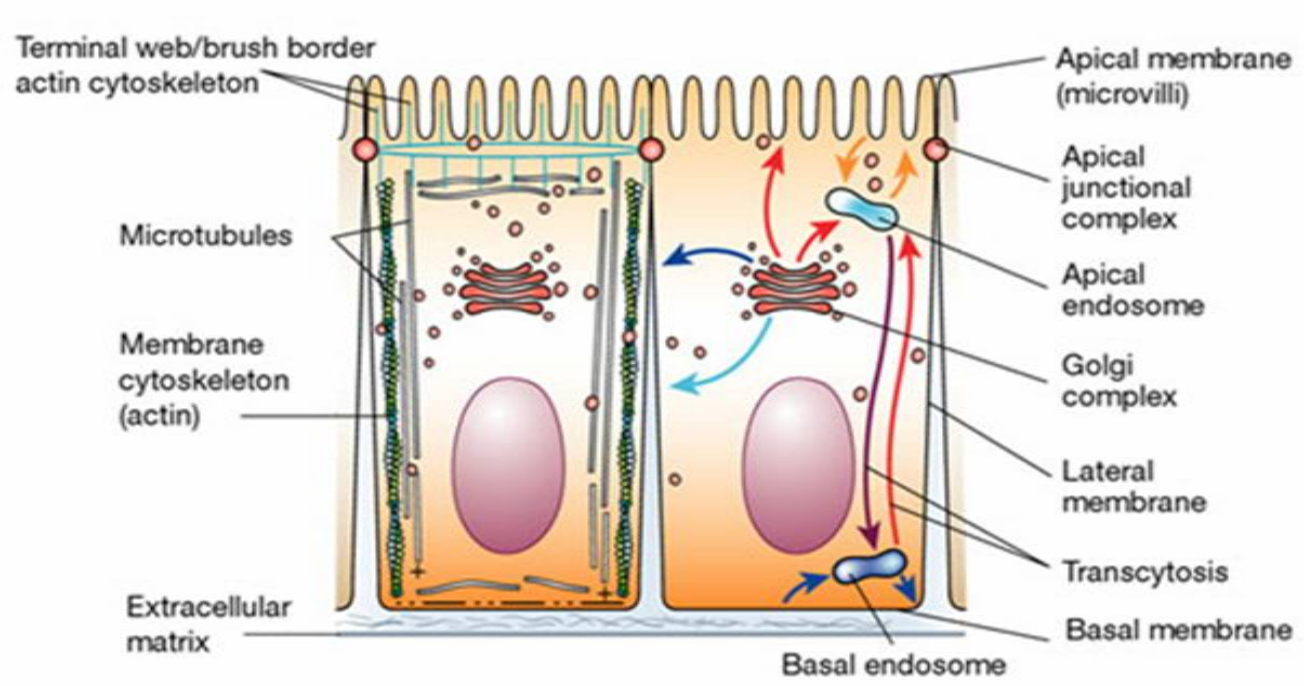

Figure 1−5 Schematic representation of polarized epithelial cells.

Left, organization of the actin and microtubule cytoskeletons; right, organization of vesicle transport pathways to different plasma membrane domains either directly from the Golgi complex, or indirectly via apical or basal endosomes through endocytic or transcytotic pathways (62).

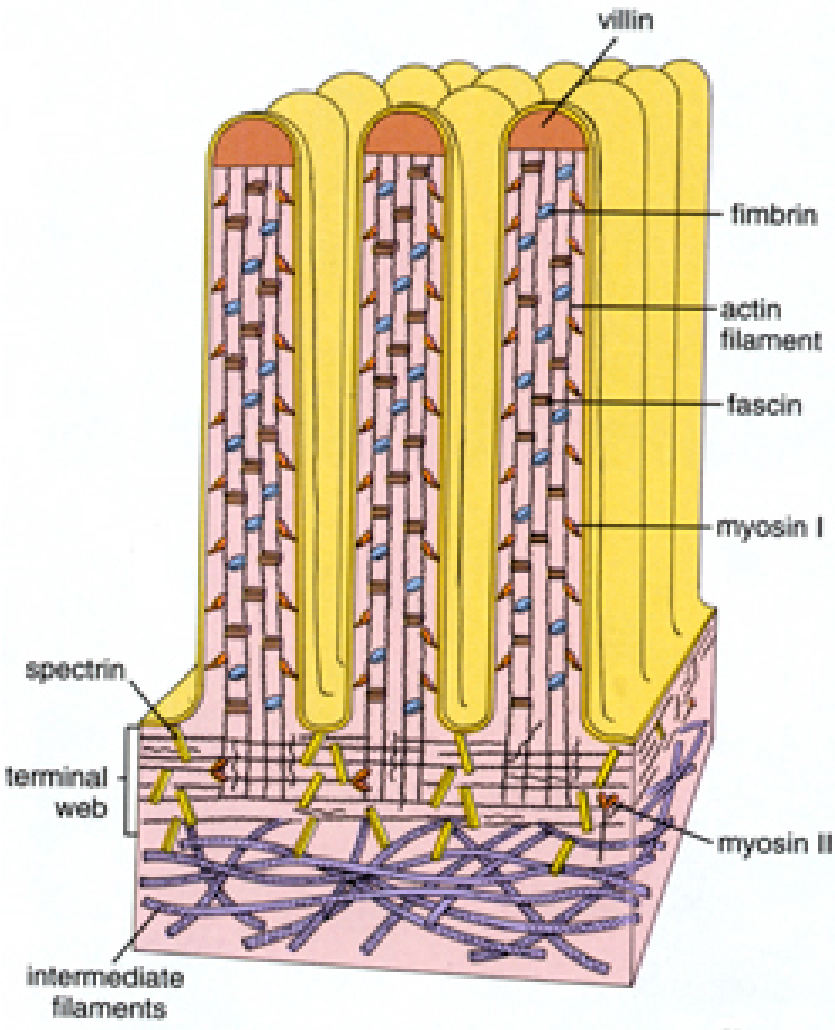

Figure 1−6 The ultrastructure of microvilli in intestine epithelial cells.

Microvilli are made of actin filaments with fimbrin and villin crosslinking the filaments, myosin I attaches filaments to the membrane, actin filaments of the microvilli are linked into the actin filaments of the terminal web, the terminal web is made of other actin filaments associated with tropomyosin, spectrin and myosin II.
http://anatomy.iupui.edu/courses/histo_D502/D502f04/lecture.f04/cell.f04/cellf04.html

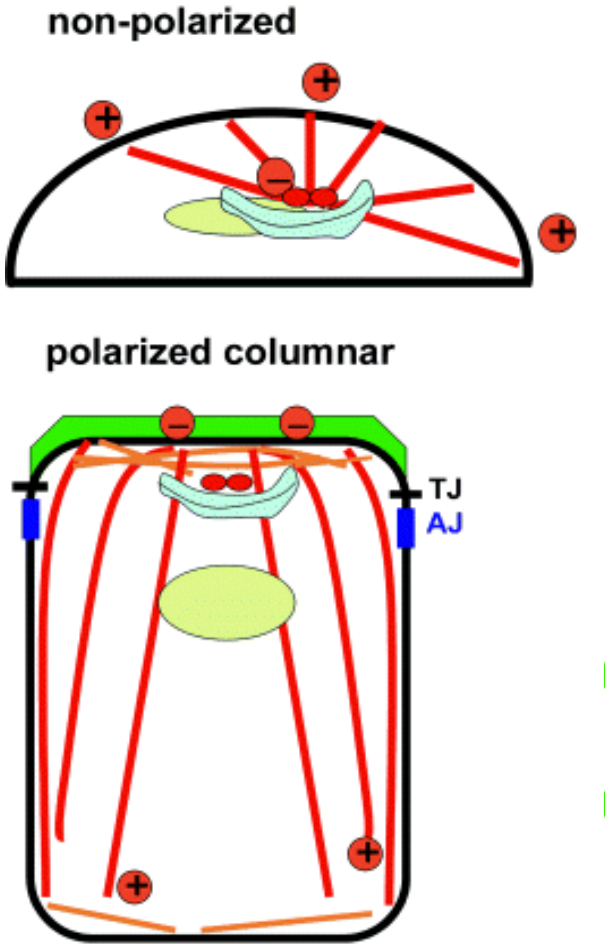

Figure 1−7 Model for the development of microtubule asymmetry in epithelial cells.

In nonpolarized cells, microtubules (MTs) (red lines) nucleate in the perinuclear region and remain anchored with their minus-ends to the centrosome (red dots). Cultured columnar epithelia have an apical and basal MT web composed of short filaments (light red) in addition to vertical MTs of uniform polarity with the minus-end facing the luminal surface (green) that is at the cell apex. TJ = tight junctions above AJ in polarized cells (60).

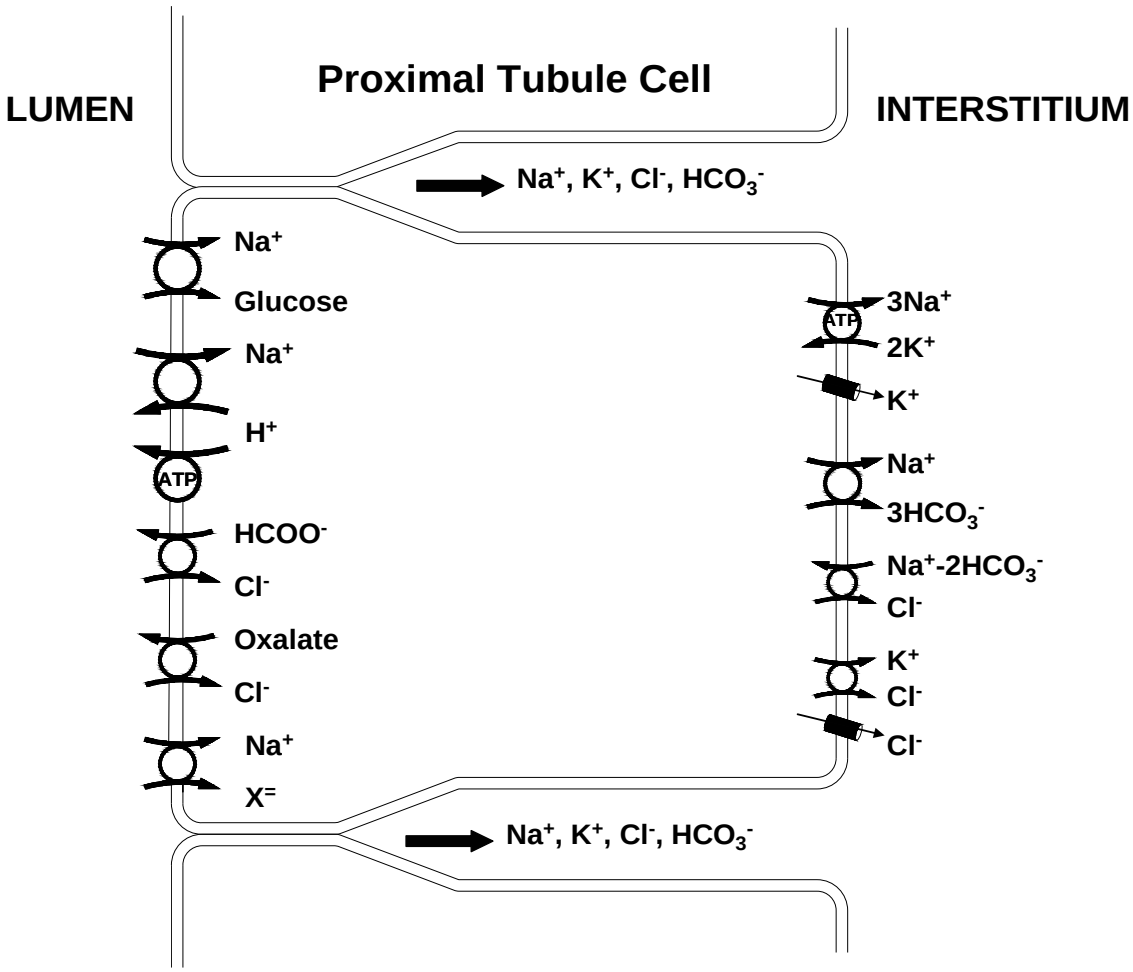

Figure 1−8 Major transporters in renal proximal tubule cells.

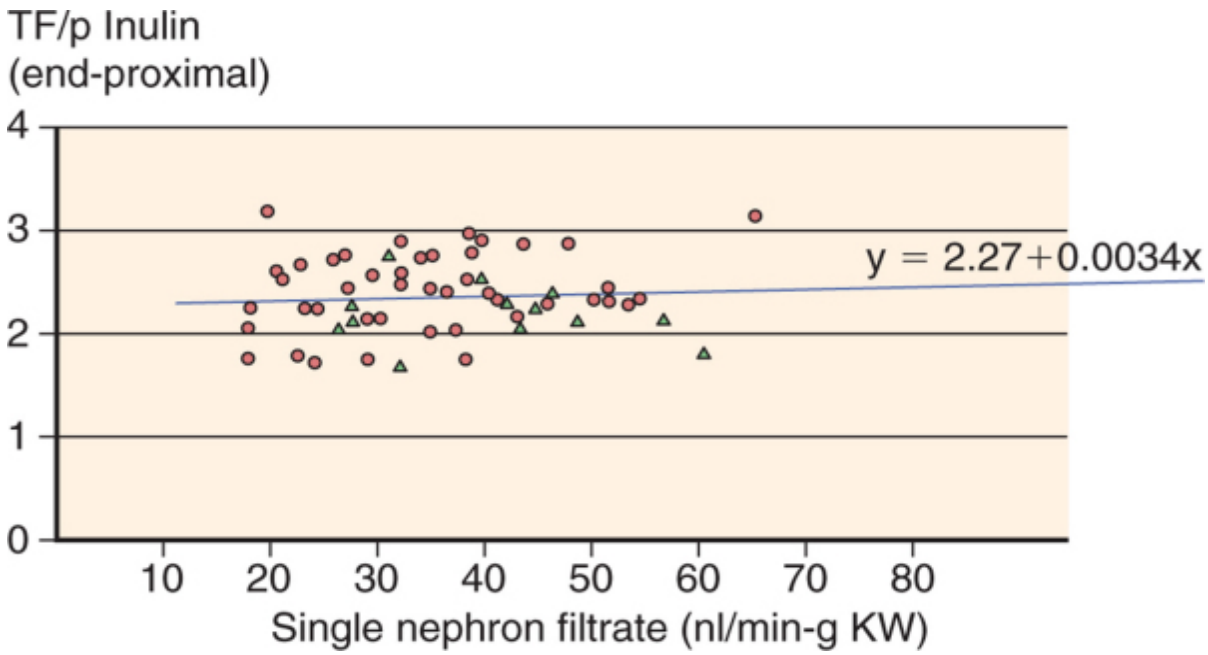

Figure 1−9 Glomerular tubular balance.

Fractional water absorption by the proximal tubule does not change as a function of single nephron glomerular filtration rate (76).

Chapter 2 Brush Border Microvilli-the Mechanosensor for Proximal Tubule Cells

2.1 Introduction

Glomerulotubular balance was first established in rat kidney via micropuncture (76), where variation in glomerular filtration was accompanied by a constant fractional reabsorption of NaCl, $NaHCO_3$ and water. The mechanisms for glomerulotubular balance include both peritubular capillary effects and luminal factors (30, 37, 92). Perhaps the most important luminal factor is a direct effect of axial flow velocity on reabsorption (72), i.e. perfusion-absorption balance (95). Renal clearance and micropuncture studies *in vivo* have demonstrated that an enhancement in luminal flow rate (glomerular tubular filtration) increased Na^+, HCO_3^- and water absorption in the proximal tubule in rat and dog. At the molecular level as shown in Figure 1-8, the primary pathway for proximal Na^+ transport is into the cell through the Na^+-H^+ exchanger isoform 3 (NHE3) within the luminal cell membrane and out across the peritubular cell membrane via the Na^+, K^+-ATPase. The reabsorption of filtered HCO_3^-, on the other hand, depends on the secretion of H^+ ions across the brush border membrane, which involves both NHE3 and an apical ion pump, H^+-ATPase (11, 32, 100).

The mechanism by which a perturbation of luminal fluid flow could be translated into a change in reabsorptive flux has been elusive. Early attention focused on the

microanatomy of the luminal membrane, which is configured as a regular hexagonal array of densely packed microvilli of uniform height (the "brush border," which has been identified by light microscopy) (58). At one time, the proximal-tubule brush border was considered to be a possible unstirred layer; however, calculations indicated that there was unlikely to be significant convective stirring within this pile (4). Moreover, the diffusion barrier between the bulk luminal fluid and the cell membrane was unlikely to hinder Na^+/H^+ exchange (45). Two studies suggested that increases in axial-flow velocity recruited new transporters into the luminal membrane. Preisig (71) examined recovery of cellular pH from an acute acid load *in vivo* (ammonium pulse) and found that increases in luminal flow rate enhanced NHE3 activity. Maddox *et al.* (51) subjected rats to acute changes in vascular volume to obtain hydropenic, euvolemic, and volume-expanded groups, with respective grouping according to decreased, normal, and increased glomerular-filtration rate. When brush-border membrane vesicles were prepared from each of these groups and Na^+-H^+ kinetics were assessed, it was found that the maximum flux velocities stratified in parallel with the glomerular-filtration rate.

Ultimately, perfusion-absorption balance must derive from an afferent sensor of fluid flow rate in series with a cascade of effector steps, which activate luminal transporters or insert new transporters into the plasma membrane. Model calculations led Guo *et al.* (35) to propose that the proximal tubule microvilli are such sensors. In this role, their regularity in height and spacing appeared to be advantageous because the bending deformation of the microvilli would be both small and uniform. In this model, it was

proposed that the critical component was the actin cytoskeleton, which is abundant within and beneath the brush border (58). The model given in Guo *et al.* (35) described how the actin-filament bundle that is the central core of the microvillus deforms under hydrodynamic loading. The proposed role for the microvilli is that they cannot only sense fluid drag forces, but they can also amplify these forces through their mechanical lever arm as they are transferred to the intracellular cytoskeleton at the terminal web, where the actin-filament bundle within the microvillus attaches at its roots to the main cell body. To serve the hypothesized function, the microvilli should be relatively stiff structures that are able to transmit the torque (bending moment), without significant bending, because of the hydrodynamic drag acting on the their tips (90). In this scheme of signal transduction, specific interaction between the proximal-tubule cytoskeleton and the luminal membrane transporters is a critical feature. In this regard, at least one such connecting molecule has been identified, namely, ezrin, which is a kinase-anchoring protein that links NHE3 and the actin cytoskeleton (48). With respect to vacuolar H^+-ATPase, there exists not only indirect interaction between the pump and the actin cytoskeleton provided via NHE3 regulating factor (NHERF) binding, but also direct binding between V1 complex of the pump and actin (32, 85).

The aim of this Chapter is to provide evidence that establishes the mechanosensory function of proximal tubule microvilli. We pursue the investigation of flow-dependent Na^+ and HCO_3^- absorption by dissecting and perfusing mouse proximal tubule *in vitro* to eliminate confounding neurohumoral factors as well as changes within the peritubular

environment (experimental data provided by Dr. T. Wang, Yale University). When the perfusion rate of the tubule is varied, there are changes in both luminal fluid velocity and tubule diameter, and both velocity and diameter are incorporated into a mathematical model for calculating the drag and torque on the microvilli. Here, we show that variations in microvillous torque are linearly proportional to changes in volume reabsorption as well as HCO_3^- absorption, key evidence in support of the mechanosensory hypothesis. Disruption of the actin cytoskeleton significantly abolished both flow-dependent Na^+ and HCO_3^- absorption, indicating that an intact cytoskeleton is required.

2.2 Material and Methods

2.2.1 Reagents

Dextran-80, EIPA, bafilomycin, and cytochalasin D were purchased from Sigma (St. Louis, MO).

2.2.2 Methods

Animals

Black C57/6J mice, which were purchased from The Jackson Laboratory, were used for studying flow-dependent proximal-tubule transport. Breeding pairs of NHE3 knockout mice were obtained from Gary Shull's laboratory (University of Cincinnati) (88). Homozygous wild-type ($NHE^{+/+}$) and null ($NHE3^{-/-}$) mice were obtained by breeding heterozygotes. Ages of null ($NHE3^{-/-}$) animals were matched with their wild-type

controls. Control and experimental groups were studied under identical experimental conditions. The experiments were conducted under animal protocol 2004–10522 approved by the Institutional Animal Care and Use Committee.

Isolation of Single Tubules

All animals were maintained on a normal diet and tap-water until the day of the experiment. The mice were anesthetized by i.p. injection of 50 mg of pentobarbital per kg of body weight. Kidneys were then removed and cut in coronal slices. Individual tubules were dissected in cooled (4°C) Hanks' solution containing 137 mM NaCl, 5 mM KCl, 0.8 mM $MgSO_4$, 0.33 mM Na_2HPO_4, 1 mM $MgCl_2$, 10 mM Tris·(hydroxymethyl)amino-methane hydrochloride, 0.25 mM $CaCl_2$, 2 mM glutamine, and 2 mM L-lactic acid. Proximal tubules (S_2) were perfused with an ultrafiltrate-like solution at perfusion rates of 5, 10, 15, 20, and 25 nl/min. The perfusion rates were adjusted by changing the gravity of the reservoir connected to the perfusion pipette and were measured by using constant-bore glass capillary tubes. The solution for luminal perfusion contained 125 mM NaCl, 22 mM $NaHCO_3$, 1 mM $CaCl_2$, 1.2 mM $MgSO_4$, 2 mM glutamine, 2 mM lactic acid, 10.5 mM glucose, 5 mM KCl, and 1.2 mM phosphoric acid. The bath medium contained 101 mM NaCl, 22 mM $NaHCO_3$, 1 mM $CaCl_2$, 1.2 mM $MgSO_4$, 2 mM glutamine, 2 mM lactic acid, 10.5 mM glucose, 5 mM KCl, 1.2 mM phosphoric acid, 32.5 mM Hepes, and 5 g/dl albumin. All solutions were bubbled with 95% O_2/5% CO_2 and had a pH of 7.4. The osmolalities of the bath and perfusate were adjusted to 300 mosmol of KgH_2O by the addition of either H_2O or NaCl. The extensively dialyzed (methoxy-^{3}H)inulin was added

to the perfusate at a concentration of 30 μCi/ml (1 Ci = 37 GBq) as a volume marker. Proximal tubules (S_2) that were isolated from mouse kidney were perfused at 37-38°C in a 1.2-ml temperature-controlled chamber. Bath fluid was changed continuously at a rate of 0.5 ml/min to maintain the constancy of pH and bath osmolality during the experiment (18). The first period of collection began after an equilibration time of 30-60 min. For each experimental period, three timed collections of tubular fluid were made.

Measurement of Jv

The volume of the perfusate and collected samples were measured in a fixed-volume collection pipette, and ^{3}H-inulin concentrations in those samples were determined in an LS5801 liquid scintillation counter (Beckman Coulter) (9). The rate of net fluid reabsorption (J_v) was calculated according to the ^{3}H-inulin-concentration changes between the original and collected fluid according to the following equation: $J_v = V_o - V_L$, where V_L is the measured rate of fluid collection, $V_o = V_L$ (IN_L/IN_o), and IN_L/IN_o is the ratio of radioactive inulin in collected and perfusion fluid, respectively. The rates of fluid absorption were expressed per millimeter of the proximal tubule.

Measurement of J_{HCO3}

The HCO_3^- concentration in the perfusate and collected tubular fluid was measured using the microcalorimetric method (Picapnotherm) as described previously (64). Samples were stored under oil, and the volumes obtained in 15-nl aliquots were compared with $NaHCO_3$ standards. The rate of HCO_3^- absorption (J_{HCO3}) was calculated according to the

HCO_3^- concentration changes between the original and collected fluid. J_{HCO3} is expressed per minute per millimeter of proximal tubule.

Measurement of Tubular Inner Diameters

Tubular inner diameters were measured from the center of the tubule under the different perfusion rates and recorded by using a charge-coupled device (CCD) video camera. Three measurements were made from each flow rate, and the means of those volumes were calculated.

Statistics

Control and experimental groups were studied under identical experimental conditions. Data are presented as means ± SE. Student's *t* test was used to compare control and experimental groups. The difference between the mean values of an experimental group and a control group was considered significant at $P < 0.05$.

2.3 Mathematical Model

The elastohydrodynamic model given by Guo *et al.* (35) quantitatively predicts the forces and torques acting on each microvillus and the bending deformation that results from this hydrodynamic loading. Nevertheless, this model does not allow us to determine easily how the drag and torque on the microvilli change with flow and diameter because it requires the detailed flow around each microvillus as their spacing changes in response to

tubule diameter changes. To analyze our experimental results, we present a simpler global model in which the detailed geometry of the microvilli and their spacing is not needed. This global model is independent of the detailed velocity profiles derived in Guo *et al.*, except that it utilizes the following two important conceptual simplifications. (*i*) The flow at the edge of the brush border is confined to a thin-tip-interaction layer of thickness δ<150 nm, where the velocity decays rapidly from its value at the brush-border edge to its value in the interior, and (*ii*) the velocity within the main body of the brush border, which occupies ≈95% of the brush border thickness, L, is nearly uniform and driven by the local axial-pressure gradient in the tubule and not the fluid shear stress in the tubule lumen. Guo *et al.* show that the slip velocity at the brush-border edge is only ≈ 1/400 of the tubule center-line velocity, and the uniform flow in the main body of the brush border is again 1/400 of this edge velocity, making it a nearly stagnant flow that is five orders of magnitude smaller than the velocity in the lumen. These vastly different velocity scales enable us to separate the drag and torque on each microvillus into the following two components: a uniform drag, D_{body}, acting over the main body L - δ of the microvillus, and a tip drag, D_{tip}, acting in the thin interaction layer of thickness δ. The corresponding components for the torque are T_{body} and T_{tip}. Furthermore, the shear stress acting at both the base of the tip-interaction layer and the base of the microvilli are negligible because the flow within the body of the brush border is negligible.

By using the above simplifications, one can define two distinct control volumes in Figure 2-1 and apply a local force balance per unit of tubule length. For the first control volume,

we consider a unit length of the entire interior of the proximal tubule (tubule lumen plus brush border). A force balance requires that the drag force $D_{tot}N$, where D_{tot} is the drag on the entire microvillus and N is the number of microvilli per unit of tubule length, be balanced by the force due to the pressure gradient dP/dz per unit of length acting over the entire interior cross-section whose radius is $R + L$, where R is the radius of the tubule lumen without the brush border.

$$\frac{dP}{dz} \cdot \pi \cdot (R+L)^2 = D_{tot} \cdot N \tag{2-1}$$

Note that in Eq. 2-1, the shear force on the apical membrane of the epithelial cell vanishes because the wall shear stress is negligible.

To determine the drag due to only the microvilli tips, D_{tip}, we consider a second cylindrical control volume whose radius is $R + \delta$. A similar force balance to that used in writing Eq. 2-1. requires that:

$$\frac{dP}{dz} \cdot \pi \cdot (R+\delta)^2 = D_{tip} \cdot N. \tag{2-2}$$

As noted previously, the shear force at the cylindrical side wall of this second control volume also vanishes because it is at the base of the tip-interaction layer, where the fluid shear is negligible. The drag force that acts only on the body of the microvillus, D_{body}, is the difference between the drag in Eqs. 2-1 and 2-2.

$$D_{body} = D_{tot} - D_{tip} = \frac{\pi}{N} \cdot \frac{dP}{dz} \cdot \left[(R+L)^2 - (R+\delta)^2 \right] \tag{2-3}$$

The total torque on each microvillus, T_{tot}, is the sum of the tip T_{tip} and body T_{body} torques. The detailed solutions in Guo *et al.* (2000) show that of the total drag on a 2.5-μm microvillus, 74% appears within 150 nm of the brush-border edge and is due to the fluid shear stress in the tip-interaction layer, whereas the remainder is due to the viscous loss in the interior of the brush border. Because $\delta << L$ or R, the lever arm for the drag force on the tip is approximately the total length L of the microvilli. However, because the drag force on the main body of the microvillus acts uniformly along its length because the flow in the interior is uniform, this drag acts as if it were applied approximately at the center of the microvillus. Thus,

$$T_{tot} = T_{tip} + T_{body} = D_{tip} \cdot L + D_{body} \cdot \frac{L}{2}. \tag{2-4}$$

By substituting Eqs. 2-2 and 2-3 into Eq. 2-4, one obtains,

$$T_{tot} = \frac{\pi}{N} \frac{dP}{dz} \cdot L[R^2 + R(L+\delta) + \frac{L^2}{2}], \tag{2-5}$$

where terms of order δ^2 have been neglected.

Because the axial water flow in the brush border contributes very little to total flux, the total local perfusion rate Q, which satisfies Poiseuille's law, is given by the flux in the lumen,

$$Q = \frac{\pi R^4}{8\mu} \cdot \frac{dP}{dz} \ , \tag{2-6}$$

where μ is the viscosity of the fluid. The local axial-pressure gradient, *dP/dz*, can now be written in terms of *Q* by using Eq. 6, and this result can be substituted into Eq. 2-5, yielding the following:

$$T_{tot} = \frac{1}{N} \cdot \frac{8\mu}{R^4} \cdot Q \cdot L \left[R^2 + R(L+\delta) + \frac{L^2}{2} \right]. \tag{2-7}$$

Eq. 2-7 is an expression for the total torque on the microvillus in terms of *Q*, *R*, μ, and microvillus geometry *N* and *L*.

It is difficult to evaluate Eq. 2-7 in absolute terms unless *N* is measured experimentally by using electron microscopy. However, in our perfusion experiments, the length of the tubule segment is fixed, and therefore, *N* does not change as the tubule diameter increases with flow. Only the spacing of the microvilli along the tubule cross-section changes. Thus, one can take the ratio of the torques on the microvillus at any two perfusion rates, and *N* will cancel out. If we take *r* as a convenient reference state, we obtain the ratio of the total torque at any perfusion rate and diameter relative to the reference state *r* as follows:

$$\frac{T}{T_r} = \frac{R_r^{\,2}}{R^2} \left(\frac{1 + \dfrac{L+\delta}{R} + \dfrac{L^2}{2R^2}}{1 + \dfrac{L+\delta}{R_r} + \dfrac{L^2}{2R_r^{\,2}}} \right) \left(\frac{\mu}{\mu_r} \right) \frac{Q}{Q_r} \tag{2-8}$$

Eq. 2-8 is the critical relationship that enables us to relate reabsorption J_v and J_{HCO3} to torque and compare theory and experiment. There are two subtle points in the derivation of Eq. 2-8. Because of the reabsorption, there is a radial pressure gradient in the brush border, but it can be shown that *dP/dz* will be nearly constant across the brush border if reabsorption per unit of length is uniform or slowly varying. We also assume that when a tubule expands at constant length, the spacing of the microvilli changes but their length *L* remains the same.

2.4 Experimental Results

2.4.1 Increasing perfusion rate enhances the fluid and HCO_3^- reabsorption.

Because the proximal tubule absorbs Na^+ isosmotically, fluid transport rates are used widely as a surrogate for Na^+ absorption. As shown in Figure 2-2A, fluid absorption (J_V) and HCO_3^- reabsorption (J_{HCO3}) was measured in isolated mouse proximal tubules at perfusion rates of 5, 10, 15, 20, and 25 nl/min, respectively. Our results (Figure 2-2B) show that J_v increased significantly from 0.79 ± 0.05, to 1.05 ± 0.07, 1.24 ± 0.10, 1.60 ± 0.19, and 1.58 ± 0.21 $nl \cdot min^{-1} \cdot mm^{-1}$ when the perfusion rate increased from 5 nl/min to 10, 15, 20, and 25 nl/min. Similarly, Figure 2-2C displays the rate of HCO_3^- absorption in response to the changing perfusion rate. HCO_3^- absorption rates are also proportionally increased with increased perfusion rates ($R^2 = 0.99$). The overall J_{HCO3} was doubled when the perfusion rate went from 5 to 25 nl/min. This is the first demonstration that Na^+ and HCO_3^- absorption is regulated by axial flow velocity in mouse proximal tubules in vitro.

It is important to note that a five-fold increase in flow rate produces only a two-fold increase in both J_v and J_{HCO3}.

2.4.2 Increasing perfusion rate increases tubule diameter.

Our previous fluid shear-stress model (35) for predicting microvillous torque suggested that the nonlinearity in the J_v and J_{HCO3} vs. perfusion curves in Figure2-2B and C might be due in part to flow-dependent changes in tubule diameter. A change in tubule diameter would not only affect the magnitude of the fluid shear stress acting on the microvilli tips, but it would also cause ultrastructural changes in the microvilli distribution within the brush border, as observed by Maunsbach *et al.* (59). We have examined the effect of increasing flow on tubule inner diameter (Figure 2-3). The proximal tubules were perfused *in vitro* at perfusion rates of 5, 10, 15, 20, and 25 nl/min. A 50% increase is observed in inner diameter between the low and high perfusion rate, and the response is nonlinear. Because the shear stress ($\tau = 32\frac{\mu}{\pi}\frac{Q}{D^3}$) at the brush-border edge is inversely proportional to the diameter cubed (for a given axial flow) in Poiseuille flow, these large changes in diameter can have a profound effect on the fluid shear stress acting on the microvilli tips and, hence, the torque that they experience. This cubic dependence implies that increases in luminal diameter will blunt the flow-dependent increase in microvillous torque. It is possible that such diameter changes may have played a role in the inability of previous investigators to discern flow-dependent transport *in vitro*.

2.4.3 Comparison between mathematical prediction and experimental results.

We next assessed the correlation of microvillus torque with fluid and HCO_3^- absorption. By using Eq. 2-8, the change in torque T at any perfusion rate Q to any reference perfusion rate Q_r can be related as long as the relative change in the tubule diameter $2R$ for that measured Q is also known. In this calculation, we assume that L = 2.5 μm, δ = 150 nm, and $\mu = \mu_r$ because the viscosity is unchanged. Furthermore, because Figure 2-2 provide the measured relationship between J_v/J_{HCO3} and Q, Eq. 2-8 or Figure 2-3A and B can be used to plot the relationship between J_v and T as well as J_{HCO3} and T. Figure 2-4 B and D shows the relationship between changes in torque and changes in J_v and J_{HCO3}, respectively. In both panels, the reference values used for torque, T_r, and $(J_v)_r$ or $(J_{HCO3})_r$ were both measured at the perfusion rate of 5 nl/min. This observed relationship between both J_v and T and J_{HCO3} and T is almost perfectly linear, suggesting that the flow-dependent changes of transport activity are modulated directly by the changes in microvillous torque.

It is striking that the changes in tubule diameter in response to Q provide a linear relationship between T and Q (microvilli function as a linear transducer) when the relationships between Q and R and between T and R are both nonlinear. Note that there are two competing nonlinear effects. As Q increases, it causes R to increase, which decreases the torque T because the fluid shear acting on the microvilli tips decreases as the tubule diameter expands. This decrease in torque, deriving from tubule distention,

offsets the increase in *T* that results from the increase in *Q*. Note that the increase in *T* is less than a factor of two over a 5-fold increase in *Q*, as shown in Figure 2-4 and *C*.

2.4.4 Effect of cytochalasin D in modulating flow-dependent Na^+ and HCO_3^- reabsorption.

These changes in microvillous torque in response to axial flow need to be transmitted to the terminal web, where the actin-filament bundle within the microvillus attaches at its roots to the main cell body. We hypothesize that this force on the cytoskeleton leads to an alteration of transport activity by modulation of membrane transporter NHE3 and H^+-ATPase. To examine this hypothesis, the effects of cytochalasin D, an actin cytoskeleton inhibitor (25), on flow-dependent proximal-tubule transport was studied. As shown in Figure 2-5A, addition of 3 μM cytochalasin D did not change the baseline J_v at low flow rate, but it abolished the flow-stimulated increase in J_v (1.56 vs. 0.76 in control and 0.94 vs. 0.81 $nl \cdot min^{-1} \cdot mm^{-1}$ in the cytochalasin group at perfusion rates of 20 and 5 nl/min, respectively). Similar effect also was witnessed when we examined HCO_3^- absorption in the absence and presence of 3 μM cytochalasin D in the luminal perfusate, shown in Figure 2-5B. These results indicated that 3 μM cytochalasin D has no toxicity to cells but inhibits actin cytoskeletal signaling, which is critical to the flow-stimulated Na^+ and HCO_3^- transport in the proximal tubule. In contrast, cytochalasin D abolished the increment of transport activity due to enhanced flow, consistent with our hypothesis that the transduction of signals from brush border to terminal web via the actin cytoskeleton is

essential for the modulation of Na^+ and HCO_3^- transport mechanisms regulated by axial flow in proximal tubules.

2.4.5 Role of NHE3 and H^+-ATPase in modulation of flow-dependent Na^+ and HCO_3^- reabsorption

Because NHE3 is the major ion transporter that is responsible for absorption of 50-60% of the filtered Na^+ and HCO_3^- in the proximal tubule (87, 88), we examined flow-dependent Na^+ and HCO_3^- absorption in NHE3 knockout mice. Figure 2-6 shows a summary of the data from the NHE3 knockout mice. In addition to the significant reduction of baseline J_v at low flow rate, as reported (77, 88), the increments in flow-stimulated Na^+ and HCO_3^- absorption were reduced 57 (0.34 vs. 0.80 nl·min^{-1}·mm^{-1}) and 35% (45.1 vs. 69.2 pmol·min^{-1}·mm^{-1}), respectively, in NHE3-null mice compared with wild-type (Tables 2-3; Figure 2-6). The slope of the flow-dependent change in J_v is significantly different between the NHE3 null mice and control (0.023 ± 0.008 vs. 0.056 ± 0.017, $P < 0.05$). In addition, the absolute changes and the percentage changes from lower and higher flow rates were also diminished significantly in NHE3 null mice. These results suggested that NHE3 activity can be stimulated by increasing axial flow. Although 44% of the flow stimulated increase in J_v is still retained because of increased axial flow, this increment of J_v must be mediated by NHE3-independent Na^+ transport mechanisms, such as Na^+/glucose-cotransport, and/or a para-cellular Na^+ transport pathway.

The mechanism of this stimulation of J_{HCO3} by flow in the NHE3-null mouse is likely due to altering H^+-ATPase activity when flow rate is increased. To test this hypothesis, we perfused tubules from wild-type mice and examined the effects of EIPA, bafilomycin, and EIPA plus bafilomycin on flow-dependent HCO_3^- transport. Data are summarized in Tables 2-4 and Figure 2-7, J_{HCO3} increased 69.2 pmol·min^{-1}·mm^{-1} (from 68.8 to 137.9 pmol·min^{-1}·mm^{-1}) when flow rate increased from 4 to 20 nl/min under control conditions. Using similar perfusion rates, EIPA inhibited 40% (ΔJ_{HCO3} = 41.7, $P > 0.05$), and bafilomycin inhibited 43% (ΔJ_{HCO3} = 39.2, $P < 0.05$) of the flow-stimulated J_{HCO3} increase. The increment of J_{HCO3} due to enhanced flow rate was reduced by 97% (ΔJ_{HCO3} = 1.99, $P < 0.0001$) when both EIPA and bafilomycin were added to the luminal perfusate, indicating that both NHE3 and H-ATPase activity are regulated by tubular flow.

2.5 Discussion

The primary hypothesis of this study is that flow-dependence of kidney proximal tubule Na^+ and HCO_3^- reabsorption is signaled by the hydrodynamic torque on epithelial microvilli. The experimental model has been the isolated perfused proximal tubule of the mouse, and our results are the first demonstration of flow-dependence in the *in vitro* setting. A long standing controversy exists due to contradictory observations between *in vivo* and *in vitro* studies on glomerular tubular balance. Previously, Burg and Orloff (76) had observed that in rabbit proximal tubule a 3-fold increase in perfusion rate produced a 37% increase in volume reabsorption, which was not statistically significant (Table 2-6

and Figure 2-8A). As a result these investigators concluded that glomerular tubular balance was “not an intrinsic property of the proximal tubule”. However, with reference to Eq. 2-7, we notice that the total torque on the microvilli varies directly with luminal perfusion and inversely with luminal diameter. This functional relationship implies that when perfusion rate is increased, relatively small amounts of tubular distention will suffice to nullify any increase in torque. We reconsidered the data from Burg and Orloff (9) as shown in Figure 2-8 (86). As the perfusion rate increased from 6 to 18 nl/min, tubular diameter and *Jv* increased by 41% and 37%, respectively, in rabbit proximal tubule compared to 30% and 60% in mouse proximal tubule. Application of Eq. 2-8 predicts an increase of torque by 38% in rabbit and 61% in mouse and, thus, a comparable change in fluid reabsorption. It appears that rabbit proximal tubules were more distensible than mouse tubules, so that perfusion-dependent changes in luminal diameter precluded large deviations in microvillous torque.

Increasing luminal flow in the proximal tubule in rats has been found to enhance the luminal-membrane density of NHE3, a finding in brush-border membrane vesicles (51) and also in direct examination of pH recovery by the intact cell (71). Consistent with these observations, we found that perfusion-absorption balance is reduced significantly in NHE3-deficient mice. What this study adds to existing knowledge is the finding that nontoxic doses of cytochalasin abolish the flow-dependent increase in Na^+ reabsorption. This finding supports the model assumption that the actin cytoskeleton is a key mediator for transduction of the hydrodynamic force on microvilli to the change in NHE3 density

within the luminal cell membrane. The range of membrane proteins that respond to this hydrodyamic force and biochemical signals that affect this traffic remain as important objectives for future investigation.

With respect to the components of HCO_3^- reabsorption, it was found that total HCO_3^- flux was inhibited by about one-third with luminal EIPA, and the effect of bafilomycin was similar. Together, the two inhibitors abolished ~80% of HCO_3^- reabsorption, suggesting some compensatory HCO_3^- flux when only a single inhibitor was used. The potency of each inhibitor is comparable to prior observations from in vivo microperfusion in the mouse (88). What is new here is that both components of proximal proton secretion appear to be flow dependent, and there seems to be little difference in the relative magnitude of the flow effect on each transporter. Although the absolute value of HCO_3^- reabsorption is reduced in NHE3-null mice, the relative effect of flow on this flux is identical to that in control tubules.

The present study is incomplete in a variety of aspects: the spectrum of luminal transporters that are modulated by flow remains to be identified; beyond the implication of the actin cytoskeleton, the cellular mediators of the flow effect are unknown; the luminal transporters that are modulated by peritubular protein remain to be identified; and the cellular mediators of the peritubular effect are also unknown. If this observation is robust, it will need to be understood in relation to the convergence of luminal and peritubular signaling systems. Finally, as the signal strength of luminal and peritubular

effects is better defined, it will be important to examine both effects in a model nephrovascular unit to see how their superimposition yields glomerulotubular balance.

Table 2-1 Effects of luminal flow rate on fluid and bicarbonate reabsorption in proximal tubules

n	V_0, nl/min	L, mm	Jv, nl/min/mm	J_{HCO3}, pmol/min/mm	ID, μm	T/Tr
18	5.03±0.30	0.86±0.03	0.77±0.05	61.1±4.9	12.9±0.5	1.00±0.08
12	10.34±0.44	0.82±0.05	0.99±0.08	88.4±5.8	15.3±0.6	1.41±0.14
12	15.25±0.34	0.79±0.03	1.19±0.08	102.8±7.2	17.3±0.7	1.56±0.13
12	20.31±0.54	0.84±0.04	1.33±0.10	118.9±7.3	18.3±0.6	1.78±0.14
7	25.80±0.61	0.79±0.09	1.41±0.06	140.3±9.5	18.9±0.8	2.10±0.20

Values are means ± SE. n, No. of perfused tubules; L, tubular length; V_0, perfusion rate; ID, inner tubular diameter; T, total torque; T_r, torque measured at the perfusion rate of 5 nl/min (5 g/dl of albumin were used in this study) (19).

Table 2-2 Effects of cytochalasin on fluid absorption in proximal tubule of mouse kidney

	N	V_0, *nl/min*	*L, mm*	J_v, *nl/min/mm*	J_{HCO3}, *pmol/min/mm*
Control	11	4.84 ± 0.19	0.64 ± 0.04	0.76 ± 0.09	68.8±5.5
Cytochalasin	10	4.91 ± 0.39	0.86 ± 0.03	0.81 ± 0.04	51.5±6.4
Control	12	19.77 ± 0.83	0.73 ± 0.02	1.56 ± 0.16*†	137.9±4.3
Cytochalasin	9	19.52 ± 1.40	0.87 ± 0.03	0.94 ± 0.10†	74.2±6.6†

N, number of perfused tubules; V_0, perfusion rates; L, length of the perfused tubule; J_V, fluid absorption, J_{HCO3}, HCO_3^- reabsorption. Cytochalasin was added to the luminal perfusate at a concentration of 3 μM [19].

*Significant difference from low perfusion rate ($P < 0.05$).

†Significant difference between the control and cytochalasin groups ($P < 0.05$).

Table 2-3 Flow-dependent proximal tubule transport in wild-type and NHE3 knockout mice

Genotype	*N*	V_0 *(nl/min)*	*L (mm)*	J_v, *nl/min/mm*	J_{HCO3}, *pmol/min/mm*
NHE3+/+	7	3.84 ± 0.17	0.69 ± 0.04	0.75 ± 0.04	68.8±5.5
NHE3-/-	7	3.73 ± 0.38	0.64 ± 0.06	0.47 ± 0.07+	45.7±5.0†
NHE3+/+	16	17.98 ± 0.10	0.72 ± 0.02	1.55 ± 0.18*	137.9±4.3
NHE3-/-	9	16.90 ± 1.45	0.65 ± 0.04	0.82 ± 0.09*†	90.8±5.4‡

N, number of perfused tubules; V_0, perfusion rates; L, length of the perfused tubule; J_V, fluid absorption; J_{HCO3}, HCO_3^- reabsorption; NHE-$3^{+/+}$, Na/H-exchanger-3 wild-type mice; NHE-$3^{-/-}$, Na/H-exchanger3 null mice[19].

*Significant difference from low perfusion rate ($P < 0.05$).

†Significant difference between $NHE3^{+/+}$ and null mice ($P < 0.05$).

Table 2-4Effects of EIPA, bafilomycin, and cytochalasin on fluid absorption under low and high perfusion rates

	4 nl/min		20 nl/min			
	n	Jv_a, nl/min/mm	n	Jv_b, nl/min/mm	ΔJ_v	$\Delta Jv / Jv_a \cdot 100$
Control	7	0.75±0.04	12	1.55±0.18	0.80±0.18	106.67±24.00
EIPA	12	0.61±0.08	12	0.95±0.09†	0.34±0.11*	55.74±18.03
Bafilomycin	8	0.83±0.10	7	1.31±0.07	0.48±0.12	57.83±14.46
EIPA+Bafilomycin	7	0.64±0.03*	8	0.92±0.03*	0.28±0.04*	43.75±6.25*

Values are means ± SE. n, No. of perfused tubules; Jv, fluid absorption; ΔJv, the differences in Jv between perfusion rate of 4 and 20 nl/min; ΔJv/Jva·100, present changes in fluid reabsorption from control; KO, knockout. EIPA, bafilomycin, and cytochalasin were added to the luminal perfusate at concentrations of 10, 0.1, and 3 μM, respectively[19].

* Significant difference from control (*P < 0.05;†P < 0.01).

Table 2-5 Effects of EIPA, bafilomycin, and cytochalasin on bicarbonate absorption under low and high perfusion rates

	4 nl/min		20 nl/min			
	n	J_{HCO3a}, pmol/min/mm	n	J_{HCO3b}, pmol/min/mm	ΔJ_{HCO3}	$\Delta J_{HCO3} / J_{HCO3a} \cdot 100$
Control	7	68.8±5.5	12	137.9±4.3	69.2±7.0	100.5±10.2
EIPA	12	46.7±5.6*	12	88.4±10.4†	41.7±11.8	89.2±25.2
Bafilomycin	8	52.8±8.2	7	92.0±7.9‡	39.2±11.4*	74.3±21.5
EIPA+Bafilomycin	7	17.9±3.1‡	8	19.9±4.1‡	2.0±5.1‡	11.1±28.6†

Values are means ± SE. n, No. of perfused tubules; J_{HCO3}, the rate of bicarbonate absorption; ΔJ_{HCO3}, the differences of J between perfusion rate of 4 and 20 nl/min; $\Delta J_{HCO3}/J_{HCO3a}\cdot 100$, present changes in bicarbonate reabsorption from control. EIPA, bafilomycin, and cytochalasin were added to the luminal perfusate at concentrations of 10, 0.1, and 3 μM, respectively.

* Significant difference from control (*P < 0.05;†P < 0.01;‡P < 0.001).

Table 2-6 Effect of Flow Rate on Fluid Absorption by Rabbit Proximal Straight Tubules

	V_0, *nl/min*	*Jv, nl/min/mm*	*ID, µm*
Rabbit*	6.0	0.420	17.000
	18.0	0.570	24.000
Mouse†	6.0	0.856	12.413
	18.0	1.372	16.155

Means of results for four experiments are shown. The mean of the differences in absorption between control and experimental periods (pairing the results from each tubule) is 0.15±0.08, P>0.10

* Burg and Orloff (76); † Du et al. (17)

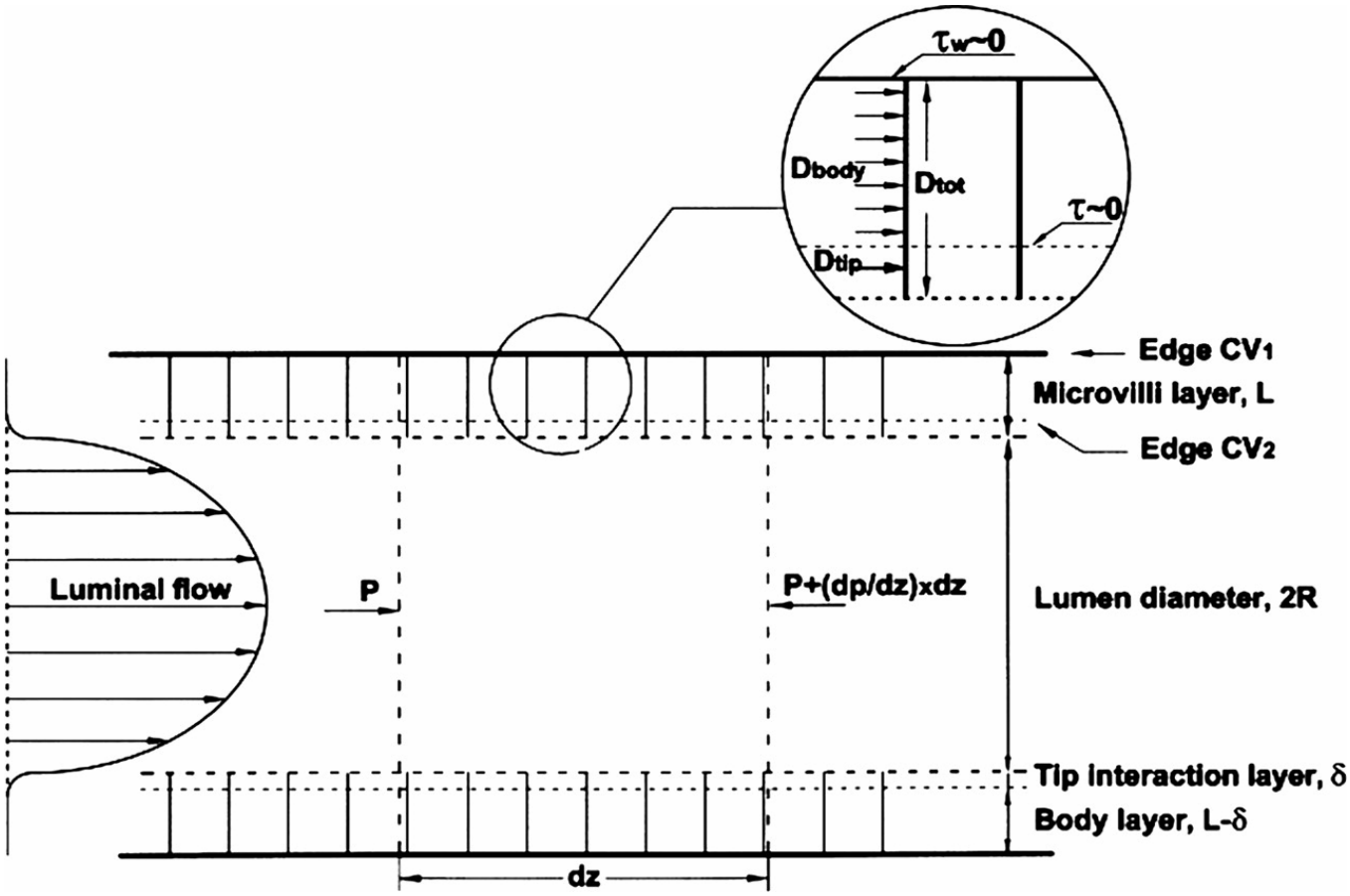

Figure 2−1 Control volumes 1 and 2 (CV1 and CV2) used to obtain the drag forces Dbody and Dtip on each microvillus.

Control volumes used in Eqs. 1 and 2 are shown. CV1 contains the entire tubule lumen including complete brush-border microvilli layer, whereas CV2 contains the tubule lumen and only the tip-interaction layer of the brush-border microvilli. The fluid shear stress at the base of CV1 and at the base of CV2 are both negligible.

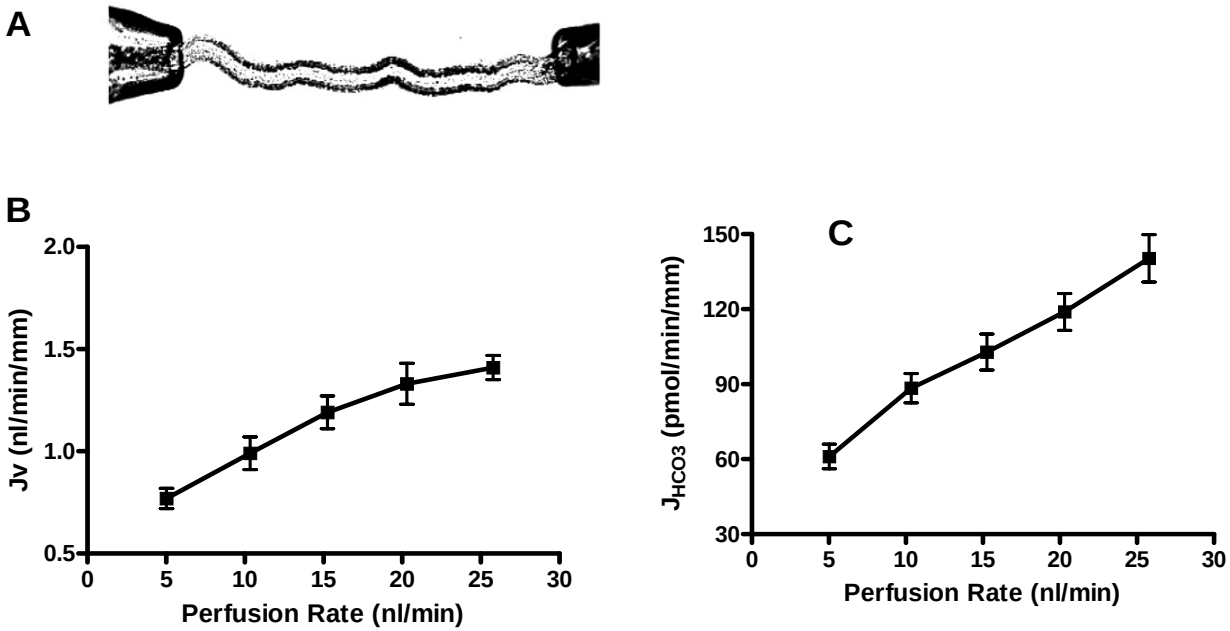

Figure 2−2 Effects of tubular flow rate on fluid (Jv) and HCO_3^- (J_{HCO3}) reabsorption in isolated proximal tubules of mouse kidney (17).

(A) Photograph taken from an experiment showing that an isolated proximal tubule held with perfusion (right) and collecting (left) pipettes under the microscopy. (B) Flow-dependent proximal-tubule transport. Jv was measured under perfusion rates of 5, 10, 15, 20, and 25 nl/min. (C) Flow-dependent proximal tubule HCO_3^- reabsorption. J_{HCO3} was measured under perfusion rates of 5, 10, 15, 20, and 25 nl/min.

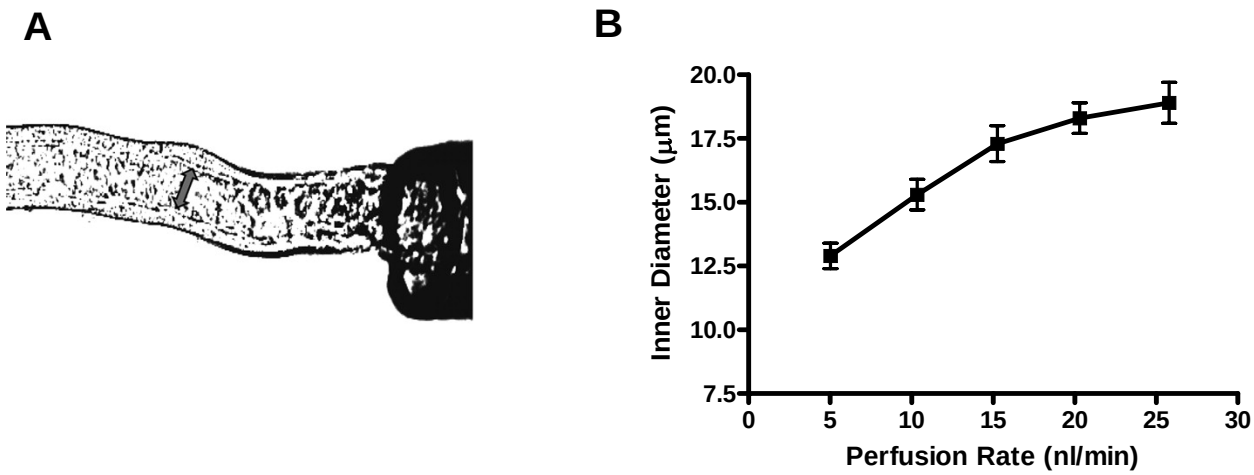

Figure 2−3 Effects of tubular flow rate on inner tubular diameters (17).

(A) Photograph taken from an experiment showing the measurement of inner diameters. (B) Changes of tubular inner diameters in response to perfusion rate. Inner diameters (ID) were measured at the perfusion rate of 5, 10, 15, 20, and 25 nl/min.

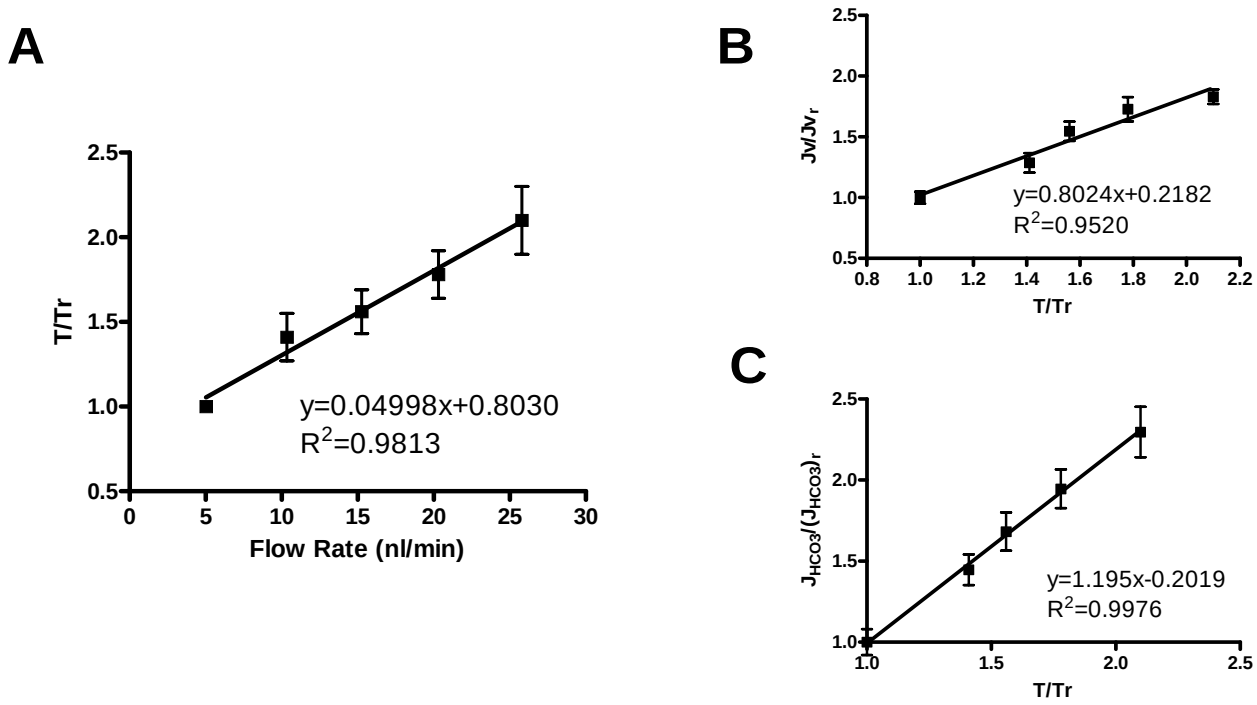

Figure 2−4 Analysis of the changes of transport activity and total torque in response to increased perfusion rates.

(A) The relationship between increasing perfusion rates and changes in torque. T, total torque of the microvilli (body and tip); Tr, reference value of the total torque at the perfusion rate of 5 nl/min; T/Tr, ratio of total torque at related perfusion rates of 10, 15, 20, and 25 nl/min to the reference value at a perfusion rate of 5 nl/min. (B) The proximal-tubule transport activity corresponding to changes of torque. The data of T/Tr and Jv/Jvr were obtained from the calculation at perfusion rates of 5, 10, 15, 20, and 25 nl/min. The relationship between the changes of torque and changes of transport activity are proportional. (C) Effect of increased flow rates on torque (T/Tr) and HCO_3^- absorption ($J_{HCO3}/J_{HCO3}r$), where r denotes the reference torque and J_{HCO3} is at the flow rate of 5 nl/min.

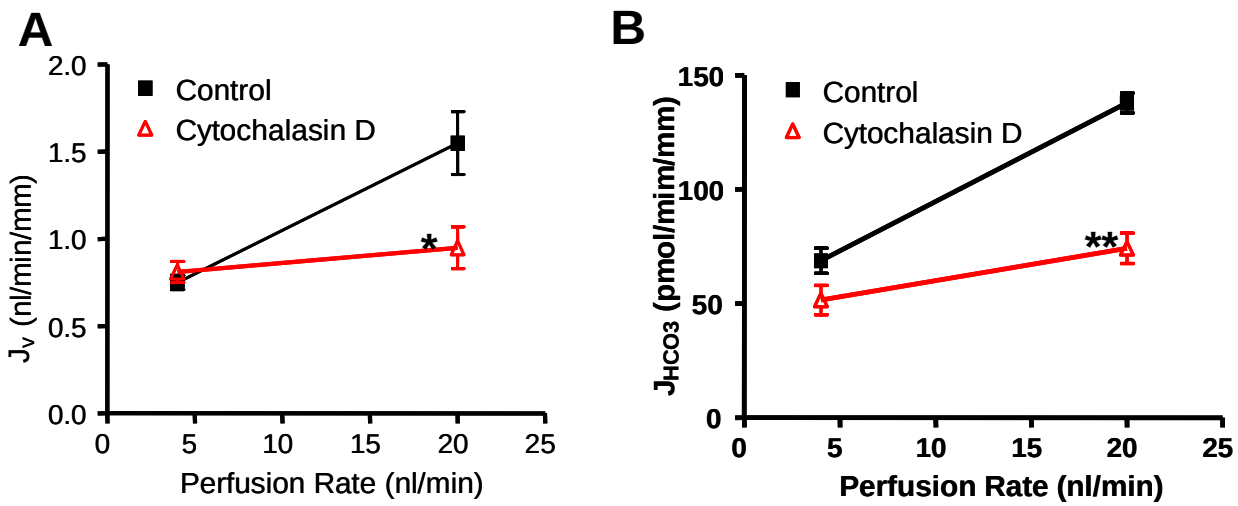

Figure 2−5 Role of cytoskeleton on flow-dependent fluid and HCO_3^- absorption.

(A) Effect of cytochalasin D on flow-dependent Jv in proximal tubules. The Jv was measured at low and high perfusion rates in the absence and presence of 3 µM cytochalasin D in the luminal perfusion solution. Cytochalasin D abolished the increment of Jv due to enhanced perfusion rate. *, $P < 0.05$, compared with controls. (B) Effect of cytochalasin D on flow-dependent J_{HCO3} in proximal tubules. J_{HCO3} were measured at low and high perfusion rates in the absence and presence of 3 µM cytochalasin D in the luminal perfusion solution.

*Significant difference from control ($P < 0.05$).

**$P < 0.01$.

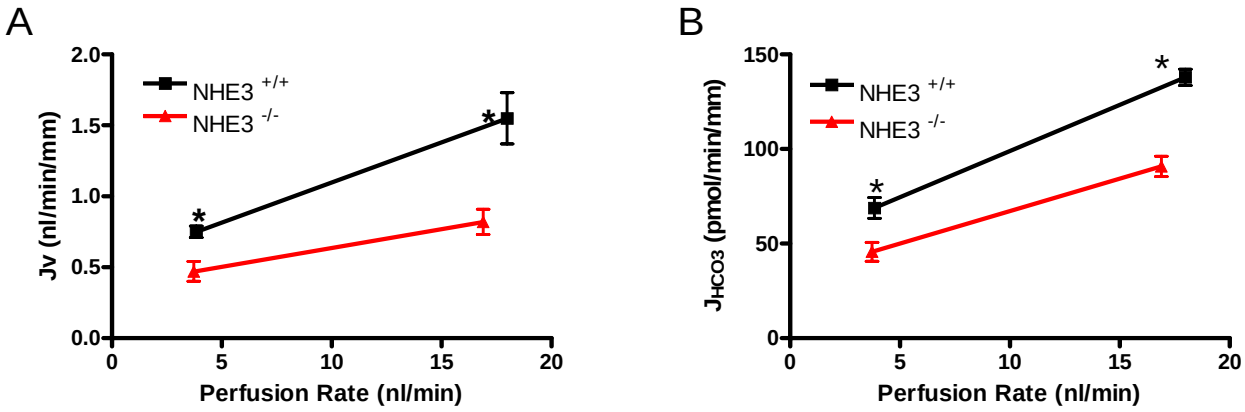

Figure 2−6 Flow-dependent fluid (A) and HCO_3^- (B) absorption in wild-type and NHE3 knockout mice.

*Significant differences between Jv and in wild type and NHE3 knockout mice at the low and high perfusion rate ($P < 0.05$).

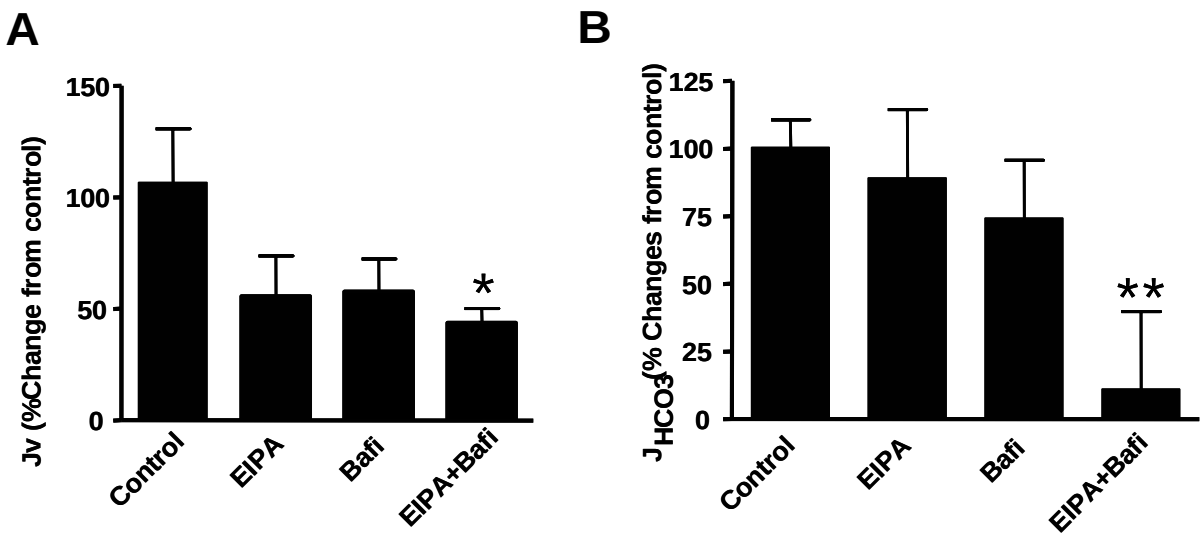

Figure 2−7 Effect of EIPA, bafilomycin on Jv and J_{HCO3} in proximal tubules.

Jv and J_{HCO3} were measured at low and high perfusion rates in the absence and presence of 10 μ M EIPA and 0.1 μ M bafilomycin, respectively, in the luminal perfusion solution.

*Significant difference from control ($P < 0.05$).

**$P < 0.01$.

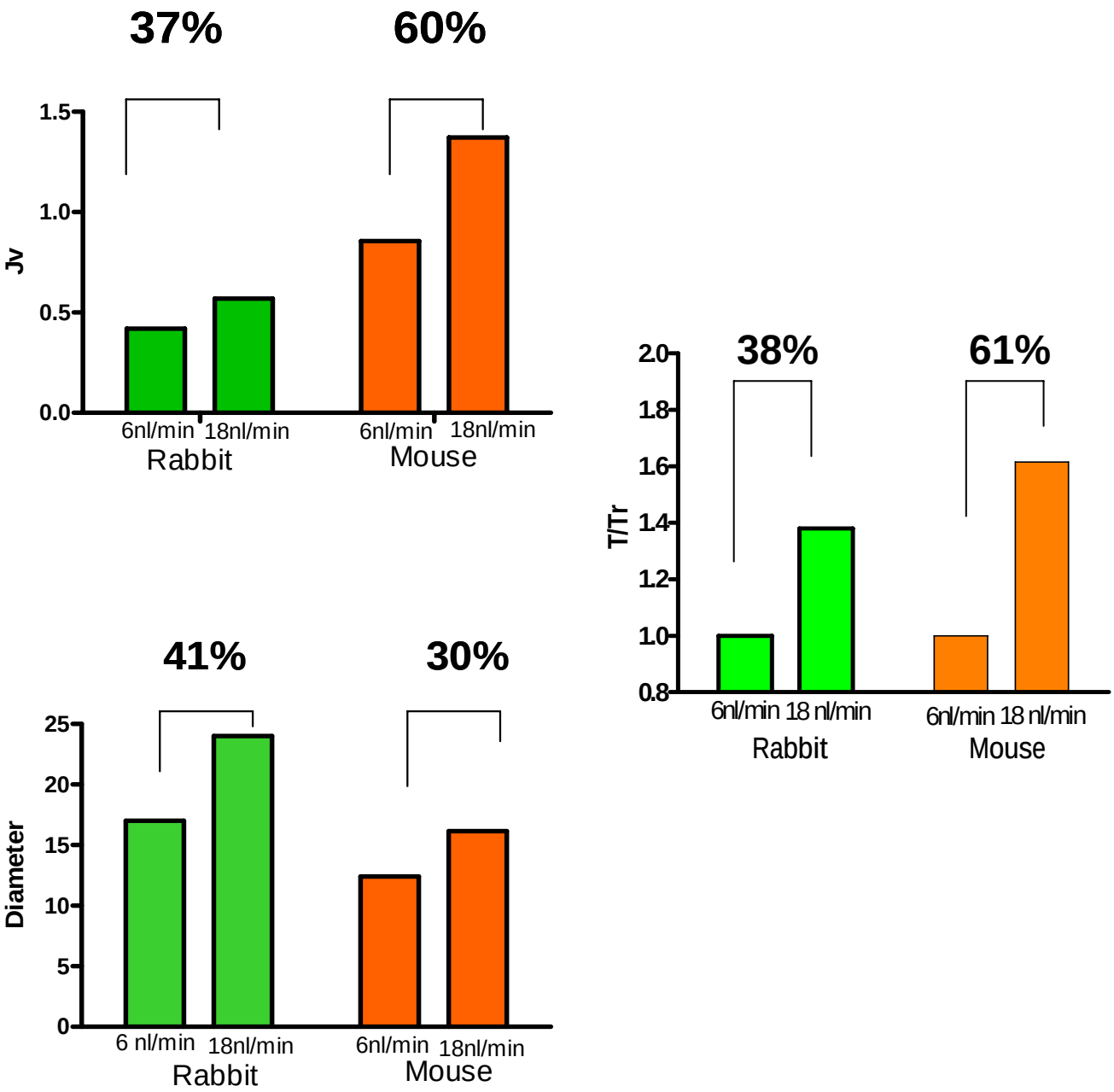

Figure 2−8 Comparison of flow-induced changes in fluid absorption (a), torque (b) and inner diameter (c) between rabbit and mouse proximal tubules.

Chapter 3 Proximal Tubule Cell Cytoskeletal Responses to Flow

3.1 Introduction

Fluid shear stress (FSS) produced by renal tubular flow modulates tubular epithelial salt and water reabsorption, as well as H^+ and K^+ secretion (19, 31, 55, 75, 76). In kidney proximal tubule, Schnermann (76) demonstrated four decades ago that there is a nearly proportional change in Na^+ and HCO_3^- reabsorption with variation in glomerular filtration rate (GFR), namely "Glomerulo-Tubular Balance". The physiological importance of this regulation is to prevent loss of solute following increases in GFR, and to preserve of adequate distal delivery of sodium and fluid when GFR is reduced. This highly-regulated intake of Na^+ and HCO_3^- is dependent upon the polarized delivery of transporter proteins, such as the Na^+/H^+ antiporter (NHE3) and H^+-ATPase to the apical membrane (51, 71). Our *in vitro* microperfusion studies have previously shown that luminal flow modulates both NHE3 (17) and H^+-ATPase (19) activities, while disruption of the actin cytoskeleton by treatment with cytochalasin D (cD) abolished this flow-dependent behavior (17), indicating that an intact actin cytoskeleton is essential for proximal tubule cells (PTCs) to transmit flow-induced mechanical forces and subsequently modulate transport.

In PTCs, the actin cytoskeleton forms unique arrangements at the apical and basal aspects of the cell that help to define the specialized structure and function of these membrane domains. The apical membrane, distinguished by a tight junction (TJ), contains a brush

border, which includes microvilli (58) and the terminal web. The microvillar actin core is connected to the terminal web, a dense layer of short actin filaments that underlies the entire apical membrane of the PTCs. The terminal web is supported at its periphery by a bundle of actin filaments forming a girdle, a dense peripheral actin band (DPAB), around the cell at the level of the adherens junctions (AJ), which is a major site of contact between neighboring cells. At the basal membrane, focal adhesions (FA) anchor the cells to the extracellular matrix.

In contrast to vascular endothelial cells (ECs), the effect of FSS on cytoskeleton organization of cultured PTCs remains poorly understood. One recent study on mouse PTC showed that PTCs undergo a change in phenotype in response to FSS and there is a marked redistribution of F-actin (25). This study was limited to F-actin and was largely observational. Another finding on renal podocytes (26) demonstrated that FSS can cause lamellipodia formation and diminish stress fibers as well as the presence of vinculin in FA. FSS-induced PTC cytoskeletal reorganization and the coordinated remodeling of junctional complexes (TJ and AJ) have yet to be examined. In the present study, we exposed immortalized mouse PTCs to defined laminar FSS in a parallel flow chamber and performed immunostaining on the major proteins of the actin cytoskeleton, AJ, TJ and FA. The results show that PTCs respond to FSS with a cytoskeletal reorganization of actin and junctional related proteins, which, surprisingly, is nearly exactly opposite that observed in rat fat pad ECs exposed to FSS for the same duration (81). Furthermore, we demonstrate that a FSS of only 1.0 dyne/cm^2, 1/10 the FSS used for ECs (81), can cause

the formation of both TJ and AJ. These paradoxical observations are explained in terms of a conceptual "junctional buttressing" model which relates the cytoskeletal reorganization of actin to the redistribution of various junction and actin associated proteins. Finally we suggest that the actin filament bundles within the microvilli act as the mechanosensor for PTCs.

3.2 Materials and Methods

Cell Cultures

Mouse PTCs (graciously provided by Dr. Lloyd Cantley's laboratory at Yale University, New Haven, CT) were originally derived from John Schwartz, Boston University, Boston, MA (78) and were grown to confluence on glass coverslips coated with collagen. Two different types of culture conditions were used: (a) expansion at 33^{o}C and (b) differentiation at 37^{o}C as described in (44, 78). Under expansion condition, cells were incubated at 33^{o}C with renal tubular epithelial medium (DMEM/F12, 10% fetal bovine serum, 100 U/ml penicillin, 100 μg/ml streptomycin) supplemented with interferon-γ. For greater differentiation, cells were switched to 37^{o}C three days before flow experiment in renal tubular epithelial medium only, no interferon-γ.

Cytochalasin D and Heparinase III treatment

To identify the impact of physical modifications of the apical surface on the efficiency of flow-induced TJ formation, we treated the PTCs with two different enzymes:

cytochalasin D (cD) and Heparinase III (HepIII). 15 U/ml Heparinase III (Sigma) was used to remove glycocalyx components (81), whereas 3 μM cytochalasin D was added to inhibit the sensory system through brush border microvilli (17).

Flow system and experiments

The flow system consisted of a parallel-plate channel flow chamber (Warner instruments) and a programmable syringe pump (KD Scientific). This system produces laminar flow over the cell monolayer. A flow rate was chosen to yield a τ-value of 1 dyn/cm^2 using the equation $\tau = 6\mu Q / bh^2$, where Q is flow rate, μ is medium viscosity, and b and h are channel width and height, respectively. Fluid temperature was maintained at 37^{o}C.

To study the effect of steady laminar FSS on cytoskeleton reorganization, confluent PTC monolayers were exposed to laminar flow for 5h with various perfusion solutions (serum-free culture medium, medium+Hep III, and medium+cD). Medium was overnight incubated with 5% CO_2. The 5h flow experiment duration was chosen based on Thi et al (81). Cells subject to static control were kept in the incubator, and the cultured medium was changed every hour such that the total amount of exposed medium was the same as in the flow condition to eliminate the influence of cell metabolism accumulated in the medium. Each set of experiments was repeated four times.

Labeling of cytoskeletal structures

After exposed to laminar FSS, cells were stained with the following monoclonal antibodies: *1*) anti-ZO-1, *2*) E-cadherin, *3*) anti-vinculin, *4*) paxillin, and 5) α-tubulin. F-actin was labeled by phalloidin and nucleus was labeled by To-PRO 3. The cells were fixed with PLP (8% paraformaldehyde, 0.1M lysine and 0.01M sodium periodate in phosphate buffer, pH 7.4, 22^{o}C), quenched for 15min with 0.5M ammonium chloride in 0.1% BSA-PBS and then permeabilized with Triton X-100, blocked in serum buffer, and finally labeled with primary antibodies for 1h. Alexa Fluor 488 or 594 goat anti-mouse IgG were used as secondary antibodies. The slide was covered with 15µl of Vectashield mounting medium (Vector Laboratories) and sealed with nail polish.

Fluorescence images were captured using a confocal microscope (Zeiss, LSM 510). Z-stacks were performed by acquiring 10-12 images with a fixed 1-µm z interval at optimal confocal planes. Quantification of the fluorescence intensity profiles were analyzed using ImageJ software (NIH) for 30 cell pairs. Each cell pair was randomly selected at z plane of interest (apical and basal region), within a region with a fixed range of 22µm with the apposition membrane approximately in the middle (81). In each of the seven paired images at the bottom of Figures 1 and 2 the intensity data on the control and sheared cells were normalized by the maximum intensity at the midplane of the region and all measurements scaled relative to this maximum value, which was defined as 100% (29).

To detect the distribution of interested protein in the Z direction, XZ images were obtained for each of four independent experiments. The images were then processed by ImageJ software (NIH) that calculated pixel intensity along line profiles. The intensity at

any given location is the mean of 10 images collected from four independent experiments. The total protein expressions were estimated by calculating the areas under each intensity curve by using Prism 4.0 (Graph Pad Software).

Protein extraction and immunoblotting

Proteins were extracted from PTCs in lysis buffer (50 mM Tris-HCl, 150 mM NaCl, 50mM EDTA, 1% TX-100, 1 μM PMSF, and 1× complete protease inhibitor cocktail) for 10 min on ice. The homogenate was clarified by centrifugation at 16,000 ×g for 20 min at 4°C, and the supernatant was collected. Protein concentrations were then determined by using a BCA Protein Assay kit (Pierce). Equal amounts of proteins (20 μg) were denatured by heating at 65°C for 15 min in 10μl of sample buffer containing 62.5 mM Tris, 2% SDS, 5% 2-mercaptoethanol, 10% glycerol, and 0.001% bromophenol blue. Samples were then separated by SDS/PAGE (15%) and transferred to PVDF membrane (Millipore). Membranes were probed with the polyclonal anti-actin antibody (A2066, Sigma, 1:200), followed by a peroxidase–conjugated secondary antibody (Jackson Laboratories; 1:5,000). The bands were visualized by an ECL method (Amersham Biosciences) and quantified by ImageJ (NIH). Statistical comparisons were based on at least three separate immunoblot assays. Comparisons were made relative to control conditions and significance was accepted at $P < 0.05$.

SEM

For SEM analyses, control PTCs were fixed in primary fixative (3% glutaraldehyde in 0.1M sodium cacodylate and 0.1M sucrose, pH 7.4), post-fixed with osmium tetroxide, and dehydrated through an ethanol series. Fixed cultures were critical-point-dried with CO_2 as the transitional fluid, sputter-coated with gold-palladium (EMS, model 550), and then examined with an ISI SS40 SEM at 10 kV (Yale University).

3.3 Results

3.3.1 Flow-Induced actin cytoskeleton reorganization.

Confluent PTCs were cultured for five days and then exposed under either 0 or 1 dyn/cm^2 (which is equivalent to 30 nl/min in isolated single proximal tubule (17)) of FSS for 5h (81). After exposure, the cells were fixed, stained for F-actin, and examined by confocal microscopy. Similar to the observation on PTCs in the FSS-induced phenotype study of Essig et al. (24), we witnessed a marked change of F-actin distribution. Fluorescein phalloidin staining showed the presence of two distinct and spatially separated actin microfilament populations, one located basally and the other apically. In the basal region of the no-flow treated cell, numerous long, thick cytosolic stress fibers were found running the entire length of the PTCs (Figure 1*Ad*), which might be associated with cell-matrix interactions between the epithelium and substratum. Apically, microfilaments are organized into a relatively thin circumferential actin network at apical cell-cell contacts (Figure 3-1 *Aa*). In addition to the simple linear junctional outlining in most areas, gaps between cells were frequently observed (Figure 3-1 *Aa*, arrows). Exposure of PTCs to FSS caused dramatically diminished thick stress fibers at the basal surface (Figure 3-

1*Ae*); in addition, some short, randomly arranged actin bundles appeared throughout the cells. At this time, cells were found continuously apposed to each other at cell-cell junctions near the apical surface where we observed more prominent DPAB (Figure 3-1*Ab*). The normalized fluorescence intensity at the apical junctional sites in the sheared cells was found to be significantly higher than in the control cells for all four experiments (Figure 1A*c*; $p<0.01$); whereas the intensity values in the basal region was significantly higher in the no-flow cells than in the sheared cells (Figure 1A*f*; $p<0.01$). Five-fold increase of the magnitude of FSS led to a more significant accumulation of actin filaments at peripheral cell borders near the apical surface (data not shown).

To test whether FSS affects the total actin expression, we performed western blot and fluorescence line intensity analyses on the *XZ*-images of actin staining (Figure 3-2). The area under the intensity curve for control cells was 476, which was not significantly different from that of sheared cells (476. 3, see Figure 3-2*B*). The western blot results further confirmed that FSS only caused actin to shift from the basement membrane to the apical region without changing its total protein expression (Figure 3-2*C*).

3.3.2 Flow-induced tight junction and adherens junction formation.

To investigate flow-stimulated TJ and AJ distribution, we examined TJ-associated protein ZO-1 and a transmembrane AJ protein E-cadherin in PTCs. In the absence of FSS, ZO-1 did not even form an apical cell-cell contact structure but appeared as isolated rings surrounding individual cells (Figure 3-1*Ba*). This separation corresponds to two

outermost peaks in the intensity profile shown in Figure 3-1*Bc* (*blue*). The cytosol also exhibited a certain amount of anti-ZO-1 staining as dot-like structures (Figure 3-1*Ba*, *arrowhead*). Exposure to 5h FSS induced a significant reassembly of intercellular junctions. After shear, a continuous distribution with dramatically reinforced junction staining pattern of ZO-1 was observed (Figure 3-1 *Bb*). Similarly, a majority of punctuate staining of intracellular E-cadherin at cell-cell interfaces in static culture became continuous and localized at the position of cell-cell junctions after imposition of FSS (Figure 3-1 *C*). The intensity values at the junctional region for both proteins were significantly higher in the sheared cells than in the no-flow cells (Figure 3-1 B&C-*c*; $p<0.01$).

3.3.3 Flow-induced focal adhesion redistribution.

Vinculin and paxillin, two adaptor proteins at FA, were examined to study the effect of FSS in the modulation of FA. Double detection of vinculin with F-actin showed that under static conditions, vinculin sparsely localized at the cell border near the basement membrane (Figure 3-3 *Ad*), and was either absent or weak at the apical surface (Figure 3-3 *Aa*). A dramatic reinforcement of vinculin staining (red) was found in the presence of FSS. In both regions, not only did vinculin localize along lateral cell membranes in a punctate pattern (Figure 3-3 *Abe*, arrow), but it also localized circumferentially around the nucleus (Figure 3-3 *Abe*, arrowhead). The fluorescence intensity profiles of both control and treated cells are shown in Figure 3-3 *Ac* and Figure *3-3Af,* respectively. In control cells the intensity profile was relatively flat indicating that the vinculin

distribution was uniform throughout the cell. In contrast, in cells stimulated with FSS, fluorescence intensity was markedly higher at both the periphery of each cell and the interior of the cells. Paxillin, on the other hand, co-localized with F-actin at stress fibers ends under control condition (Figure 3-3 *Ba*, arrows). After 5h FSS, a predominant upregulation of paxillin was found (Figure 3-3 *Bb*). The intensity profile clearly delineated a FSS-induced increment of paxillin expression (Figure 3-3*Bc*).

3.3.4 Possible mechanosensor of proximal tubule cells.

The foregoing experiments focused on the diverse cytoskeletal responses of PTCs after exposure to FSS. How do PTCs detect the FSS? Many studies have suggested that the sensing apparatus is likely to be cytoskeletal elements or a structure that lies at the apical membrane surface. Several candidates have been identified in various cell types. We mainly focused on the following three candidates: microvilli (17, 35), finger-like structures on the apical membrane of PTCs, which contain a core of actin filaments (58); primary cilia, which consist of a 9+0 arrangement of microtubules (89); and glycocalyx (81), a thin "cell-coat" observed on the surface membrane of ECs. To confirm that each of these structures is present on the surface of PTCs, we used scanning electron microscopy (SEM) and confocal microscopy. The SEM result showed that PTCs exhibited dome shape, with an apical domain bearing numerous microvilli (Figure 3-4*A*). Then we stained α-tubulin to investigate whether primary cilia are present in our cells. Interestingly, no cilia formed in PTCs cultured for five days (Figure 3-4 *B*), the condition that we used in our FSS studies. However, after culturing the cells for eight days, primary

cilia were observed sticking about 2-3 μm above the apical membrane (Figure 3-4 *B*). This result ruled out the possibility that primary cilia would contribute to FSS-induced cytoskeletal reorganization of PTCs under our experimental condition. Next, to test whether the glycocalyx or microvilli play a sensor role in regulating mechanotransduction in PTCs, we perfused the monolayer with the addition of Heparinase III (HepIII) (to digest the glycocalyx) or cD (to disrupt the actin filaments), and analyzed the co-localization of F-actin and ZO-1. Not surprisingly, we found that TJ still form after 5h of FSS with the presence of HepIII (Figure 3-4 *C*). In comparison, cD treatment resulted in disruption of actin filaments with the actin bundles reorganized into aggregates throughout the cytoplasm, as well as discontinuous distribution of ZO-1 visualized as wavy ribbons at the cell borders (Figure 3-4 *C*). Clearly, TJ were not formed in the presence of cD.

3.4 Discussion

The experiments in this paper have led to two important and unexpected observations. First, the cytoskeletal reorganization of F-actin and associated linker and junction proteins in response to FSS in cultured confluent PTC is nearly diametrically opposite to that observed for ECs (10) which were also subjected to FSS for 5h. In the latter paper, provided an intact glycocalyx is present, there was a DPAB, few basal stress fibers, a dispersed distribution of vinculin and clearly defined continuous TJ in the control state as indicated by the localization of ZO-1. This organization was greatly altered after FSS with a breakdown of peripheral actin bands, a formation of stress fibers, a movement of

vinculin to cell-cell adhesion sites at the basement membrane and a disruption of TJ. These observations are just opposite that observed in the present study. Second, cultured PTCs, though confluent, do not form either AJ or TJ in their control state. Quite remarkably, a FSS of only one dyne/cm2 appears to be a critical precondition for the formation of both AJ and TJ. This FSS is only one tenth that applied in the EC studies in (81). The magnitude of the FSS would appear to be very significant since a FSS of one dyne/cm2 is typical of PTCs in vivo, whereas a FSS of 10 dynes/cm2 is more typical of ECs in vivo.

Another fundamental observation is that in the case of ECs, the integrity of the glycocalyx layer is essential for the mechanotransduction of FSS. The experiments by Thi et al. (81) reveal that if the endothelial surface layer is compromised either by enzymatic treatment or the use of DMEM solution without plasma proteins, cytoskeletal reorganization is completely abolished demonstrating that an intact glycocalyx plays a critical role in transmitting FSS to the underlying cytoskeleton. This is explained in terms of a "bumper car" model shown in Figure 3-5 A & B wherein the bending moment applied at the edge of the glycocalyx layer is instrumental in applying a rotational moment on ECs that leads to a disruption of the AJ and its peripheral actin band which functions much like a rubber bumper at the perimeter of the cell. The key observation in Figure 3-5 B is that the moment applied by the integrated clockwise torque on the EC is resisted by an opposing moment applied at the AJ and when this moment exceeds the strength of the VE-cadherin bonds there is a disruption of the AJ with a disassembly of

the DPAB and a migration of vinculin to cell borders to form new basal attachments and stress fibers.

PTCs also contain a layer of acidic glycoproteins coated on the surface of brush border microvilli (73). However, this layer had little effect on cytoskeletal reorganization in PTCs in response to FSS as shown in Figure 3-1 C (left). Our results indicate that the brush border microvilli on the apical surface of PTCs play the same role as the EC glycocalyx in that the fluid drag on these protuberances produces a rotational moment on the cell in response to FSS. Morphometric analysis revealed that the surface density of microvilli was approximately 3.0/μm2 and their average height about 0.8 μm. This density is approximately one order of magnitude less than in vivo, where the microvilli form a highly organized, closely spaced, hexagonal array, and their height is about 1/3 that observed in vivo (57). The average spacing of microvilli in Figure 3-4 A is 0.55 μm and, thus, their spacing is nearly comparable to their height allowing the flow to penetrate deep into the brush border. Therefore, the total force from the fluid flow that contributes to the rotational moment about the base of the cell includes two components, one from the drag on the microvilli and one from the fluid shear stress acting on the apical membrane. The combined moment is comparable to that in vivo where the rotational moment is due nearly exclusively to the drag acting on the microvilli tips at the edge of the brush border (outer 10%), Guo et al.(35), since the lever arms from the base of the cell are nearly the same for both force components.

Why do confluent ECs and PTCs respond in such a different manner to FSS? This can be explained with the aid of the conceptual "junctional buttressing" model shown in Figure 3-5 C&D. In Figure 3-5 C the PTCs are in a control state. As deduced from Figure 3-1, under control conditions without flow, there are neither AJ nor TJ. The most important clue is the fact that, the cells, though confluent and touching at their base, do not have TJ as indicated by the distribution of ZO-1 in Figure 3-1B. There is a strong expression of stress fibers at the base of the cell, as indicated by Figure 3-1A, which causes a firm adhesion of the cell to its substrate. This creates a tension in the cell membrane, due to the compressive resistance of the internal cytoskeleton, which in turn produces a rounding of the apical surface and a pulling away of a cell from its neighbor at its basolateral surface. The cells have the appearance of tall cuboidal domes. Cell junctions can not form until there is a disruption of the stress fibers at the basal surface and a release of this membrane tension. For the AJ to form, E-cadherin in the vesicle like structures observed in Figure 3-1C must form adhesive bonds between cells. Even a small FSS will cause these tall cuboidal cells to tilt and their basolateral surfaces to come in contact as shown in Figure 3-5D. This also causes a release of actin stress fibers at the basal surface and the formation of a DPAB as part of AJ assembly as shown in Figure 1A. In our experiments not shown, a higher FSS of 5 dynes/cm2 was applied and stronger peripheral actin bands were observed. Since adhesion of cells to matrix proteins is mediated by membrane receptors, particularly integrins, it is likely that the basal membrane of flow-stimulated PTCs was the site of accumulation or renewal of integrins.

Vinculin and paxillin interacting with newly recruited integrins at FA appears to act as the new basal support for these tall epithelial cells.

The studies by Thi et al. (81) show that a much larger FSS is required to produce cytoskeletal reorganization in ECs. A threshold FSS of close to 10 dynes/cm2 was needed to initiate remodeling, a value close to the measured physiological range. In contrast, a FSS of only 1.0 dyne/cm2 is required for PTCs. This difference in FSS magnitude is largely due to cell geometry. Tall, cuboidal cells have large bending moments about their base, whereas the flat ECs appear to pivot about the plane of their AJ where their actin bumpers are in alignment, as seen in Figure 3-5A and the lever arm (distance from this plane) is much shorter. A second major difference is that in ECs stress fibers extend from the basal to apical margins of the cell providing for a direct structural link between forces applied at the apical surface to FA at the base. In PTCs one expects that such direct links would be few in view of the tall, cuboidal geometry. Therefore, the need for stress fibers linking basal adhesions to the apical surface of the cell would be greatly reduced as observed in Figure 3-1.

The current study identified the importance of FSS in formation of TJ and AJ and the dramatic cytoskeletal reorganization in PTCs in response to FSS. This finding is important and could elucidate our understanding of FSS-induced proximal tubule transport mechanisms described in (17) and (19) for HCO3- and Na+ reabsorption. The elucidation of the signal transduction pathway of FSS-induced cytoskeletal reorganization in PTCs and the identification of the elements involved in such a pathway

may be helpful in further characterizing FSS-induced cytoskeletal-related protein trafficking in PTCs. A possible role for the actin cytoskeleton has been suggested by Dubinsky et al. (21), who propose that the cytoskeleton can mediate cross-talk between apical and basolateral transporters. The possibility is also quantitatively examined in the recent mathematical model by Weinstein et al. (93) for the overall tubular transport using the microvilli torque hypothesis first proposed in Guo et al. (35). Further studies are needed to investigate whether FSS-induced cytoskeleton reorganization favors the membrane transporter protein trafficking in PTCs.

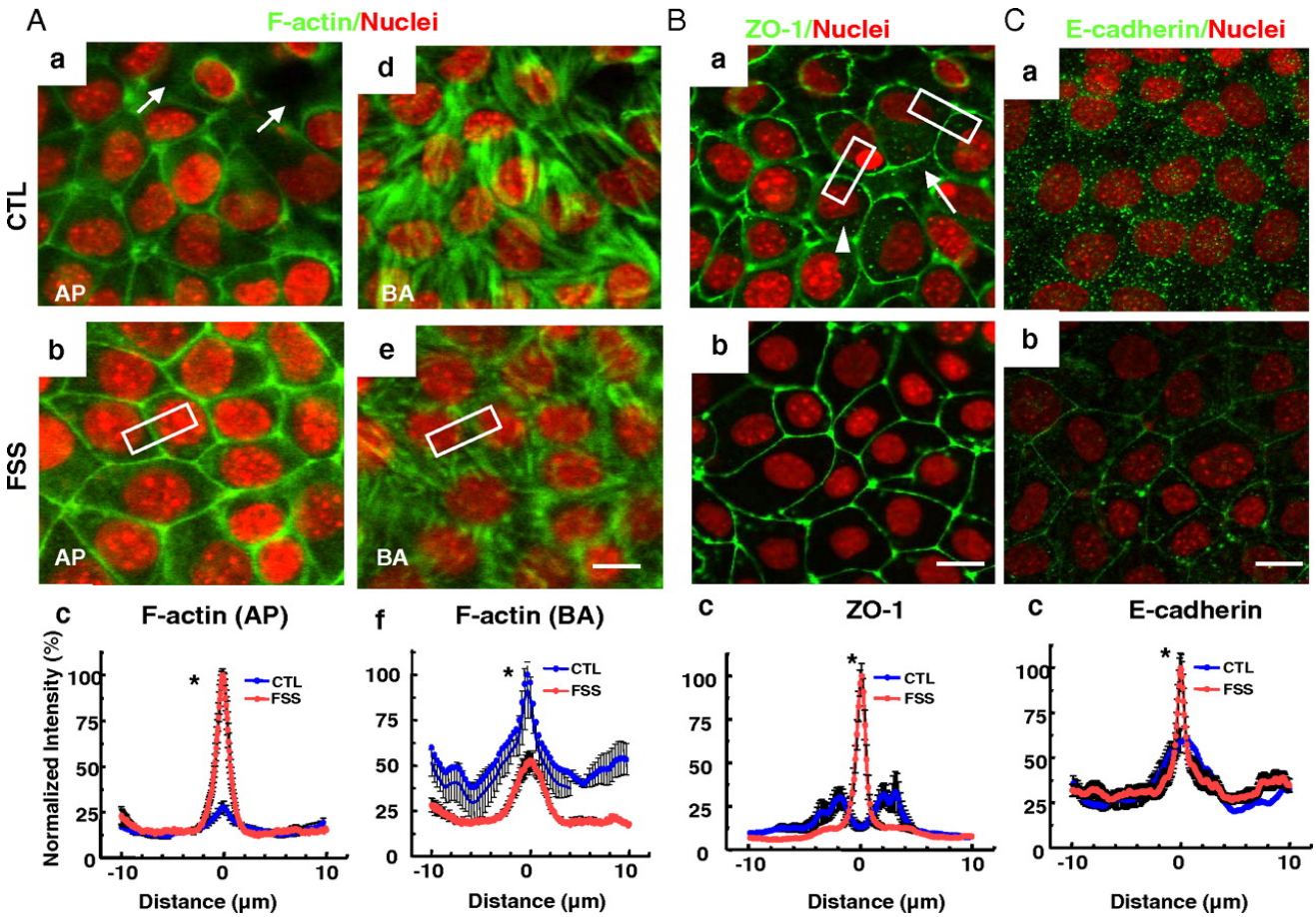

Figure 3−1 Reorganization of confluent mouse proximal tubule cell cytoskeleton and junctional complexes in response to fluid shear stress

PTCs were exposed to laminar FSS of 1 dyn/cm^2 for 5 h at 37°C. Effects of FSS on distribution of F-actin (*A*), ZO-1 (*B*), and E-cadherin (*C*) were analyzed by immunofluorescence confocal microscopy. Quantification of each protein distribution in cells under static control (blue) or FSS treatment (red) conditions was plotted by using ImageJ. Note the shift from bimodal to single-peak distribution signifying formation of TJs (*Bc*) and formation of peak intensity signifying formation of cadherin-related, AJ-associated DPABs (*Cc*).

All data are presented as mean ±SEM, $n = 40$ (*, $P < 0.01$).

Arrows, gaps between cells; arrowhead, intracellular localization; white rectangles, regions used to obtain average intensity profile; BA, cell base; AP, cell apex; CTL, control condition. (Scale bar, 10 μm.)

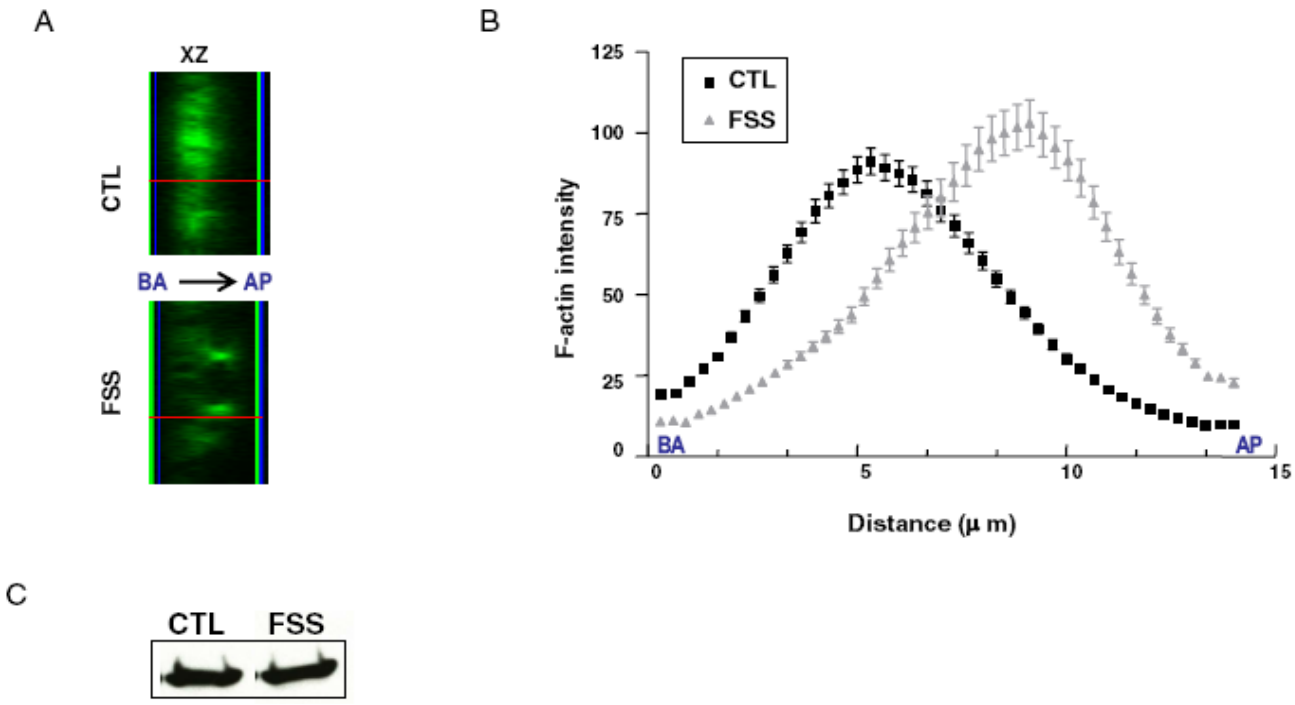

Figure 3−2 Fluid shear stress alters F-actin localization, but not expression, in cultured proximal tubule cells.

(*A*) F-actin (green) localization in *XZ* images. Cells were either under control or exposed to FSS for 5 h and then subjected to immunostaining of F-actin. (*B*) The fluorescence intensity distribution for F-actin along *Z* direction. Line was chosen randomly across the entire cell height as indicated in the *XZ*-images. Intensity profiles were plotted by using ImageJ. Data are presented as mean ± SEM, n=200. (*C*) Western blot analysis for actin under control and FSS treatment, respectively.

No significant difference was found when comparing actin expression between the two conditions. Each blot is representative of three experiments.

CTL, control condition; FSS, fluid shear stress; BA, base; AP, apex.

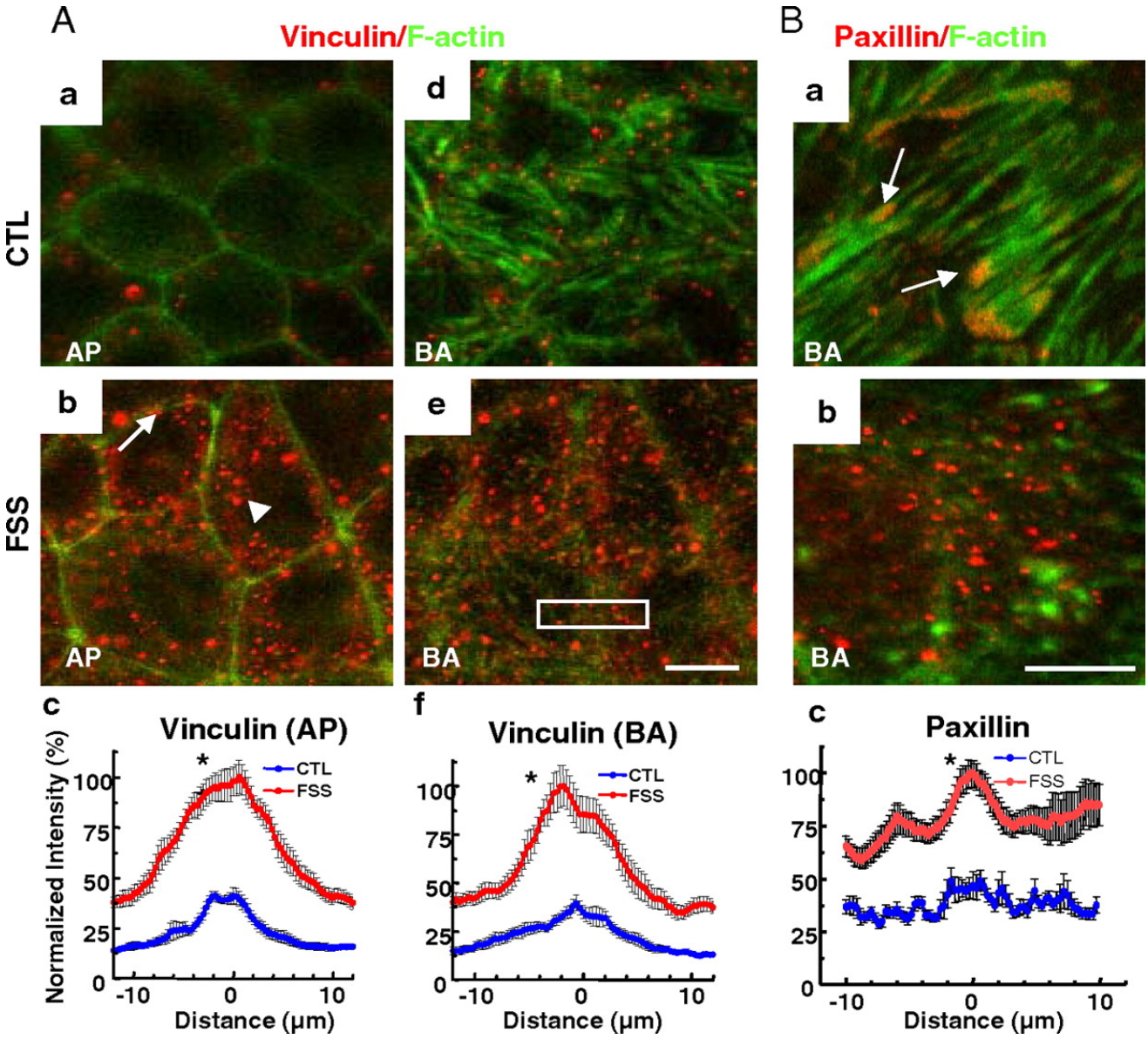

Figure 3−3 Reorganization of the proximal tubule cell cytoskeleton and focal adhesions in response to shear.

(***A***) Distribution of F-actin (green) and vinculin (red) in control (***a*** and ***d***) and FSS-stimulated cells (***b*** and ***e***), whereas ***c*** and ***f*** show quantification of vinculin distribution in the absence (blue) or presence (red) of FSS. Note the large enhancement of vinculin distribution in both AP and BA regions. Arrow, vinculin localized at cell junction sites; arrowhead, nucleus periphery. (***B***) Localization of paxillin (red) in cells subjected to static control (***a***) or with FSS stimulation (***b***). Arrows, paxillin localized at the termination of stress fiber sites. Quantification of paxillin in the absence (blue) or presence (red) of FSS is shown in (***c***). Note the large enhancement of paxillin distribution, signifying the formation of basal focal attachments in response to FSS.

All data are presented as mean ±SEM, $n = 40$ (*, $P < 0.01$).

AP, cell apex; BA, cell base; CTL, control condition. (Scale bar, 10 μm.)

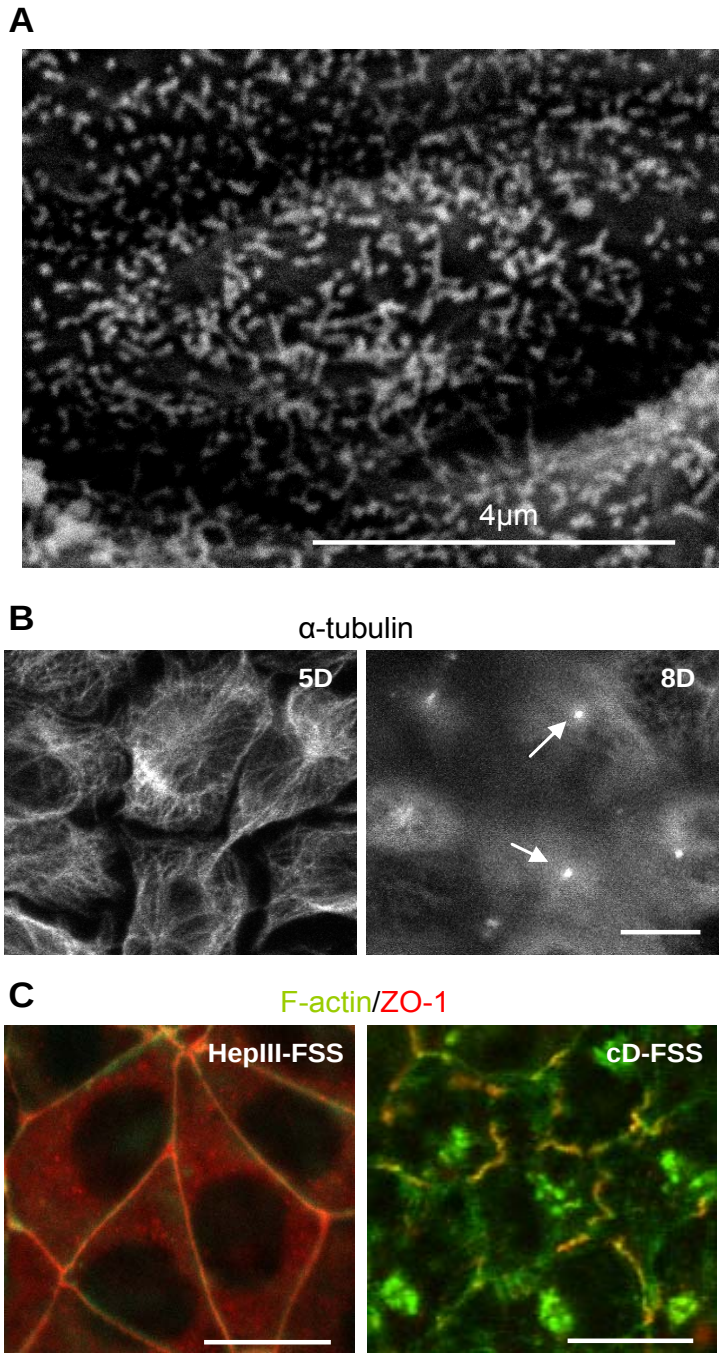

Figure 3−4 Possible mechanosensor for mouse proximal tubule cells.

(*A*) SEM picture of PTCs shows that the epithelium possesses numerous microvilli. (*B*) Antitubulin immunofluorescence staining of 5-d and 8-d cultured PTCs. Arrows, primary cilia. Note the complete absence of primary cilia at day 5 and formation at day 8. (*C*) Colocalization of F-actin (green) and ZO-1 (red) after exposed to 5 h of FSS in the presence of HepIII (*Left*) and cD (*Right*). Note that there was no difference in TJ formation (ZO-1) or appearance of AJs and DPABs after HepIII treatment, signifying that the glycocalyx plays an insignificant role in response to FSS. In contrast, both the TJs and the AJs were markedly disrupted by cD, indicating the primary role of F-actin in the cytoskeletal response to FSS. (Scale bar, 10 μm; otherwise as indicated.)

PTC=proximal tubule cell, HepIII=heparinase III, TJ=tight junction, AJ=adherence junction, DPAB=dense peripheral actin band, cD=cytochalasin D, FSS=fluid shear stress

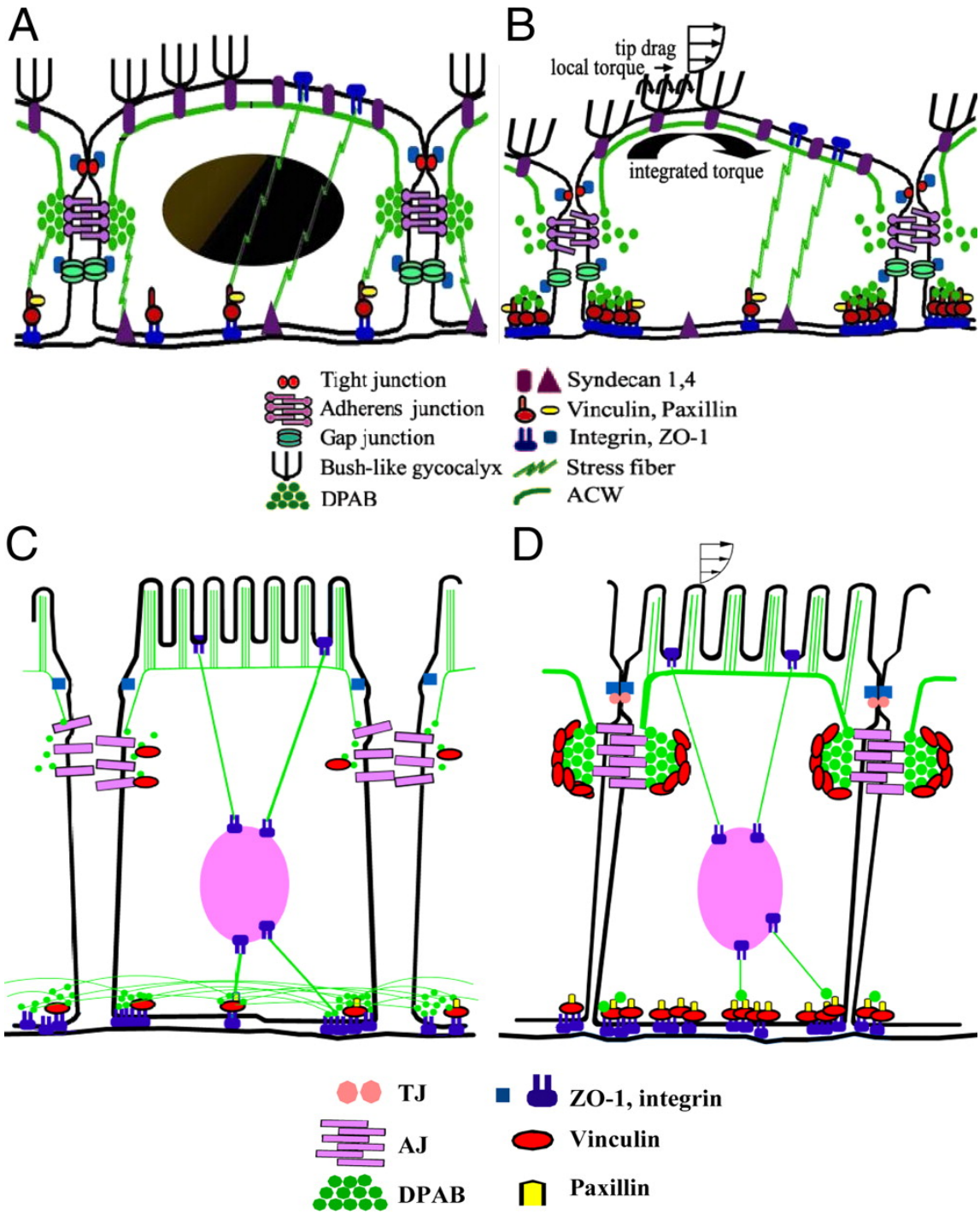

Figure 3−5 A conceptual "junctional buttressing" model for the cytoskeleton reorganization and junctional formation of mouse proximal tubule cells in response to fluid shear stress in comparison with "bumper-car" model for endothelial cells.

(***A*** and ***B***) EC "bumper-car" model (previously published in ref. (81)). (***A***) In control state, EC displays an intact DPAB that is localized to the AJ, functioning as a rubber fender of a bumper car that is constantly undergoing small collisions with its neighbors. (***B***) FSS causes a breakage of weak cadherin bonds, a disruption of AJs, and a disassembly of DPABs. (***C***) Regarding PTCs, there are neither AJs nor TJs under control conditions. These cells express numerous cytosolic stress fibers at their bases, which are in contact with one another at their periphery. This creates a tension in the membrane that pulls the membrane toward the base and forms a rounded canopy of cell membrane at the apical surface. (***D***) After exposure to FSS, stress fibers disappear from cell base and AJs, TJs, and DPABs form. More vinculin and paxillin accumulates at basolateral sites. Apically, more intense vinculin distribution was also found at the level of the AJ after 5 h of FSS.

EC = endothelial cell, DPAB = dense peripheral actin band, PTC = proximal tubule cells, FSS = fluid shear stress, TJ = tight junction, AJ = adherens junction

Chapter 4 Flow-Mediated Membrane Transporter Upregulation and Trafficking

4.1 Introduction

Fluid shear stress (FSS) produced by renal tubular flow modulates tubular epithelial salt and water reabsorption, as well as H^+ and K^+ secretion (19, 31, 55, 75, 76). In kidney proximal tubule, Schnermann (76) demonstrated four decades ago that there is a nearly proportional change in Na^+ and HCO_3^- reabsorption with variation in glomerular filtration rate (GFR), namely "glomerular tubular balance" (GTB). The physiological importance of this regulation is to prevent loss of solute following increases in GFR, and to preserve adequate distal delivery of sodium and fluid when GFR is reduced. This highly-regulated intake of Na^+ and HCO_3^- depends on the activity of a host of specialized transporting proteins that are located on the specific plasma membrane domains of proximal tubule cells. Acute Na^+ reabsorption across the proximal tubule is mediated primarily by apical entry via NHE3 and extrusion via basolateral sodium pumps (Na^+/K^+-ATPase). HCO_3^- reabsorption is regulated by apical transporters NHE3 and vacuolar H^+-ATPase (V-ATPase), and basolateral Na^+/HCO_3^- cotransporter. It has been reported that increases in axial flow velocity recruit new Na^+/H^+ transporters (mainly NHE3) into the luminal membrane (51, 71). Our previous in vitro microperfusion studies have also shown that luminal flow modulates both NHE3 (17) and V-ATPase (19) activities. It is not clear whether this is due to trafficking of apical membrane proteins from the large pool of subapical endosomes to the cell surface, increased activity of transporters in the plasma

membranes, or both. One recent mathematical model by Weinstein et al. (93) quantitatively predicted that coordinated regulation of both luminal and peritubular transporters are required for the overall Na+ reabsorption to be able to preserve the integrity of cell volume and composition during variations in Na+ reabsorption. The effect of FSS on trafficking of the basolateral membrane proteins has yet to be examined.

Cytoskeletal elements, such as microtubules, actin filaments, and their associated molecular motors are intimately involved in mechanical signaling in multiple cell types (16, 43, 68). Inhibition of actin stress fiber development by cytochalasin D blocks FSS-induced gene expression in osteoblasts (68). Cadherins do not function as cell adhesion molecules and do not transmit mechanical signals in the absence of cytoskeletal attachment (34, 67). Microtubule disruption with nocodazole blocked both FSS-induced morphological change and actin stress fiber induction in bovine aortic endothelial cells (54). In mouse proximal tubules, we have observed a strikingly linear relationship between the hydrodynamic torque produced by the drag force acting on brush border microvilli and Na+ and HCO3- reabsorption. This process was interrupted by cytoskeletal disassembly. Cytoskeletons are dynamic structures and undergo dramatic remodeling in the presence of FSS. A conceptual “junctional buttressing” model (20) was proposed recently to describe the phenomenologic changes of actin cytoskeleton and its junctional linker proteins of mouse proximal tubule (MPT) cells when exposed to FSS. The changes include a formation of tight and adherens junctions, a disappearance of basal stress fibers, and an accumulation of focal adhesion proteins at the basement membrane. Whether

FSS-induced cytoskeleton reorganization plays any role in modulating protein activity is unknown.

In this study, we examined the distribution of NHE3, V-ATPase and Na^+/K^+-ATPase in an immortalized MPT cell line by immunofluorescence and western blot analysis and found that in the absence of luminal flow, the distribution of apical transporters across the cytoplasm was diffuse, with no compartment being more prevalent in either NHE3 or proton pump immunostaining. Sodium pumps were seen mostly at the basolateral membrane, interacting with actin stress fibers. After activating the cell monolayer with FSS, both NHE3 and proton pump proteins were found to translocate to the apical membrane. Membrane sodium pump expression increased two-fold in comparison with control condition. Since disruption of the actin cytoskeleton blunts flow-induced Na+ and HCO3- reabsorption, we tested whether this would also block the translocation of all three transporters and increment of their expression. Our data suggests that FSS-induced NHE3 and sodium pump trafficking are largely dependent on an intact actin cytoskeleton, whereas the proton pump depends mainly on the microtubule cytoskeleton. Taken together, FSS causes upregulation of all three transporters and the trafficking to their specific membrane compartments. Cytoskeletal networks are essential to this flow-dependent process and are protein specific.

4.2 Material and Methods

Chemicals and Antibodies

All chemicals were obtained from Sigma, except where otherwise noted, and except for the following: cell culture media (Invitrogen); penicillin and streptomycin (GIBCO-BRL); ECL western blot reagent (Amersham Biosciences); and PVDF membranes (Immobilon).

Primary antibodies were obtained from either commercial sources or from independent investigators. The polyclonal antibody against NHE3 used for immunostaining was kindly provided by Dr. M. Knepper (NIH). The anti-NHE3 mouse monoclonal (3H3) was a gift of Dr. D. Biemesderfer (Yale University). The rabbit polyclonal antibody against the 33kD V-ATPase subunit E was purchased from Santa Cruz Biotechnology. The Na+/K+-ATPase antibody (6H and α5) was a gift from Dr. M. Caplan (Yale University). And secondary antibodies, including the fluorescein-labeled goat anti-rabbit or goat anti-mouse IgG antibodies were purchased from Molecular Probes and peroxidase-conjugated goat anti-rabbit or goat anti-mouse IgG were purchased from Jackson Laboratories.

Cell Culture and Laminar Flow Experiment

MPT cells (obtained from Dr. Lloyd Cantley, Yale University) were grown until confluence on glass coverslips coated with collagen. Cells were first cultured in epithelial medium (DMEM/F12, 10% fetal bovine serum, 100 U/ml penicillin, 100 μg/ml streptomycin) supplemented with interferon-γ at 33 ^{o}C and then switched to 37 ^{o}C three days before flow experiment in renal tubular epithelial medium only, no interferon-γ (44,

78). Cells were incubated in serum-free medium without hormones or growth factors for 24 hours before the experiments.

The flow system, which has been characterized previously (20), mainly consisted of a parallel-plate channel flow chamber and was kept at 37^{o}C. Confluent MPT monolayers were exposed to laminar flow for 5h at 1 dyne/cm^2 (which is equivalent to 30 nl/min in vivo) with various perfusion solutions (serum-free culture medium, medium+cytochalasin D, and medium+Colchicine) at 37 ^{o}C. Medium was incubated overnight in a 95% O_2/5% CO_2 incubator. The 5h flow experiment duration was chosen in consistence with our previous study (20). Cells subject to static control were kept in the incubator, and the cultured medium was changed every hour such that the total amount of exposed medium was the same as in the flow condition to eliminate the influence of cell metabolism accumulated in the medium. Each set of experiments was repeated three times.

Immunohistochemistry

Immunofluorescence was performed as previously described (20). After fixation, the cells were quenched, permeabilized, blocked with 10% goat serum buffer and then processed for immunodetection. Primary antibodies were diluted in the blocking buffer and the cells were incubated for 1h at room temperature. Bound antibodies were detected with Alexa-594-labeled secondary antibodies. F-actin was labeled by FITC-phalloidin and

microtubule by α-tubulin. The coverslips were mounted on glass slides and sealed with nail polish.

Fluorescent marker and antibody distribution were monitored with a Zeiss LSM 510 confocal laser-scanning microscope and experimental images were imaged at the laser gain that was used to establish negligible fluorescence for the controls. Z-series of 0.5-μm optical sections was taken through cells. The sections were then added together with LSM Image browser software (Zeiss, Germany). XZ images were obtained through the dashed line indicated on each XY image. Two-dimensional image analysis was performed with ImageJ software (NIH). The intensity of fluorescence for the experiments was measured by randomly choosing 10 cells on each Z-plane. The average pixel intensity per square micrometer for each of three images and an average of these three measures was recorded. Fluorescence intensities were normalized such that the maximum protein intensity was assigned a value of 100%.

Western Blot Analysis

After the indicated flow treatment, cells were rinsed twice with cold PBS and extracted with cold lysis buffer containing 50 mM Tris HCl, 150 mM NaCl, 50 mM EDTA, 1% TX-100, and 1x complete protease inhibitor cocktail (Complete; Roche Molecular Biochemicals). Cell lysates were then centrifuged (4oC, 14,000 rpm, 20 min), and equal amounts of total protein from the supernatants were used for Western blot analysis. For membrane protein, cells were collected, homogenized, and microcentrifuged (4 ^{o}C, 1,500

rpm, 15min) to remove nuclei and cell debris. Supernatants were further centrifuged (4oC, 63,000 rpm, 60 min), and pellets were resuspended in lysis buffer and collected as the cell membrane protein extraction. Protein concentrations were determined using a BCA Protein Assay kit (Pierce, Rockford, IL). Samples were stored at -80 ^{o}C until analyzed.

For the Western blot analysis, equal amounts of total protein were resolved by 4-12% SDS-PAGE and immunoblotted with antibodies against NHE3, the Na^{+}/K^{+}-ATPase α1 subunit, V-ATPase. Subsequently, the membrane was probed with secondary antibodies, followed by incubation with ECL Western blot reagent. Relative intensity of protein bands was quantified by ImageJ (NIH, Bethsa, MD). All comparisons were made relative to control conditions (no FSS).

Statistical Analysis

The results are expressed as means ± SEM from combined experiments. Significance of differences was assessed using Student's t test and was reported at the $P < 0.05$ level.

4.3 Results

4.3.1 Fluid shear increases apical NHE3 abundance and cytochalasin D inhibits this effect.

A double-label immunofluorescence study was carried out in order to determine the localization of NHE3 and actin microfilaments in MPT cells in response to 5h FSS

treatment at 1dyne/cm2. NHE3 in MPT cells grown in a static condition was found to be weakly distributed on the surface of the plasma membrane (Figure 4-1Aa). In some cells, we were not able to detect NHE3 expression (Figure 4-1Aa, arrows). From the enlarged XZ image, we detected a weak NHE3 staining in the apical domain of the control cells. This was confirmed by quantitative region scan analysis (Figure 4-1B). Using the perijunctional actin ring as a landmark to align the fluorescence intensities across multiple scans, we found that NHE3 intensity peaked at a location just below the F-actin peak of the apical actin ring, indicating a majority of cytosolic NHE3 distribution (Figure 4-1B). Approximately 22% of the total NHE3 was located in the apical plasma membrane of these cells. Following exposure to a FSS of 1 dyne/cm^2 for 5h, concomitant with dramatic actin cytoskeleton reorganization (20, 25), the overall expression of NHE3 was found to be greatly increased. In addition, we witnessed a translocation of NHE3 to the apical surface membrane of MPT cells (Figure 4-1Ab, XZ). Now ~30% of NHE3 was located apical to the actin ring. We used Western blot analysis to confirm that the FSS-induced increase in NHE3 occurred at the apical membrane. FSS treatment increased the fluorescence of membrane NHE3 protein by 252 ± 24% compared with control ($P<0.05$, N=3) (Figure 4-1C, D). By contrast, the total amount of NHE3 protein fluorescence in cell lysates increased by 213 ± 30% ($P<0.05$, n=3). This suggests that apical insertion of NHE3 is one of the mechanisms of FSS-induced Na^+ reabsorption. In the presence of cytochalasin D, as illustrated in Figure 4-1Ac, there were drastic changes in the distribution of actin: stress fibers were disrupted; the perijunctional actin band disappeared and formed large subcortical aggregates. The FSS-induced increment of

NHE3 staining was almost completely diminished, and the antigen was relocated into an intracellular compartment (Figure 4-1Ac). Importantly, FSS was no longer able to stimulate NHE3 apical abundance, indicating that the FSS-induced activation of NHE3 trafficking and expression are dependent upon an intact cytoskeleton in MPT cells.

4.3.2 Shear stress induces upregulation of Na^+/K^+-ATPase expression and translocation.

Next, we tested the distribution and abundance of Na^+/K^+-ATPase in MPT cells after FSS stimulation. Figure 2A shows that under control conditions, Na^+/K^+-ATPase was weakly localized at the cell lateral membrane. More intense sodium pump staining was observed near the cell-cell contacts in the basement membrane (Figure 2Aa, arrows). Colocalization of Na^+/K^+-ATPase and F-actin were found in the enlarged xz image (Figure 4-2Aa, XZ), consistent with a previous report showing Na^+/K^+-ATPase very tightly interacts with the membrane cytoskeleton (63). Remarkably, cells that are treated with FSS exhibited a greater surface expression of Na^+/K^+-ATPase (Figure 4-2 Ab) as compared with the control cells. The increase in membrane Na^+/K^+-ATPase expression occurred both at the cell periphery and interior. Western blotting showed a ~1.5 fold increase in total cellular Na^+/K^+-ATPase expression and a twofold increase in membrane Na^+/K^+-ATPase expression. Importantly, the observed inhibitory effects of actin disruption resulted in a markedly reduced expression of sodium pumps at the cell surface, which was obvious by immunostaining (Figure 4-2Ac). These results suggest that acute

stimulation of Na^+/K^+-ATPase by FSS results at least in part from stimulation of exocytic insertion of Na^+/K^+-ATPase protein, which requires actin cytoskeleton integrity.

4.3.3 Shear stress induces V-ATPase trafficking and cytochalasin D had no effect on this activity.

We then tested the distribution of another apically localized protein, V-ATPase. Under static conditions, only 30% of the cells possess V-ATPase staining and they are mostly concentrated in subapically located endocytic vesicles (Figure 4-3Aa). In flow-treated cells an upregulation of V-ATPase occurred: V-ATPase was found in every cell, with greater localization at the cell surface and reduced levels in the subapical domain (Figure 4-3Ab, XZ). We also tested the protein levels of V-ATPase in the membrane and in whole cell lysates by immunoblotting and found increased levels in cells treated with FSS (Figure 4-3C). The average band intensity for the whole cell lystates in control cells was 82 ± 27% lower than the band obtained from the FSS-treated cells (Figure 4-3D). In the apical membrane of the control cells, the average pixel intensity was 181 ± 27% lower than in the FSS-treated condition. Surprisingly, in cD-FSS treated cells, V-ATPase remained primarily localized to the apical surface (Figure 4-3Ac). The fluorescence intensity and distribution remained similar to what was observed in FSS treatment condition. Taken together, these data show extensive FSS-induced translocation to the apical membrane and upregulation of V-ATPase expression, and this effect apparently is actin cytoskeleton-independent.

4.3.4 Colchicine inhibits shear-induced V-ATPase trafficking.

Studies on other polarized epithelial cells have suggested that microtubules are involved in the targeting of intracellular vesicles to the apical pole of epithelial cells (1, 36, 66). In colchicine-treated rats, Brown and coworkers (8) found a great reduction in apical V-ATPase content. We therefore assessed the effect of colchicine on FSS-induced V-ATPase trafficking in cultured MPTs by double-staining of V-ATPase and α-tubulin. In control cells, the immunofluorescence for the α-tubulin antibodies exhibited radial or reticular patterns in the cytoplasm, and intense fluorescence was observed in the perinuclear region (Figure 4-4Aa, arrows), presumably in the microtubule organizing center (MTOC) region. From the XZ plane, microtubules were found mainly arranged in bundles of filaments running along the apical-basal axis of the cells (Figure 4Aa, XZ). V-ATPase was found mostly beneath the apical tubulin "cap". To evaluate the relative localization of microtubules in MPT cells, we doubly labeled rhodamin-phalloidin and α-tubulin and observed that the microtubule meshwork and actin bundles overlap in the apical regions (Figure 4-4B). After FSS stimulation, the distribution of microtubules seemed to be accumulated in smaller cytoplasmic areas. Interestingly, a "tail" like structure was often found connected to the cell periphery (Figure 4-4Ab, arrows). Furthermore, the circular structures of MTOCs around the nuclei were dramatically reduced to strongly fluorescent focal regions. V-ATPase staining showed two spatially separated populations, one located inside of the microtubule circle and the others outside. The ones outside of the microtubule surroundings appear more condensed compared to the insiders (Figure 4-4Ab, arrowheads) and localized more on the surface of the apical

membrane (Figure 4-4Ab, XZ). A single dose of colchicine resulted in a strong loss of microtubules in MPT cells (Figure 4-4Ac, green). We observed only residual labeling located in the subapical region, which may belong to stable microtubules located in the terminal web. Importantly, treatment with colchicine also resulted in a marked decrease in the surface expression of V-ATPase (Figure 4-4Ac, red), which is consistent with previous in vivo findings (7) that colchicine treatment caused the normally tight apical band of V-ATPase staining to be replaced by a scattered distribution of labeled vesicles throughout the cell cytoplasm. It is not known whether colchicine perfusion-induced V-ATPase internalization is dependent on membrane endocytosis or on the dissociation of V-ATPase from the plasma membrane followed by internalization due to interactions with the cytoskeleton. Taken together, colchicine-induced depolymerization of microtubules blunted the effect of FSS on V-ATPase redistribution and upregulation.

4.4 Discussion

The present study, carried out on immortalized MPT cells, was designed to define whether membrane transporter protein trafficking is involved in FSS-induced regulation of the protein activity. The main novel points are the following: (1) FSS-induced stimulation of NHE3 and V-ATPase activity was associated with increased apical protein abundance. (2) FSS-induced transporter trafficking was not only limited to the apical domain of the plasma membrane, where the mechanotransducers directly contact with the different flow pattern, but also involved with basolateral membrane protein activities, such as Na^+/K^+-ATPase; (3) actin cytoskeleton disruption blocked FSS stimulating effect

on upregulation and trafficking of NHE3 and Na^+/K^+-ATPase; (4) FSS-induced increase in apical V-ATPase abundance relies on microtubule network, but not actin cytoskeleton.

Laminar FSS stimulates Na+ and HCO3- absorption in the renal proximal tubule mainly by activation of the apical NHE3 and V-ATPase. This effect was repeatedly documented by groups using different experimental methods. Preisig (71) measured cellular pH recovery after an ammonium pulse in perfused proximal tubule of rat kidney in vivo. With increases in luminal flow rate (from 5 to 40 nl/min), the pH recovery mediated by NHE3 was enhanced. Maddox et al. (51) subjected rats to acute changes in vascular volume to obtain animal models with decreased, normal, and increased GFR. It was found that the NHE3 activities were in parallel with GFR. Our recent isolated single tubule perfusion study has demonstrated that the flow-dependent Na+ reabsorption was diminished in NHE3-null mice (17). And that flow impacts more than just NHE3 is supported by observations that flow dependence is seen in the presence of EIPA (NHE3 inhibitor) or in NHE3 knockout mice (19). How the flow modulates luminal transporter activity is less understood. Acute regulation of protein activity is mediated predominantly by changes in maximal velocity of the exchanger (Vmax). Such Vmax effects can be achieved by rapid changes either in the number of the exchanger molecules at the cell surface or in the number of exchange cycles per molecule per second (turnover number) or both. Accumulating evidence suggests that rapid regulation of NHE3 activity in epithelial cells usually involves, at least in part, changes in the amount of NHE3 at the

plasma membrane by changes in regulated exo- and endocytosis (2, 15, 42, 47, 97). For example, EGF, FGF and clonidine stimulate NHE3 activity through accelerating NHE3 exocytosis, whereas dopamine inhibits NHE3 activity partly through stimulating NHE3 endocytosis (40, 42). Also under basal conditions in PS120 fibroblasts and in polarized epithelial cell lines, the human colon cancer cell line Caco-2 and the renal proximal tubule cells line OK, NHE3 cycles on and off the plasma membrane. Our results confirm that luminal protein trafficking to the apical plasma membrane is one mechanism by which FSS may activate membrane proteins that mediate ion transport events. We observed ~2.5-fold increase in membrane NHE3 expression and ~ 2.8-fold increase in membrane V-ATPase expression following FSS treatment. The difference here in comparison with others is that the total amount of NHE3 and V-ATPase were both altered. Our explanation is that under stimulated condition, proteins are more active so that the baseline of the protein expression is higher than under static conditions. Experiments under different flow rates thereby need to be performed to clarify this assumption.

Another important purpose of the current study was to provide evidence that peritubular transporters can be activated by luminal flow. According to the prediction by a recent mathematical model derived by Weinstein et al (93), the peritubular transporters must be modulated by luminal flow to support Na^+, HCO3-, and water exit to the interstitium and blood from the cell when apical transporter activity is increased. The authors calculated two key parameters: sodium flux and cell volume in the absence or presence of

peritubular transporters. It showed that increases in luminal transporter density alone produce at most a 30% increase in Na+ flux versus a linear range under a normal physiological condition. In addition, cell volume could reach to a lethal increase if there is no coordinated scaling of luminal and peritubular transporter activity. Our results show an alteration of the amount of membrane Na^+/K^+-ATPase stimulated by FSS. This increase is observed in the presence of a mild increment of the total cellular pool of Na^+/K^+-ATPase, strongly suggesting that translocation of intracellular Na-pumps to the plasma membrane occurs in response to increased luminal FSS. Whether Na+/K+-ATPase activity is regulated with application of luminal flow has not been answered. This issue has been studied more extensively, however, in intracellular Na concentration ([Na+]i)-dependent Na^+/K^+-ATPase activity. In rabbit cortical collecting duct, a rise in $[Na+]_i$ by incubation with the Na+ ionophore nystatin increased Na^+/K^+-ATPase activity and cell surface expression to the same extent (84). A Japanese group also found that $[Na^+]_i$ could directly modulate Na^+/K^+-ATPase gene expression in rat kidney cells (61). Therefore, one possible mechanism for the fate of FSS-induced Na^+/K^+-ATPase delivery to basolateral membrane ought to start from the luminal flow stimulation. Some degree of luminal transporter insertion may occur in the apical membrane, which in turn leads to an increase in [Na+]i. To maintain a low cytosolic Na level, an activation of basolateral Na^+/K^+-ATPase occurred afterward.

The current study has implicated that an intact actin and microtubule cytoskeleton is essential for FSS-induced membrane protein trafficking in MPT cells. The cytoskeleton

is a dynamic structure that maintains cell shape, often protects the cell, and enables cellular motion. In fact, our recent "junctional buttressing" model has illustrated a dramatic cytoskeleton reorganization after onset of FSS. We witnessed a formation of tight junction and adherens junction, a disappearance of basal stress fibers, and an accumulation of focal adhesion proteins in the basement membrane (20). How the cytoskeletal changes regulate transporter activities is unclear, but it could reflect a dependence on localization, assembly into higher-order complexes, or a possible direct mechanical effect of cytoskeletal elements on transport proteins. Previous studies suggest that NHE3 is associated indirectly with cytoskeleton through coordinate binding of NHE3 regulatory factor 1 (NHERF1/EBP50), a bridging molecule that also associates with ezrin, which, in turn, binds directly to actin (91). Hayashi et al (38) illustrated that disruption of the apical actin network of epithelial cells using TxB or Y-27632 resulted in massive internalization of NHE3, which is accompanied by a drastic drop in the ability of the cells to reabsorb Na+ and the osmotically obliged water. In AP-1 cells, NHE3 was extensively inhibited by capping the barbed ends of actin microfilaments or by scavenging away monomeric actin (46). When incubated in acid medium (13) or with endothelin (69), the increase of the exocytic insertion of NHE3 protein was also inhibited by cD in OK cells. With respect to Na^+/K^+-ATPase, it has been shown that Na+/K+-ATPase is tightly connected with ankyrin/fodrin-actin membrane cytoskeleton. In epithelial cells, ankyrin links fodrin to the Na^+/K^+-ATPase, and ankyrin binding coordinately assembles the E-cadherin and Na^+/K^+-ATPase at the basolateral membrane. It is implied that E-cadherin may play a role in stabilizing and assembling the membrane

cytoskeleton and the Na^+/K^+-ATPase at the basolateral cell surface of MDCK cells (64). From the above, it is likely that dramatic cytoskeleton reorganization in response to flow might favor the protein activation and targeting. The consensus on how such effects take place has not been reached.

V-ATPase trafficking in response to FSS was found to be dependent upon intact microtubules, but not on actin filaments, which is interestingly in line with observations in several other cell types. In yeast (96), nocodazole, an agent that disrupts microtubules, partially blocks dissociation of V-ATPase in response to glucose depletion. By contrast, latrunculin, an actin disrupting drug, has no effect on glucose-dependent dissociation of V-ATPase complex. In osteoclasts, immunofluorescence analysis shows an intimate colocalization between V-ATPase and microtubule, but not actin filaments (82). Hence, there is the possibility that vesicles containing the V-ATPase do not require actin filaments to target to their destination, but instead a local depolymerization in the actin network might allow vesicles to traverse the dense subapical network of filaments and to gain access to the plasma membrane. Perhaps, this explains why HCO_3^- reabsorption in isolated MPT was not completely abolished when treated with cytochalasin D in comparison with the combination of EIPA (NHE3 inhibitor) and bafilomycin (V-ATPase inhibitor) (19). We did not perform the colchicine treatment on the other two sodium transporters but would expect a similar effect on NHE3 but not Na^+/K^+-ATPase. It is known that microtubules do not appear to be important for generation and/or maintenance of basolateral proteins, such as Na^+/K^+-ATPase, but more involved in the transport of

membrane proteins to the apical pole of the epithelial cells (1, 36). Studies have found that basolateral localization of Na^+/K^+-ATPase remains unaffected in cells that are treated with colchicine, which is associated with the unaffected subcellular distribution of spectrin, actin, and ankyrin. On the other hand, NHE3 and NHERF are targeted to the basolateral membrane in proximal tubules of colchicine-treated rats (74).

In summary, we have described a novel effect of FSS that may contribute to the understanding of the mechanism of "perfusion-absorption balance" and have, in the process, revealed a role for cytoskeleton in the FSS-induced trafficking of the transporters to their functional membrane domains. These observations raise the possibility that, under physiological circumstances, membrane transporter activity may be regulated by altering the partition of exchangers between endosomes and the surface membrane. Our current study does not rule out the possibility that the turnover rate of transporters also increases in response to FSS stimulation. The functional aspect of FSS-induced transporter activity will be examined in the future.

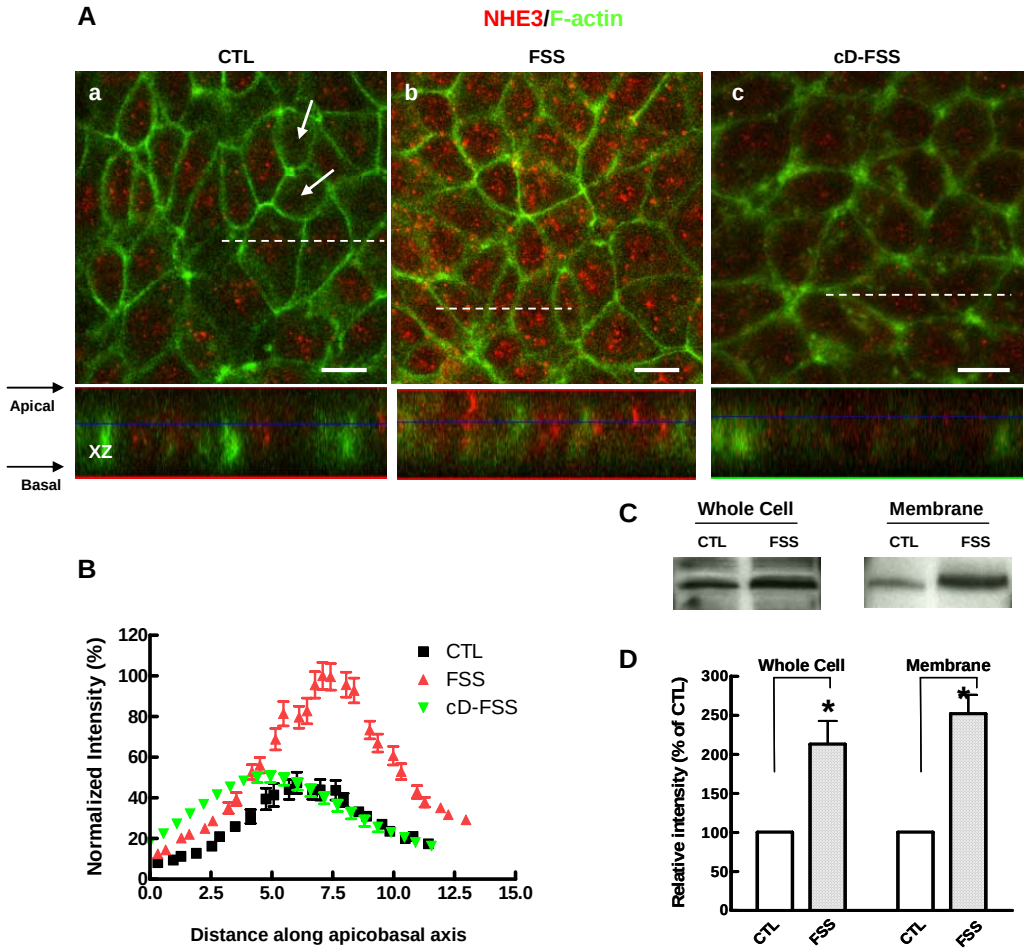

Figure 4−1 Effect of fluid shear stress on NHE3 trafficking and expression in confluent mouse proximal tubule cells.

(A) Immunofluorescence images of MPT cells under CTL (a), FSS (b), and cD-FSS conditions (c). The antibody stained for NHE3 (red) and actin filaments (green), respectively. XY image is taken from where the blue line is indicated in the XZ image. XZ images were obtained through the dash line on the corresponding XY images. In control, NHE3 staining appears more prominent in the cytoplasm just below the apical actin ring. Some areas were stained weakly or had no immunostaining (arrows). After 5h FSS, the NHE3 staining was stronger and the stained areas were larger than those in control cells. (B) Distributions of normalized NHE3-stained fluorescence intensity. The values were normalized such that the mean maximum value in the stimulation group was 100% in each experiment. The fluorescence intensity of the cells was shifted to the right (apical side of the cells) after application of FSS (red). This effect was blunted with the addition of cD (green). (C) Western blot analysis showing NHE3 levels in whole cells (left) under CTL and FSS condition, and membrane NHE3 levels (right). Clearly, FSS induced both total and membrane NHE3 expression; membrane NHE3 expression has more increment in comparison than the whole cell expression, indicating an exocytic insertion of NHE3 occurred. (D) Quantification of NHE3 expression.

Data are mean ± SEM, n=3; Bars, 10μm. *$p<0.05$.

MPT=mouse proximal tubule, CTL=control, FSS=fluid shear stress, cD=cytochalasin D

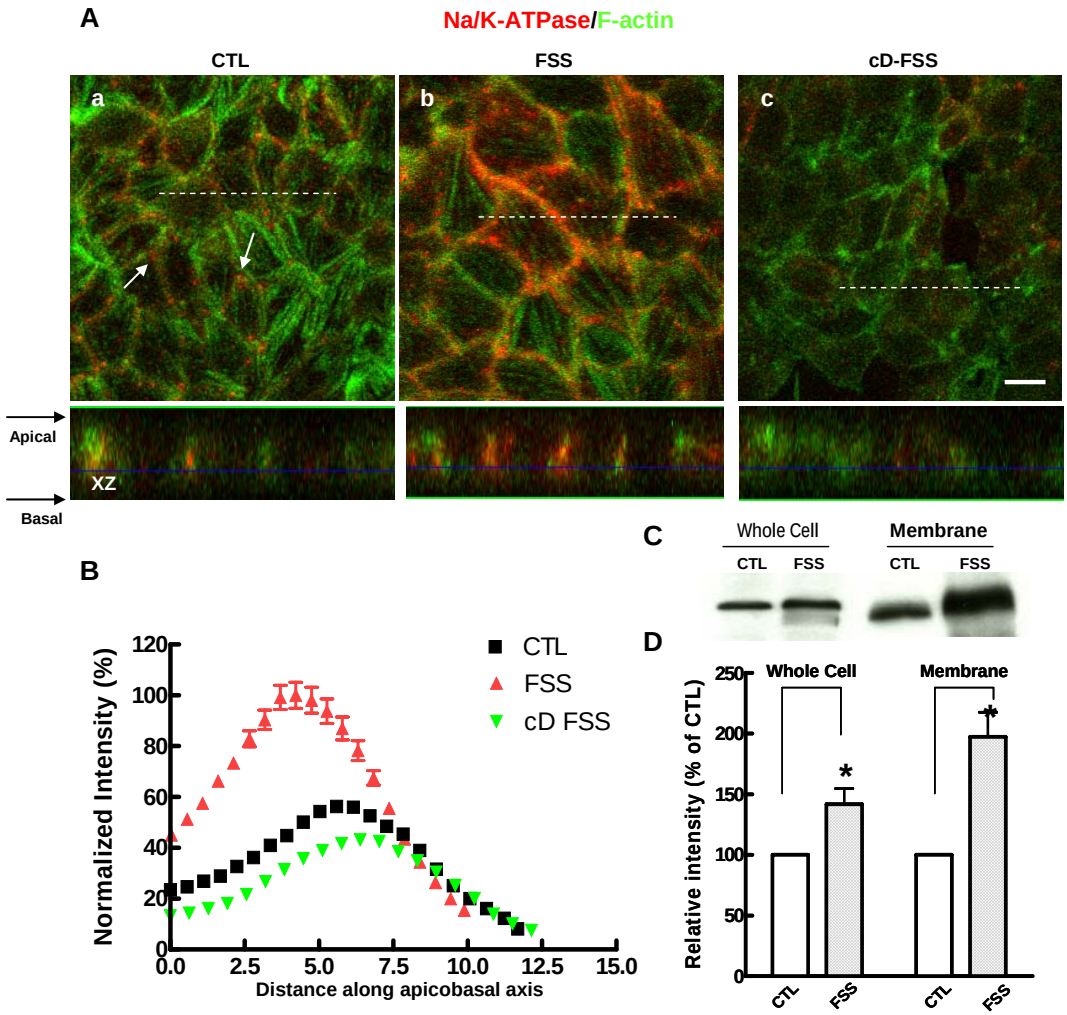

Figure 4−2 Effect of fluid shear stress on Na+/K+-ATPase trafficking and expression in mouse proximal tubule cells.

(A) Immunofluorescence images of MPT cells under CTL (a), FSS (b), and cD-FSS conditions (c). The antibody stained for Na^+/K^+-ATPase (red) and actin filaments (green), respectively. In control, Na^+/K^+-ATPase weakly distributed mainly at the basolateral membrane with some intensive staining near the cell-cell contacts (arrows). After 5h FSS, an elevation in membrane Na^+/K^+-ATPase expression was observed both at the cell periphery and cytosol. Cytochalasin D significantly blunted the flow-dependent effects. (B) Distributions of normalized Na^+/K^+-ATPase -stained fluorescence intensity. The values were normalized such that the mean maximum value in the stimulation group was 100% in each experiment. The fluorescence intensity of the cells was shifted to the left (basal side of the cells) after application of FSS (red). This effect was blunted with the addition of cytochalasin D (green). (C) Representative immunoblots showing cell total (left) and membrane (right) expression of Na^+/K^+-ATPase. (D) Quantification of Na^+/K^+-ATPase expression.

Data are mean ± SEM, n=3; Bars, 10μm. *$p<0.05$.
MPT=mouse proximal tubule, CTL=control, FSS=fluid shear stress, cD=cytochalasin D

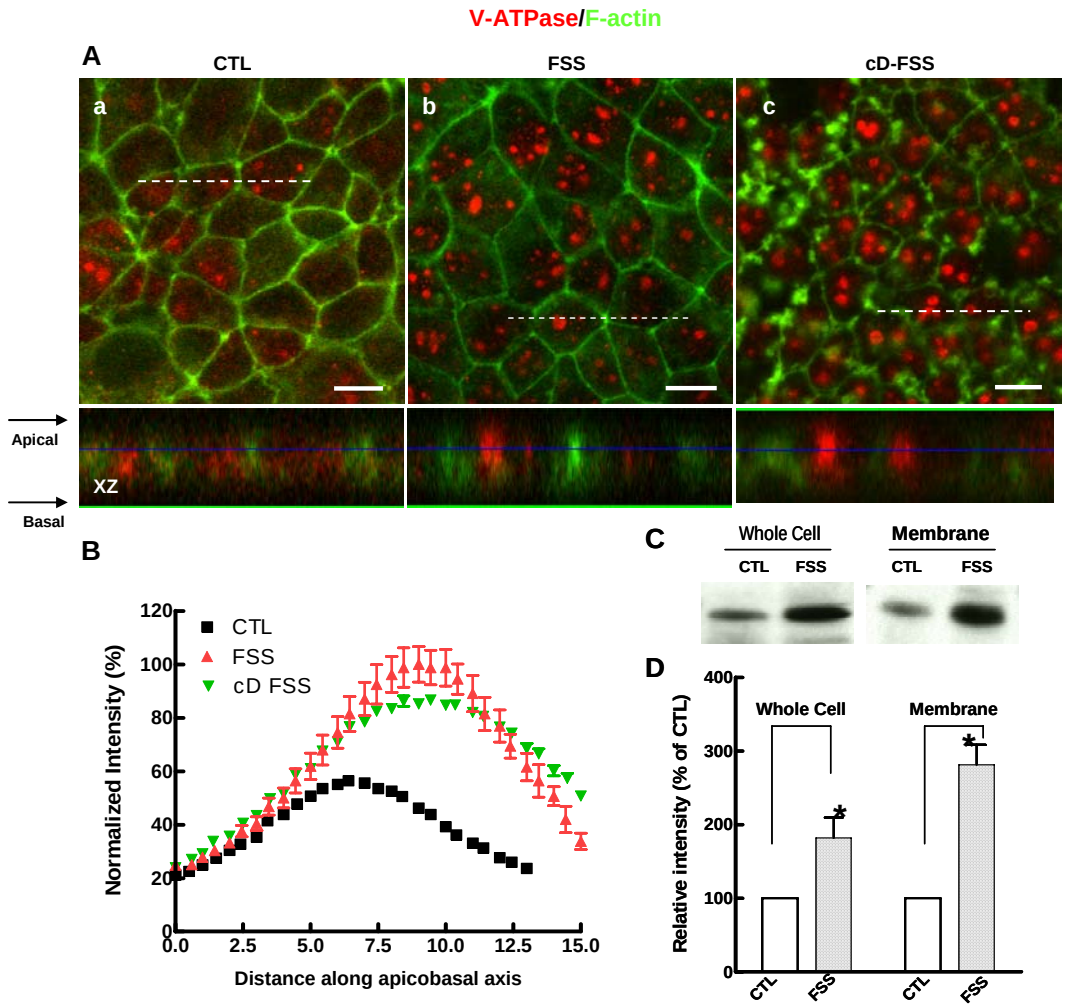

Figure 4−3 Effect of fluid shear stress on V-ATPase trafficking and expression in mouse proximal tubule cells.

(A) Immunofluorescence images of MPT cells under control (a), FSS (b), and cD-FSS conditions (c). The antibody stained for V-ATPase (red) and actin filaments (green), respectively. In control, only 30% of the cells express V-ATPase. After 5h FSS, V-ATPase was expressed more evenly and brightly in every cells. There is a translocation of V-ATPase witnessed in the XZ image. Cytochalasin D did not affect the flow-dependent upregulation of V-ATPase. (B) Distributions of normalized V-ATPase fluorescence intensity. The values were normalized such that the mean maximum value in the stimulation group was 100% in each experiment. The fluorescence intensity of the cells was shifted to the left (basal side of the cells) after application of FSS (red). (C) V-ATPase was detected by Western blot analysis on whole cell lysate (left) or on membrane protein (right). (D) Quantification of V-ATPase expression.

Data are mean ± SEM, n=3; Bars, 10μm. *$p<0.05$.
MPT=mouse proximal tubule, CTL=control, FSS=fluid shear stress, cD=cytochalasin D

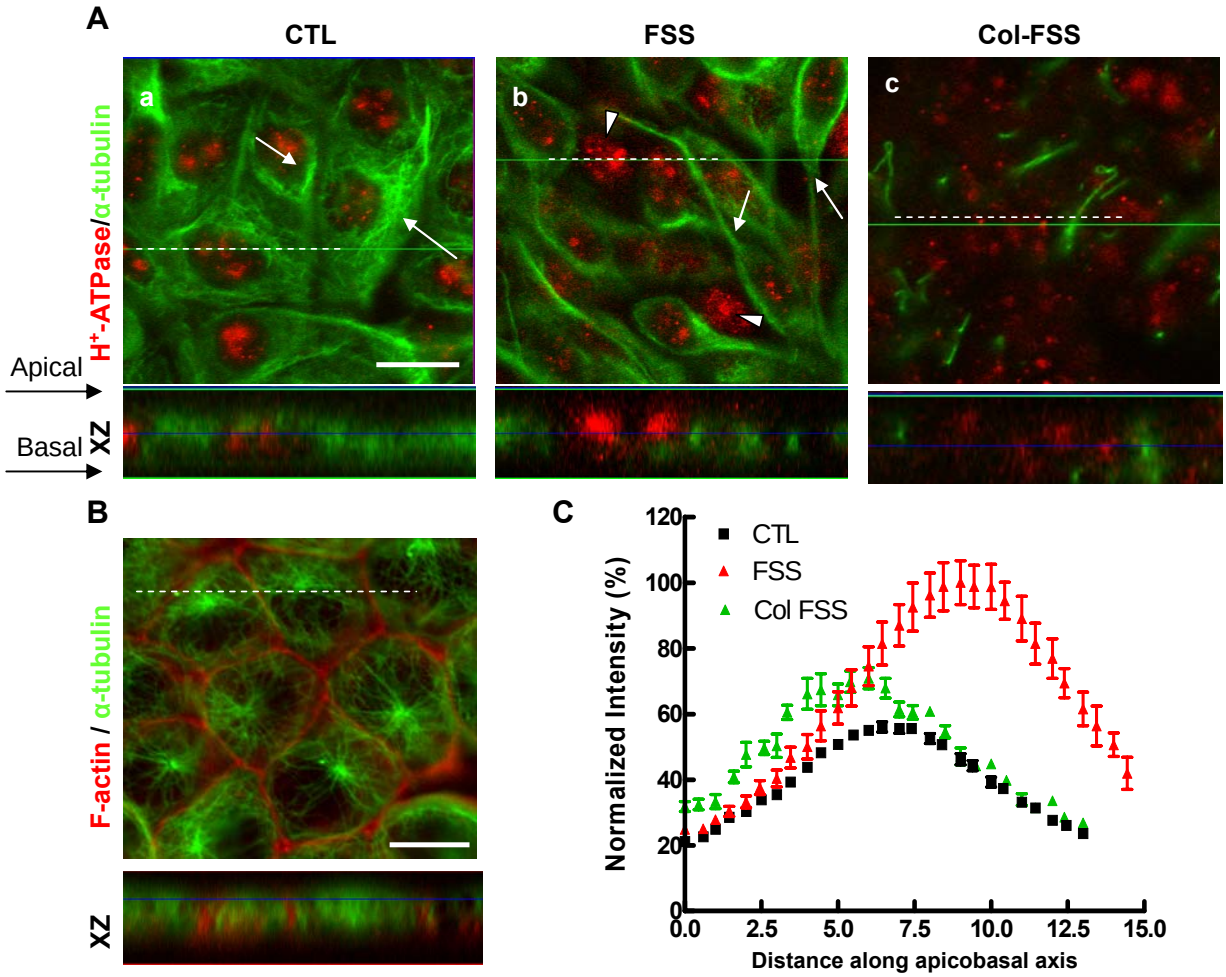

Figure 4−4 Colchicine inhibited fluid shear stress-induced upregulation of V-ATPase in mouse proximal tubule cells.

(A) Immunofluorescence images of MPT cells under control (a), FSS (b), and col-FSS conditions (c). The antibody stained for V-ATPase (red) and α-tubulin (green), respectively. In control, α-tubulin exhibited radial patterns in the cytoplasm, and intense fluorescence was observed in the perinuclear region (arrows). After 5h FSS, α-tubulin was accumulated in smaller cytoplasmic areas. A "tail" like structure was often found connected to the cell periphery (arrows). V-ATPase expressed outside the microtubule surrounding appeared more condensed (arrow heads) and more exposed to the apical surface (XZ). Colchicine led to a strong loss of microtubules and a marked decrease of V-ATPase localization. (B) Distributions of normalized V-ATPase fluorescence intensity. The values were normalized such that the mean maximum value in the stimulation group was 100% in each experiment. The fluorescence intensity of the cells was shifted to the left (basal side of the cells) after application of FSS (red). (C) V-ATPase was detected by Western blot analysis on whole cell lysate (left) or on membrane protein (right). Representative immunoblots showing cell total (left) and membrane (right) expression of V-ATPase. (D) Quantification of V-ATPase expression.

Data are mean ± SEM, n=3; Bars, 10μm. *$p<0.05$.
MPT= mouse proximal tubule, FSS=fluid shear stress, col=colchicine

Chapter 5 Conclusion

In this dissertation we explored a long-standing mystery in mouse proximal tubule: the mechanism of glomerular tubular balance (GTB), wherein changes in glomerular filtration rate are balanced by equivalent changes in tubular reabsorption, thus maintaining a constant fractional reabsorption of fluid and solutes. GTB is independent of direct neurohumoral control, and thought to be mediated by the additive effects of luminal and peritubular factors. The impact of the luminal flow rate has been termed "perfusion-absorption balance", and has been demonstrated in rat microperfusion studies. Luminal flow has been found to influence the transport of ions, small molecules and volume reabsorption. The main focus of the present work is the mechanism underlying flow-mediated Na^+ and HCO_3^- reabsorption. First, we have developed a new theory to calculate the forces and torques on the microvilli and demonstrated that flow-induced changes of proximal tubule absorption are torque-dependent. Changes in luminal diameter are inversely correlated to the changes in torque, which explained the difference between in *vivo* and in *vitro*, and between mouse and rabbit proximal tubule in increments of Na^+ reabsorption by higher flow. Second, we have demonstrated that an intact actin cytoskeleton is required for the torque-dependent reabsorption. Third, we have witnessed a dramatic reorganization of actin cytoskeleton and junction formation in the presence of flow stimulation. Surprisingly, the responses of proximal tubule epithelial cells are almost exactly opposite to what has been seen in endothelial cells. Finally, flow-dependent upregulation and trafficking of transporters was confirmed for both luminal

and peritubular membrane domains. Interestingly, not all membrane transporter activities are dependent on the integrity of an actin cytoskeleton network.

In Chapter 2, we begin our work by presenting a global theoretical model to calculate the forces and torques on the microvilli. Guo et al. (35) has proposed that brush border microvilli are the mechanosensors for proximal tubule cells and developed a mathematical model in which the detailed velocity distribution throughout the brush border was used to determine the fluid drag and torque distribution on each microvillus. This model does not allow us to easily determine how the drag and torque on the microvilli change with flow and diameter since it requires that we determine the detailed flow around each microvillus as their spacing changes in response to tubule diameter changes. To analyze our experimental results, we present a simpler global model where the detailed geometry of the microvilli and their spacing is not needed. This model calculates the ratio of the total torque T to its value T_r at a low reference flow rate by Eq. 2-8:

$$\frac{T}{T_r} = \frac{R_r^{\,2}}{R^2}\left(\frac{1+\dfrac{L+\delta}{R}+\dfrac{L^2}{2R^2}}{1+\dfrac{L+\delta}{R_r}+\dfrac{L^2}{2R_r^{\,2}}}\right)\left(\frac{\mu}{\mu_r}\right)\frac{Q}{Q_r} \tag{2-8}$$

Using this equation we calculated the change in torque and found that the relationship between increasing perfusion rates and changes in torque is almost perfectly linear and, for the first time, provided a link between a mechanical loading (hydrodynamic torque)

and physiological responses (Na^+ and HCO_3^- reabsorption). The results indicate that flow-dependent changes of transport activity are directly modulated by the changes in microvillus torque.

By using this new theory, we have reconsidered the data of Burg and Orloff (9), widely cited as a negative effect of flow on proximal sodium reabsorption in isolated rabbit proximal tubule. The flow modulated changes in fluid reabsorption, tubule diameter and the torque were compared between rabbit and mouse proximal tubules. As shown in Figure 2-8, when flow rate was increased 3 fold, torque and J_v increased by 38% and 37%, respectively, in rabbit proximal tubules. Similarly, torque and J_v increased by 61% and 60%, respectively, in mouse proximal tubule, indicating proportional changes in torque and J_v in response to flow exhibited in both species. In contrast, the tubule diameter increased by 41% in rabbit and only 30% in mouse proximal tubules. As the change in torque is inversely related to the change in tubule diameter squared, the increase in torque is significantly lower in rabbit than in mouse proximal tubules due to the enlargement of the tubule lumen in the former. It appears that rabbit proximal tubules were more distensible than mouse tubules, so that perfusion dependent changes in luminal diameter precluded large deviations in microvillus torque. Thus the reason for the absence of flow-stimulated Na^+ reabsorption in rabbit proximal tubules *in vitro* has been answered by our equations of torque-dependent transport. Even beyond the studies reported in this thesis, the new theory validates *in vitro* microperfusion technique as an invaluable tool for the future studies of GTB.

According to the hypothesis proposed by Weinbaum et al. (90), the changes in microvillus torque in response to luminal flow need to be transmitted to the terminal web where the actin filament bundle within the microvillus attaches at its roots to the main cell body. To verify this hypothesis, the effect of cytochalasin D on flow-dependent proximal tubule transport was studied. As discussed in Chapter 2, addition of 3 μM cytochalasin D did not change the baseline of J_v at low flow rate, but completely abolished the flow-stimulated increase in J_v. In comparison, flow-dependent J_{HCO3} was substantially reduced in the presence of cytochalasin D, but the reduction is not as significant as observed for changes in J_v, indicating that there might be another actin cytoskeleton-independent mechanism involved. These results suggested that 3 μM cytochalasin D has no toxicity to cells but inhibits actin cytoskeletal signaling, which is critical to the flow-stimulated Na^+ and HCO_3^- transport in the proximal tubule. In contrast, cytochalasin D completely abolished the increment of transport activity due to enhanced flow, consistent with our hypothesis that the transduction of signals from brush border to terminal web via the actin cytoskeleton is essential for the modulation of solute transport mechanisms regulated by flow in proximal tubules.

Na^+ and HCO_3^- reabsorption depend in large measure on the activity of the membrane transporter proteins. Following the previous study, the next key question one may ask is how the actin cytoskeleton modulates transporter activities in the presence of flow. To answer this question, we first investigated the responses of the actin cytoskeleton to fluid

flow in Chapter 3. In the following chapter (Chapter 4), we examined the responses of the transporter proteins to fluid flow and their interaction with the actin cytoskeleton.

We used immunofluorescence technique and stained F-actin, tight junction protein (ZO-1), adherens junction protein (E-cadherin), and focal adhesion proteins (vinculin and paxillin) in cultured mouse proximal tubule cell (PTC) line. After 5 hours of fluid shear, the distributions of these structural proteins were examined in PTC and compared with no-flow controls. A few key findings include: a) shear stress-induced disappearance of cytosolic stress fibers from the cell base and reinforcement of the cortical actin web, b) a formation of the apical junctional complexes (tight junction and adherens junction), and c) an accumulation of focal adhesion proteins at the basement membrane of PTCs. These results are the complete opposite of what has been reported in endothelial cells (81). To explain this paradox, we proposed a conceptual "junctional buttressing" model for PTCs (Figure 3-5) in which fluid shear enables the dense peripheral actin bands, tight junction and adherens junction to become more tightly connected. In control state, the cells, though confluent and touching at their base, do not have tight junctions and adherens junctions as indicated by the distribution of ZO-1 and E-cadherin. There is a strong expression of stress fibers at the base of the cells, which causes a firm adhesion of the cell to its substrate. This creates a tension on the lateral side of the cell membrane, which in turn produces a rounding of the apical surface and a pulling away of a cell from its neighbor. The cells have the appearance of tall columnar domes. Cell junctions can not form until there is a disruption of the stress fibers at the basal surface and a release of this

membrane tension which is exactly what happened when we exposed these cells under a small fluid shear (1 dynes/cm^2). Under the flow stimulation, the assembly of focal adhesions supports cell adhesion to extracellular matrix in which focal adhesions substitute for stress fibers and stabilize the cell at its base.

Another fundamental finding of this study is that a much smaller shear (1/10 of that in endothelial cell study) is required to produce cytoskeletal reorganization in epithelial cells. A threshold shear of 10 dyne/cm^2 was needed to initiate the remodeling in endothelial cells, a value close to the measured physiological range, whereas 1 dyne/cm^2 is required for PTCs. This difference in shear stress magnitude is largely due to cell geometry. Tall, columnar epithelial cells have large bending moments about their base, whereas the flat endothelial cells appear to pivot about the plane of their adherens junction where their actin bumpers are in alignment and the lever arm is much shorter.

From a "structure-function" point of view, we next carried out experiments to explore whether such a dramatic cytoskeletal remodeling would have an impact on transporter activities. Previously, we indirectly examined the effect of flow on modulation of luminal membrane NHE3 and H^+-ATPase activity by adding protein inhibitors and found that EIPA (NHE3 inhibitor) inhibited 30%, and bafilomycin (H^+-ATPase inhibitor) inhibited 48% of the flow-stimulated J_{HCO3} increase. The increment of J_{HCO3} due to enhanced flow rate was reduced by 97% when both EIPA and bafilomycin were added together. In addition, the flow-stimulated increase in J_{HCO3} was reduced by 35% in NHE knockout mice. These results indicate that both NHE3 and H^+-ATPase are modulated by flow. In

Chapter 4, we used an immunofluorescence technique to visualize the subcellular distribution of transporters (NHE3, H^+-ATPase, and Na^+/K^+-ATPase) and immunoblot analysis to quantify the expression of the transporters under both no-flow and flow condition. To test the interaction of these transporters with the actin cytoskeleton, we added cytochalasin D into the perfusate. Two important results of these new findings arise. First, fluid shear increased the overall expression of all three transporters and a translocation to their functional side of the membrane. Second, cytochalasin D disrupted the flow-induced upregulation of NHE3 and Na^+/K^+-ATPase, but did not affect the increment in flow-induced H^+-ATPase expression and its trafficking. In contrast, addition of colchicine (a microtubule depolymerizing drug) blunted the effect of flow on H^+-ATPase. The different responses between transporters may have provided an explanation as to why there is still a small flow-dependent increase in J_{HCO3} after perfusing the tubules under low and high flow rates in the presence of cytochalasin D.

Perhaps the most important aspect of this study is the demonstration that peritubular transporters, though geometrically distant from the luminal stimulation, are still modulated by flow. The inspiration for this study came from the mathematical model in Weinstein et al (93). The model suggested that peritubular transporter density has to increase in the same manner as the apical transporters when luminal flow increases in order to keep a constant cell volume. One study on proximal tubules in young spontaneously hypertensive rat (SHR) has revealed that an age-dependent change in apical NHE3 activity is similar to that observed for Na^+, K^+-ATPase and distribution.

They suggested that increased proximal tubule NHE3 activity maybe lead to an increase of Na^+/K^+-ATPase activity, and increased Na^+ reabsorption (39). But there was no direct evidence provided until now. We observed a twofold increase in overall Na^+/K^+-ATPase expression and a 2.5 fold increase in membrane Na^+/K^+-ATPase expression, which is in consistent with what have measured for NHE3 stimulation by flow. From the immunofluorescence image, we also noticed that Na^+/K^+-ATPase tends to target mainly the lateral side of the cells instead of the cell base. The mechanism by which flow upregulates Na^+/K^+-ATPase expression and targeting remains unknown.

The current study is not complete in many aspects. First of all, experimental approaches will need to be conducted to elucidate the mechanosensory function in proximal tubule cells. There are two questions that need to be addressed: 1) are microvilli the only mechanosensor for proximal tubule cells or do cilia play a role, and 2) what is the regulatory pathway between microvilli bending and transporter activities. In contrast to the mechanosensory function of microvilli proposed for the renal proximal tubule, flow-dependent transport in the distal nephron has recently been attributed to renal epithelial cilia (70). Subsequently, Liu *et al.* (49) demonstrated that flow-dependent increases in $[Ca^{2+}]_i$ occur in both principal cells with apical cilia and intercalated cells with apical microplicae that lack cilia, suggesting that these intercalated cell projections also serve a mechanosensory function. Although the linear dependence of reabsorption on microvillous torque is reassuring, this issue is difficult to resolve with certainty because of the positive correlation of hydrodynamic drag on both microvilli and cilia. Herein,

Tg737 mutant mice, with stunted cilia, will need to be utilized to test whether there is a significant change in flow-dependent fluid reabsorption. As far as the cascade of mechanotransduction in proximal tubule cells, it has been found that NHE regulatory factor (NHERF-1) colocalizes with NHE3 in microvilli of the brush border and binds to the actin-associated protein ezrin, thus linking NHE3 to the cytoskeleton. This linkage to the cytoskeleton may be particularly important for the mechanical activation of NHE3 by microvillar bending. Further experiments need to be carried out to clarify this issue.

Second, in Chapter 2, we have observed that flow induces the formation of tight junction and adherens junctions in cultured mouse proximal tubule cells. Whether this structural change links to signaling pathways that facilitate transporter trafficking or activation is also interesting to explore.

Third, a flow-dependent functional study is necessary for the purpose of understanding the mechanism of GTB. Whether flow-induced Na^+ and HCO_3^- reabsorption is due to trafficking of transporters to their functional membrane, increase of their activities or both has not been answered. Spectroscopic measurements of cytosolic pH will need to be conducted to assess the time-course of varying flow effects on NHE3 and H^+-ATPase activities.

Finally, the cross-talk between apical and peritubular transporters in response to flow stimulation needs to be investigated. As mentioned before, flow induced nearly identical changes in NHE3 and Na^+/K^+-ATPase expression. Whether there is cross-talk between

one another remains unclear. Adding inhibitors to block either apical or basolateral membrane proteins may help to elucidate this issue.

References

1. **Achler C, Filmer D, Merte C, and Drenckhahn D**. Role of microtubules in polarized delivery of apical membrane proteins to the brush border of the intestinal epithelium. *J Cell Biol* 109: 179-189, 1989.

2. **Akhter S, Cavet ME, Tse CM, and Donowitz M**. C-terminal domains of Na(+)/H(+) exchanger isoform 3 are involved in the basal and serum-stimulated membrane trafficking of the exchanger. *Biochemistry* 39: 1990-2000, 2000.

3. **Barth AI, Nathke IS, and Nelson WJ**. Cadherins, catenins and APC protein: interplay between cytoskeletal complexes and signaling pathways. *Curr Opin Cell Biol* 9: 683-690, 1997.

4. **Basmadjian D, Dykes DS, and Baines AD**. Flow through brushborders and similar protuberant wall structures. *J Membr Biol* 56: 183-190, 1980.

5. **Bergeron M, Guerette D, Forget J, and Thiery G**. Three-dimensional characteristics of the mitochondria of the rat nephron. *Kidney Int* 17: 175-185, 1980.

6. **Bretscher A**. Microfilament structure and function in the cortical cytoskeleton. *Annu Rev Cell Biol* 7: 337-374, 1991.

7. **Brown D, Sabolic I, and Gluck S**. Colchicine-induced redistribution of proton pumps in kidney epithelial cells. *Kidney Int Suppl* 33: S79-83, 1991.

8. **Brown D, Sabolic I, and Gluck S**. Polarized targeting of V-ATPase in kidney epithelial cells. *J Exp Biol* 172: 231-243, 1992.

9. **Burg MB, and Orloff J**. Control of fluid absorption in the renal proximal tubule. *J Clin Invest* 47: 2016-2024, 1968.

10. **Chan YL, Biagi B, and Giebisch G**. Control mechanisms of bicarbonate transport across the rat proximal convoluted tubule. *Am J Physiol* 242: F532-543, 1982.

11. **Chen LK, and Boron WF**. Intracellular pH regulation in epithelial cells. *Kidney Int Suppl* 33: S11-17, 1991.

12. **Claude P, and Goodenough DA**. Fracture faces of zonulae occludentes from "tight" and "leaky" epithelia. *J Cell Biol* 58: 390-400, 1973.

13. **Collazo R, Fan L, Hu MC, Zhao H, Wiederkehr MR, and Moe OW**. Acute regulation of Na+/H+ exchanger NHE3 by parathyroid hormone via NHE3

phosphorylation and dynamin-dependent endocytosis. *J Biol Chem* 275: 31601-31608, 2000.

14. **Coudrier E, Kerjaschki D, and Louvard D**. Cytoskeleton organization and submembranous interactions in intestinal and renal brush borders. *Kidney Int* 34: 309-320, 1988.

15. **D'Souza S, Garcia-Cabado A, Yu F, Teter K, Lukacs G, Skorecki K, Moore HP, Orlowski J, and Grinstein S**. The epithelial sodium-hydrogen antiporter Na+/H+ exchanger 3 accumulates and is functional in recycling endosomes. *J Biol Chem* 273: 2035-2043, 1998.

16. **Davies PF, Barbee KA, Volin MV, Robotewskyj A, Chen J, Joseph L, Griem ML, Wernick MN, Jacobs E, Polacek DC, dePaola N, and Barakat AI**. Spatial relationships in early signaling events of flow-mediated endothelial mechanotransduction. *Annu Rev Physiol* 59: 527-549, 1997.

17. **Du Z, Duan Y, Yan Q, Weinstein AM, Weinbaum S, and Wang T**. Mechanosensory function of microvilli of the kidney proximal tubule. *Proceedings of the National Academy of Sciences of the United States of America* 101: 13068-13073, 2004.

18. **Du Z, Ferguson W, and Wang T**. Role of PKC and calcium in modulation of effects of angiotensin II on sodium transport in proximal tubule. *Am J Physiol Renal Physiol* 284: F688-692, 2003.

19. **Du Z, Yan Q, Duan Y, Weinbaum S, Weinstein AM, and Wang T**. Axial flow modulates proximal tubule NHE3 and H-ATPase activities by changing microvillus bending moments. *Am J Physiol Renal Physiol* 290: F289-296, 2006.

20. **Duan Y, Gotoh N, Yan Q, Du Z, Weinstein AM, Wang T, and Weinbaum S**. Shear-induced reorganization of renal proximal tubule cell actin cytoskeleton and apical junctional complexes. *Proc Natl Acad Sci U S A* 105: 11418-11423, 2008.

21. **Dubinsky WP, Mayorga-Wark O, and Schultz SG**. Volume regulatory responses of basolateral membrane vesicles from Necturus enterocytes: role of the cytoskeleton. *Proc Natl Acad Sci U S A* 96: 9421-9426, 1999.

22. **Earley LE, and Schrier RW**. Intrarenal control of sodium excretion by hemodynamic and physica factors. In: *Handbook of Physiology, Renal Physiology*. Bethesda, MD: Am Physiol Soc, 1973, p. 763-790.

23. **Eskin SG, Ives CL, McIntire LV, and Navarro LT**. Response of cultured endothelial cells to steady flow. *Microvasc Res* 28: 87-94, 1984.

24. **Essig M, and Friedlander G**. Tubular shear stress and phenotype of renal proximal tubular cells. *J Am Soc Nephrol* 14 Suppl 1: S33-35, 2003.

25. **Essig M, Terzi F, Burtin M, and Friedlander G**. Mechanical strains induced by tubular flow affect the phenotype of proximal tubular cells. *Am J Physiol Renal Physiol* 281: F751-762, 2001.

26. **Friedrich C, Endlich N, Kriz W, and Endlich K**. Podocytes are sensitive to fluid shear stress in vitro. *Am J Physiol Renal Physiol* 291: F856-865, 2006.

27. **Furuse M, Furuse K, Sasaki H, and Tsukita S**. Conversion of zonulae occludentes from tight to leaky strand type by introducing claudin-2 into Madin-Darby canine kidney I cells. *J Cell Biol* 153: 263-272, 2001.

28. **Galbraith CG, Skalak R, and Chien S**. Shear stress induces spatial reorganization of the endothelial cell cytoskeleton. *Cell Motil Cytoskeleton* 40: 317-330, 1998.

29. **Gerges NZ, Brown TC, Correia SS, and Esteban JA**. Analysis of Rab protein function in neurotransmitter receptor trafficking at hippocampal synapses. *Methods Enzymol* 403: 153-166, 2005.

30. **Gertz KH, and Boylan JW**. Glomerular-tubular balance. . In: *Handbook of Physiology Renal Physiology*. Bethesda, MD: Am Physiol Soc., 1973, p. 763-790.

31. **Giebisch G, and Windhager EE**. Characterization of renal tubular transport of sodium chloride and water as studied in single nephrons. *Am J Med* 34: 1-6, 1963.

32. **Gluck SL, Underhill DM, Iyori M, Holliday LS, Kostrominova TY, and Lee BS**. Physiology and biochemistry of the kidney vacuolar H+-ATPase. *Annu Rev Physiol* 58: 427-445, 1996.

33. **Grindstaff KK, Bacallao RL, and Nelson WJ**. Apiconuclear organization of microtubules does not specify protein delivery from the trans-Golgi network to different membrane domains in polarized epithelial cells. *Mol Biol Cell* 9: 685-699, 1998.

34. **Gumbiner BM**. Cell adhesion: the molecular basis of tissue architecture and morphogenesis. *Cell* 84: 345-357, 1996.

35. **Guo P, Weinstein AM, and Weinbaum S**. A hydrodynamic mechanosensory hypothesis for brush border microvilli. *Am J Physiol Renal Physiol* 279: F698-712, 2000.

36. **Gutmann EJ, Niles JL, McCluskey RT, and Brown D**. Colchicine-induced redistribution of an apical membrane glycoprotein (gp330) in proximal tubules. *Am J Physiol* 257: C397-407, 1989.

37. **Haberle DA, and von Baeyer H**. Characteristics of glomerulotubular balance. *Am J Physiol* 244: F355-366, 1983.

38. **Hayashi H, Szaszi K, Coady-Osberg N, Furuya W, Bretscher AP, Orlowski J, and Grinstein S**. Inhibition and redistribution of NHE3, the apical Na+/H+ exchanger, by Clostridium difficile toxin B. *J Gen Physiol* 123: 491-504, 2004.

39. **Hinojos CA, and Doris PA**. Altered subcellular distribution of Na+,K+-ATPase in proximal tubules in young spontaneously hypertensive rats. *Hypertension* 44: 95-100, 2004.

40. **Hu MC, Fan L, Crowder LA, Karim-Jimenez Z, Murer H, and Moe OW**. Dopamine acutely stimulates Na+/H+ exchanger (NHE3) endocytosis via clathrin-coated vesicles: dependence on protein kinase A-mediated NHE3 phosphorylation. *J Biol Chem* 276: 26906-26915, 2001.

41. **Hynes RO, and Lander AD**. Contact and adhesive specificities in the associations, migrations, and targeting of cells and axons. *Cell* 68: 303-322, 1992.

42. **Janecki AJ, Montrose MH, Zimniak P, Zweibaum A, Tse CM, Khurana S, and Donowitz M**. Subcellular redistribution is involved in acute regulation of the brush border Na+/H+ exchanger isoform 3 in human colon adenocarcinoma cell line Caco-2. Protein kinase C-mediated inhibition of the exchanger. *J Biol Chem* 273: 8790-8798, 1998.

43. **Janmey PA**. The cytoskeleton and cell signaling: component localization and mechanical coupling. *Physiol Rev* 78: 763-781, 1998.

44. **Karihaloo A, Karumanchi SA, Cantley WL, Venkatesha S, Cantley LG, and Kale S**. Vascular endothelial growth factor induces branching morphogenesis/tubulogenesis in renal epithelial cells in a neuropilin-dependent fashion. *Mol Cell Biol* 25: 7441-7448, 2005.

45. **Krahn TA, and Weinstein AM**. Acid/base transport in a model of the proximal tubule brush border: impact of carbonic anhydrase. *Am J Physiol* 270: F344-355, 1996.

46. **Kurashima K, D'Souza S, Szaszi K, Ramjeesingh R, Orlowski J, and Grinstein S**. The apical Na(+)/H(+) exchanger isoform NHE3 is regulated by the actin cytoskeleton. *J Biol Chem* 274: 29843-29849, 1999.

47. **Kurashima K, Szabo EZ, Lukacs G, Orlowski J, and Grinstein S**. Endosomal recycling of the Na+/H+ exchanger NHE3 isoform is regulated by the phosphatidylinositol 3-kinase pathway. *J Biol Chem* 273: 20828-20836, 1998.

48. **Lamprecht G, Weinman EJ, and Yun CH**. The role of NHERF and E3KARP in the cAMP-mediated inhibition of NHE3. *J Biol Chem* 273: 29972-29978, 1998.

49. **Liu W, Xu S, Woda C, Kim P, Weinbaum S, and Satlin LM**. Effect of flow and stretch on the [Ca2+]i response of principal and intercalated cells in cortical collecting duct. *Am J Physiol Renal Physiol* 285: F998-F1012, 2003.

50. **Lutz KL, and Siahaan TJ**. Molecular structure of the apical junction complex and its contribution to the paracellular barrier. *J Pharm Sci* 86: 977-984, 1997.

51. **Maddox DA, Fortin SM, Tartini A, Barnes WD, and Gennari FJ**. Effect of acute changes in glomerular filtration rate on Na+/H+ exchange in rat renal cortex. *J Clin Invest* 89: 1296-1303, 1992.

52. **Madsen KM, and Brenner BM** editors. *Structure and function of the renal tubule and interstitium.* . Philadelphia: JB Lippincott, 1989, p. 606.

53. **Madsen KM, and Tisher CC**. Structural-functional relationship along the distal nephron. *Am J Physiol* 250: F1-15, 1986.

54. **Malek AM, and Izumo S**. Mechanism of endothelial cell shape change and cytoskeletal remodeling in response to fluid shear stress. *J Cell Sci* 109 (Pt 4): 713-726, 1996.

55. **Malnic G, Berliner RW, and Giebisch G**. Flow dependence of K+ secretion in cortical distal tubules of the rat. *Am J Physiol* 256: F932-941, 1989.

56. **Maunsbach AB**. Observations on the ultrastructure and acid phosphatase activity of the cytoplasmic bodies in rat kidney proximal tubule cells. With a comment on their classification. *J Ultrastruct Res* 16: 197-238, 1966.

57. **Maunsbach AB, Christensen, E. I.** In: *Handbook of Physiology: Renal Physiology*, edited by windhager E. Bethesda: Am. Physiol. Soc., 1992, p. 41-107.

58. **Maunsbach AB, Christensen, E. I.** *Renal Physiology*. Bethesda: Am. Physiol. Soc, 1992, p. 41-107.

59. **Maunsbach AB, Giebisch GH, and Stanton BA**. Effects of flow rate on proximal tubule ultrastructure. *Am J Physiol* 253: F582-587, 1987.

60. **Musch A**. Microtubule organization and function in epithelial cells. *Traffic* 5: 1-9, 2004.

61. **Muto S, Nemoto J, Okada K, Miyata Y, Kawakami K, Saito T, and Asano Y**. Intracellular Na+ directly modulates Na+,K+-ATPase gene expression in normal rat kidney epithelial cells. *Kidney Int* 57: 1617-1635, 2000.

62. **Nelson WJ**. Adaptation of core mechanisms to generate cell polarity. *Nature* 422: 766-774, 2003.

63. **Nelson WJ, and Hammerton RW**. A membrane-cytoskeletal complex containing Na+,K+-ATPase, ankyrin, and fodrin in Madin-Darby canine kidney (MDCK) cells: implications for the biogenesis of epithelial cell polarity. *J Cell Biol* 108: 893-902, 1989.

64. **Nelson WJ, Shore EM, Wang AZ, and Hammerton RW**. Identification of a membrane-cytoskeletal complex containing the cell adhesion molecule uvomorulin (E-cadherin), ankyrin, and fodrin in Madin-Darby canine kidney epithelial cells. *J Cell Biol* 110: 349-357, 1990.

65. **Nicholson SM, and Bruzzone R**. Gap junctions: getting the message through. *Curr Biol* 7: R340-344, 1997.

66. **Ojakian GK, and Schwimmer R**. The polarized distribution of an apical cell surface glycoprotein is maintained by interactions with the cytoskeleton of Madin-Darby canine kidney cells. *J Cell Biol* 107: 2377-2387, 1988.

67. **Ozawa M, Ringwald M, and Kemler R**. Uvomorulin-catenin complex formation is regulated by a specific domain in the cytoplasmic region of the cell adhesion molecule. *Proc Natl Acad Sci U S A* 87: 4246-4250, 1990.

68. **Pavalko FM, Chen NX, Turner CH, Burr DB, Atkinson S, Hsieh YF, Qiu J, and Duncan RL**. Fluid shear-induced mechanical signaling in MC3T3-E1 osteoblasts requires cytoskeleton-integrin interactions. *Am J Physiol* 275: C1591-1601, 1998.

69. **Peng Y, Moe OW, Chu T, Preisig PA, Yanagisawa M, and Alpern RJ**. ETB receptor activation leads to activation and phosphorylation of NHE3. *Am J Physiol* 276: C938-945, 1999.

70. **Praetorius HA, and Spring KR**. The renal cell primary cilium functions as a flow sensor. *Curr Opin Nephrol Hypertens* 12: 517-520, 2003.

71. **Preisig PA**. Luminal flow rate regulates proximal tubule H-HCO3 transporters. *Am J Physiol* 262: F47-54, 1992.

72. **Romano G, Favret G, Damato R, and Bartoli E**. Proximal reabsorption with changing tubular fluid inflow in rat nephrons. *Exp Physiol* 83: 35-48, 1998.

73. **Roth J, Brown D, and Orci L**. Regional distribution of N-acetyl-D-galactosamine residues in the glycocalyx of glomerular podocytes. *J Cell Biol* 96: 1189-1196, 1983.

74. **Sabolic I, Herak-Kramberger CM, Ljubojevic M, Biemesderfer D, and Brown D**. NHE3 and NHERF are targeted to the basolateral membrane in proximal tubules of colchicine-treated rats. *Kidney Int* 61: 1351-1364, 2002.

75. **Satlin LM, Sheng S, Woda CB, and Kleyman TR**. Epithelial Na(+) channels are regulated by flow. *Am J Physiol Renal Physiol* 280: F1010-1018, 2001.

76. **Schnermann J, Wahl M, Liebau G, and Fischbach H**. Balance between tubular flow rate and net fluid reabsorption in the proximal convolution of the rat kidney. I. Dependency of reabsorptive net fluid flux upon proximal tubular surface area at spontaneous variations of filtration rate. *Pflugers Arch* 304: 90-103, 1968.

77. **Schultheis PJ, Clarke LL, Meneton P, Harline M, Boivin GP, Stemmermann G, Duffy JJ, Doetschman T, Miller ML, and Shull GE**. Targeted disruption of the murine Na+/H+ exchanger isoform 2 gene causes reduced viability of gastric parietal cells and loss of net acid secretion. *J Clin Invest* 101: 1243-1253, 1998.

78. **Sinha D, Wang Z, Price VR, Schwartz JH, and Lieberthal W**. Chemical anoxia of tubular cells induces activation of c-Src and its translocation to the zonula adherens. *Am J Physiol Renal Physiol* 284: F488-497, 2003.

79. **Tang VW, and Goodenough DA**. Paracellular ion channel at the tight junction. *Biophys J* 84: 1660-1673, 2003.

80. **Thaler CD, and Haimo LT**. Microtubules and microtubule motors: mechanisms of regulation. *Int Rev Cytol* 164: 269-327, 1996.

81. **Thi MM, Tarbell JM, Weinbaum S, and Spray DC**. The role of the glycocalyx in reorganization of the actin cytoskeleton under fluid shear stress: a "bumper-car" model. *Proc Natl Acad Sci U S A* 101: 16483-16488, 2004.

82. **Toyomura T, Oka T, Yamaguchi C, Wada Y, and Futai M**. Three subunit a isoforms of mouse vacuolar H(+)-ATPase. Preferential expression of the a3 isoform during osteoclast differentiation. *J Biol Chem* 275: 8760-8765, 2000.

83. **Tsukita S, Yonemura S, and Tsukita S**. ERM proteins: head-to-tail regulation of actin-plasma membrane interaction. *Trends Biochem Sci* 22: 53-58, 1997.

84. **Vinciguerra M, Deschenes G, Hasler U, Mordasini D, Rousselot M, Doucet A, Vandewalle A, Martin PY, and Feraille E**. Intracellular Na+ controls cell surface expression of Na,K-ATPase via a cAMP-independent PKA pathway in mammalian kidney collecting duct cells. *Mol Biol Cell* 14: 2677-2688, 2003.

85. **Vitavska O, Wieczorek H, and Merzendorfer H**. A novel role for subunit C in mediating binding of the H+-V-ATPase to the actin cytoskeleton. *J Biol Chem* 278: 18499-18505, 2003.

86. **Wang T**. Flow-activated transport events along the nephron. *Curr Opin Nephrol Hypertens* 15: 530-536, 2006.

87. **Wang T, Inglis FM, and Kalb RG**. Defective fluid and HCO(3)(-) absorption in proximal tubule of neuronal nitric oxide synthase-knockout mice. *Am J Physiol Renal Physiol* 279: F518-524, 2000.

88. **Wang T, Yang CL, Abbiati T, Schultheis PJ, Shull GE, Giebisch G, and Aronson PS**. Mechanism of proximal tubule bicarbonate absorption in NHE3 null mice. *Am J Physiol* 277: F298-302, 1999.

89. **Watanabe D, Saijoh Y, Nonaka S, Sasaki G, Ikawa Y, Yokoyama T, and Hamada H**. The left-right determinant Inversin is a component of node monocilia and other 9+0 cilia. *Development* 130: 1725-1734, 2003.

90. **Weinbaum S, Guo P, and You L**. A new view of mechanotransduction and strain amplification in cells with microvilli and cell processes. *Biorheology* 38: 119-142, 2001.

91. **Weinman EJ, Cunningham R, and Shenolikar S**. NHERF and regulation of the renal sodium-hydrogen exchanger NHE3. *Pflugers Arch* 450: 137-144, 2005.

92. **Weinstein AM**. Glomerulotubular balance in a mathematical model of the proximal nephron. *Am J Physiol* 258: F612-626, 1990.

93. **Weinstein AM, Weinbaum S, Duan Y, Du Z, Yan Q, and Wang T**. Flow-dependent transport in a mathematical model of rat proximal tubule. *Am J Physiol Renal Physiol* 292: F1164-1181, 2007.

94. **Welling LW, and Welling DJ**. Surface areas of brush border and lateral cell walls in the rabbit proximal nephron. *Kidney Int* 8: 343-348, 1975.

95. **Wilcox CS, and Baylis C**. Glomerular-tubular blaance and proximal regulation. In: *The Kidney: Physiology and Pathophysiology*, edited by Seldin D, and Giebisch G. New York: Raven Press, 1985, p. 985-1012.

96. **Xu T, and Forgac M**. Microtubules are involved in glucose-dependent dissociation of the yeast vacuolar [H+]-ATPase in vivo. *J Biol Chem* 276: 24855-24861, 2001.

97. **Yip KP, Tse CM, McDonough AA, and Marsh DJ**. Redistribution of Na+/H+ exchanger isoform NHE3 in proximal tubules induced by acute and chronic hypertension. *Am J Physiol* 275: F565-575, 1998.

98. **Yu AS**. Paracellular solute transport: more than just a leak? *Curr Opin Nephrol Hypertens* 9: 513-515, 2000.

99. **Zhai XY, Birn H, Jensen KB, Thomsen JS, Andreasen A, and Christensen EI**. Digital three-dimensional reconstruction and ultrastructure of the mouse proximal tubule. *J Am Soc Nephrol* 14: 611-619, 2003.

100. **Zimolo Z, Montrose MH, and Murer H**. H+ extrusion by an apical vacuolar-type H(+)-ATPase in rat renal proximal tubules. *J Membr Biol* 126: 19-26, 1992.